1983

Analysis of the nine-point finite difference approximation for the heat conduction equation in a nuclear fuel element

Mohamed Kadri
Iowa State University

Kadri, Mohamed

ANALYSIS OF THE NINE-POINT FINITE DIFFERENCE APPROXIMATION FOR THE HEAT CONDUCTION EQUATION IN A NUCLEAR FUEL ELEMENT

Iowa State University PH.D. 1983

Analysis of the nine-point finite difference approximation for the heat conduction equation in a nuclear fuel element

by

Mohamed Kadri

A Dissertation Submitted to the
Graduate Faculty in Partial Fulfillment of the
Requirements for the Degree of
DOCTOR OF PHILOSOPHY

Major: Nuclear Engineering

Approved:

Signature was redacted for privacy.

In Charge of Major Work

Signature was redacted for privacy.

For the Major Department

Signature was redacted for privacy.

For the Graduate College

Iowa State University
Ames, Iowa
1983

TABLE OF CONTENTS

NOMENCLATURE

K	Thermal conductivity
ρ	Material density
C_p	Specific heat
S	Internal heat generation
$\bar{r}$	Spacial vector
t	Time
T	Temperature
h_c	Heat transfer coefficient
T_f	Fluid temperature
β	Ratio of space increments ($\Delta x/\Delta y$)
Δx	Space increment in x-direction
Δy	Space increment in y-direction
p	Nine-point relation parameter
T_c	Sum of corner temperatures
D_x	First derivative with respect to x
D_y	First derivative with respect to y
D_{xx}	Second derivative with respect to x
$O(h)$	Spacing truncation error
$O(\Delta t)$	Truncation error on the time step
m,n,k	Iterative steps
EBS	Convergence criteria
$T_{i,j}$	Numerical nodal temperature
$T^*_{i,j}$	Analytic nodal temperature

E_A	Absolute error
E_R	Relative error
E_{L_2}	Euclidean error norm
ν	Convergence rate
λ	Largest eigenvalue of iteration matrix
L_2	Residual norm
L_{max}	Infinite residual norm
A	Slab length in x-direction
B	Slab length in y-direction
N	Number of mesh-grid in x-direction
M	Number of mesh-grid in y-direction
K_o	Thermal conductivity at reference temperature
ξ	Porosity coefficient
q_i	Heat conducted in x-direction
q_j	Heat conducted in y-direction
F	Initial temperature
$\phi(K)$	Fuel-clad surface temperature
Δt	Increment time step
∇	Gradient operator
∇^2	Laplacian operator
a	Parameter, 0 or 1
L	Fuel element length
Q'	Linear power density
Q''	Heat flux
$\bar{T}_F$	Average fuel temperature

$T_{F\ max}$	Maximum fuel temperature
T_{FS}	Surface fuel temperature
F	Peak to average fuel element power
α	Optimum SOR parameter
α_T	Thermal diffusivity
h	Space increment in case of equally spacing
$\bar{K}$	Average thermal conductivity

1. INTRODUCTION

1.1 Review of Literature

Various numerical methods have been devised for solutions to the problems of steady-state and transient nonlinear heat conduction encountered in reactor engineering calculations. The most common of these are finite-difference methods and finite element methods using Galerkin or weighted residual procedures.

In the finite-difference methods as used in various references [1, 2, 3, 4, 5, 6, 7, 8], the differential equations are approximated by the five-point difference equations at the mesh points and are usually of low order truncation error (see Appendix A). On the other hand, finite element method based on Galerkin or weighted residual procedure require the computation of integrals at each step which may not be an easy calculation in problems such as conduction in nuclear fuel elements [9].

Another approach, which uses the Monte Carlo method to solve the heat conduction problem, is able only to solve certain specific problems because the method uses the same random walk logic as existing Monte Carlo transport computer codes. However, all published results using these methods have been limited to single medium problems. Also, there are Monte Carlo methods which solve the five-point finite difference relations; these have not proven to be competitive with other finite difference techniques [10].

A knowledge of possible temperature distributions is required by the designer of various parts of nuclear reactors. A method that approximates the differential equations of heat conduction based on the nine-point formula can achieve higher order truncation accuracy [$O(h^4)$ where h is the maximum step size]. Therefore, the nine-point approximate numerical technique has been studied in this investigation in an attempt to provide suitable ways of applying this concept to find a more accurate and faster converging results of temperature distributions in a nuclear fuel element.

1.2 Statement of Problem

The mathematical formulation of most problems in science involving rates of change with respect to two or more variables leads either to a partial differential equation, or to a set of such equations. The analytical solution of the two-dimensional heat conduction equation (Eq. 1.1) is a function T(x,y,t), which satisfies a partial differential equation at every point in a region R (Figure 1.1), and satisfies certain boundary conditions on the closed curve surrounding R. The boundary conditions for the equation contain either the function T(x,y,t), its normal derivative, or a linear combination of T(x,y,t) and the normal derivative. In most practical cases, it is extremely difficult to arrive at exact solutions to the heat conduction problems encountered with reactor engineering calculations, such as the temperature distribution in the fuel plate or fuel rod given by Equation (1.1). However, only a limited number of special types of equations have been solved analytically, and their usefulness is limited

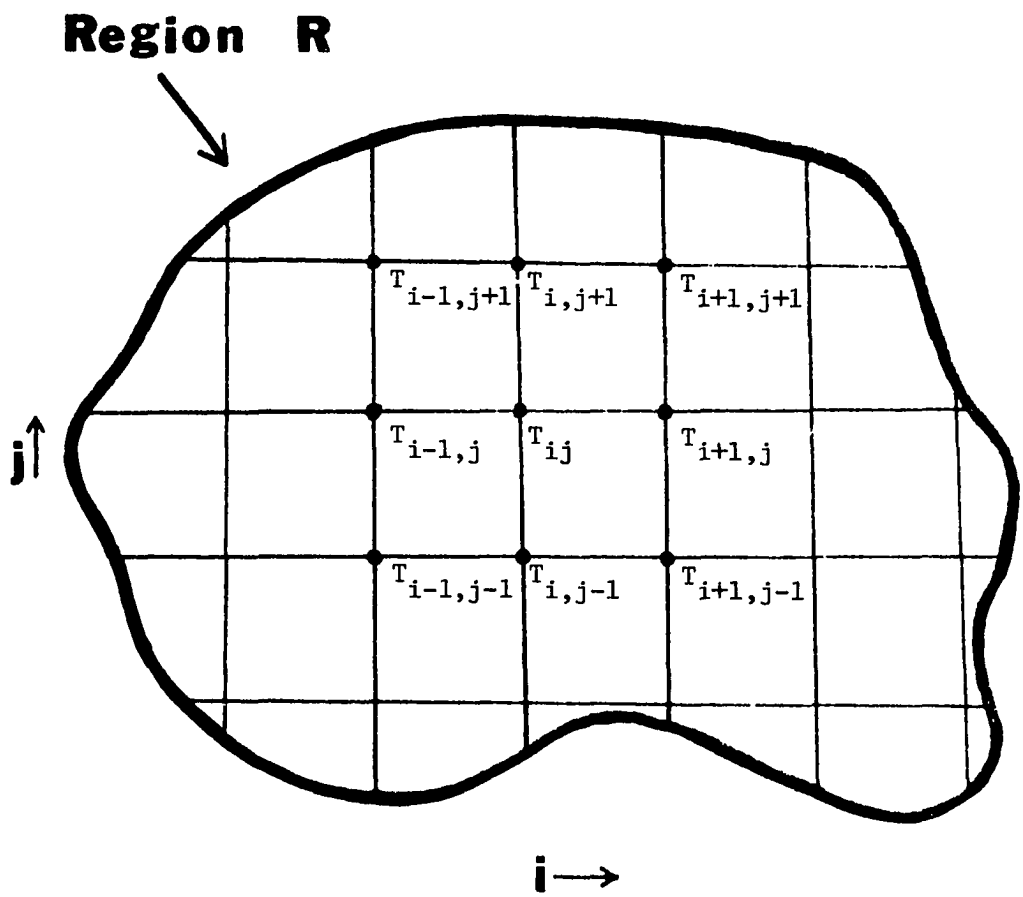

Figure 1.1. General region R with rectangular grid for finite difference application

to problems involving shapes for which the boundary conditions can be met. For such cases, it is necessary to satisfy appropriate boundary conditions on the boundary of a specified region and to match the continuity requirements within that region. However, many devised numerical methods have been developed to deal with such cases, especially for complex reactor configurations where there is almost a continuously varying distribution of material.

Of the numerical approximation methods available for solving differential equations, those employing finite differences are more frequently used than any other. In the finite difference approach, the technique is to superimpose a rectangular grid over the region in question (see Figure 1.1). The continuum model is replaced by a discrete model, i.e. the linear partial differential equation is replaced by an algebraic system of simultaneous linear difference equations [4]. In a typical practical problem, these may require a set of 1000, or more, simultaneous linear equations which must be solved using a large digital computer.

The differential equation for heat conduction throughout a stationary isotropic solid is given by [11]

$$\nabla \cdot K(\bar{r},T)\ \nabla T(\bar{r},t) + S(\bar{r},t) = \rho\ C_p\ \frac{\partial T}{\partial t} \qquad (1.1)$$

where $K(\bar{r},T)$ = thermal conductivity, ρ = density, C_p = specific heat, and $S(\bar{r},t)$ = internal heat source.

If the thermal conductivity is not a function of position or temperature, this simplifies to:

$$K \nabla^2 T(\bar{r},t) + S(\bar{r},t) = \rho C_p \frac{\partial T}{\partial t} \quad . \tag{1.2}$$

It is desirable to solve the above differential equations subject to the following types of standard boundary conditions [11, 12].

1.2.1 Boundary condition of the first kind

The temperature is specified along a boundary surface

$$T = f(\bar{r}_s,t) \quad . \tag{1.3}$$

1.2.2 Boundary condition of the second kind

The normal derivative of the temperature is specified along a boundary surface

$$\frac{\partial T}{\partial r} = f(\bar{r}_s,t) \tag{1.4}$$

where $\bar{r}_s$ is on a boundary surface, $\frac{\partial}{\partial r}$ represents differentiation along the outward normal to the surface.

1.2.3 Boundary condition of the third kind

A combination of the temperature and normal derivative is specified at a boundary.

$$K \frac{\partial T}{\partial r} + h_c T = f(\bar{r}_s,t) \tag{1.5}$$

where h_c is the convective heat transfer coefficient. This type of boundary condition is normally associated with forced convection and written as

$$K \frac{\partial T}{\partial r} = h_c(T_f - T) \tag{1.6}$$

where T_f is the temperature of the fluid in the channel of the fuel assembly. The linear partial differential equation (Eq. 1.1) is replaced by an algebraic system of simultaneous linear difference equations. There is one difference equation for each internal nodal point of the grid; this system can then, in turn, be solved by either direct or iterative techniques for the value of $T_{i,j}$ at each of the nodal points (i,j). As the grid spacing is reduced and therefore the number of nodal points increased, and if the technique converges, the numerical solution should approach the analytical solution of the partial differential equation over the region.

The finite difference equations can be obtained using a Taylor's expansion method. The most widely applied finite difference equation is the five-point equation, such as that developed in Appendix A [12, 13].

Accuracy of the finite difference technique can be improved by representing the partial differential equation by a higher order finite difference approximation developed to reduce the Taylor series truncation error.

In the present work, the nine-point finite difference equations for the heat equation for a fuel plate, considering equal and unequal spacing in the x-y Cartesian geometry, have been devised. This is accomplished by using a Taylor's series expansions about the four corner points as well as the five previously expanded points (Figure 1.1). The resulting equation is a nine-point finite difference equation. However, an important aspect to consider in the formulation of the nine-point technique is to insure higher order accuracy for the solution of the

finite difference equations.

A computer program was developed for this senario. It was designed to solve steady-state and transient heat conduction problems in two-dimensional Cartesian coordinates. The thermal conductivity, density, and specific heat may be both spatially and temperature-dependent. Heat generation rates may be dependent upon time, temperature and position. The boundary conditions, which may be surface-to-boundary or surface-to-surface, may be fixed temperatures or any combination of prescribed heat fluxes.

The point successive iterative technique and SOR methods [14, 4] were used to solve the finite difference equations which approximate the partial differential equations for a steady-state problem. The transient problem may be solved using any one of several finite difference schemes. These include an implicit technique which can range from Crank-Nicolson to the Classical Implicit procedure, an explicit method which is stable for a determined time step size [12, 4].

Thus, in this present computational study which was made on a nine-point approximation and a five-point approximation to the two-dimensional heat conduction equation, the techniques were applied to several sample problems using the successive explicit iterative techniques. The error and speed of convergence of the approximations were then compared.

The nine-point approximation used is an adaptation of a general nine-point formula for the Laplacian operator developed by Rohach [15]. The approximation was given for unequal spacing.

2. THEORETICAL DEVELOPMENTS

2.1 Derivation of Algorithm

A general nine-point relation for unequal spacing in two dimensions to the Laplacian Operator using the corner points is given by Rohach [15]. In this work the relation will be expanded to a nine-point numerical approximation of the two-dimensional heat conduction problems.

Consider the following relation (Figure 2.1):

$$(\frac{1}{\beta} - p)(T_{i+1,j} + T_{i-1,j}) + (\beta - p)(T_{i,j+1} + T_{i,j-1})$$

$$+ \frac{p}{2} T_c - 2(\frac{1}{\beta} + \beta - p)\, T_{i,j} \qquad (2.1)$$

where

$$\beta = \frac{\Delta x}{\Delta y}$$

p = a parameter

$$T_c = T_{i-1,j-1} + T_{i-1,j+1} + T_{i+1,j-1} + T_{i+1,j+1} \,. \qquad (2.2)$$

To relate the derivatives to the respective finite differences, use the Taylor series expansion. One can write

$$T(x_{r \pm 1}, y_s) = \exp\,(\pm \Delta x\, D_x)\, T_{r,s}$$

$$T(x_r, y_{s \pm 1}) = \exp\,(\pm \Delta y\, D_y)\, T_{r,s}$$

$$T(x_{r \pm 1}, y_{s \pm 1}) = \exp\,(\pm \Delta x\, D_x \pm \Delta y\, D_y)\, T_{r,s} \,, \qquad (2.3)$$

where

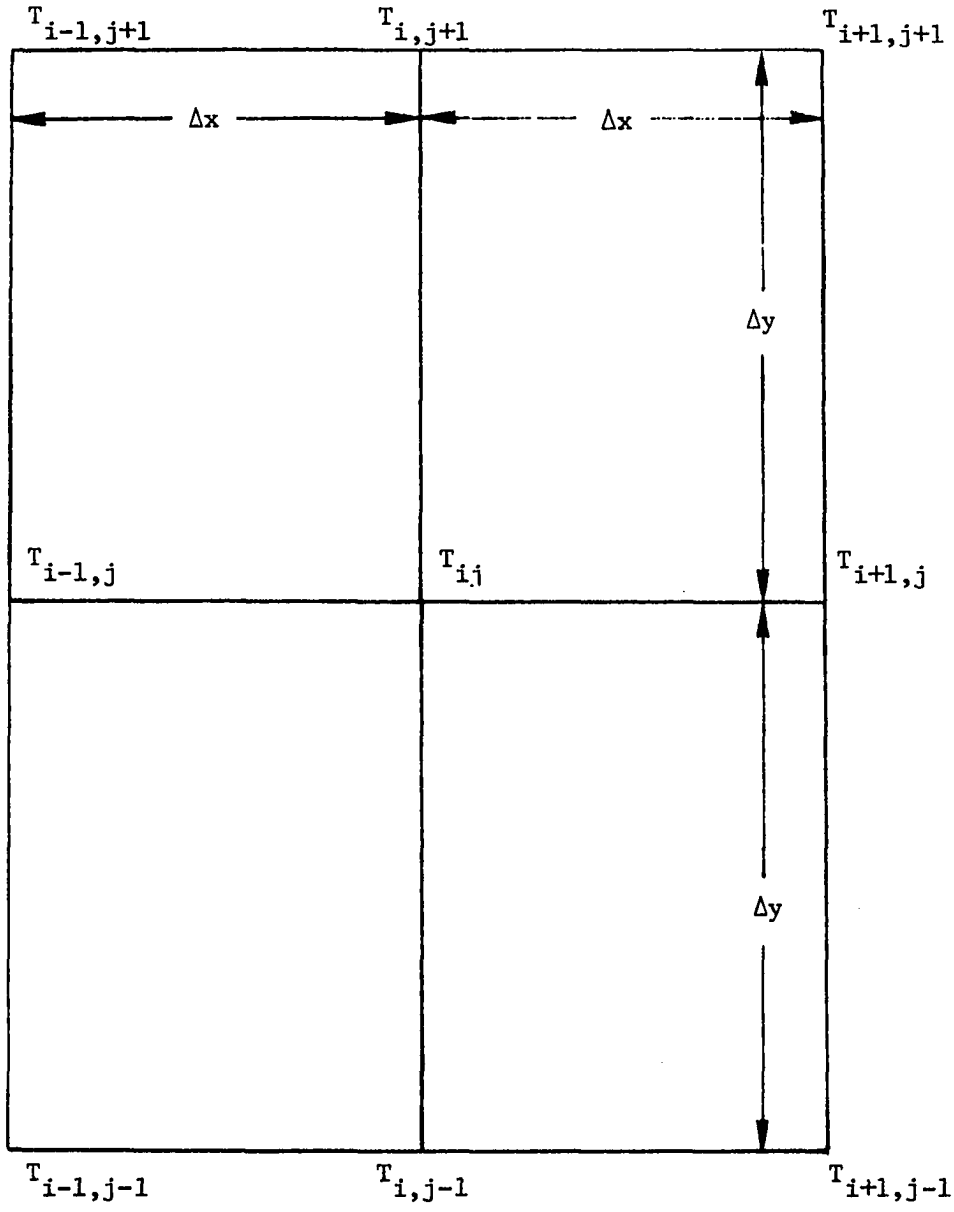

Figure 2.1. Grid used for finite difference equation development

$$D_x = \frac{\partial}{\partial x},\ D_y = \frac{\partial}{\partial y},\ D_{xy} = \frac{\partial^2}{\partial x \partial y},\ \text{etc.}$$

Δx, Δy are the spacings in the two directions. Expanding each of the four axial points about the center point results in

$$T_{i+1,j} = T_{ij} + \Delta x \frac{\partial T_{ij}}{\partial x} + \frac{(\Delta x)^2}{2!} \frac{\partial^2 T_{ij}}{\partial x^2} + \frac{(\Delta x)^3}{3!} \frac{\partial^3 T_{ij}}{\partial x^3} + \ldots$$

$$T_{i-1,j} = T_{ij} - \Delta x \frac{\partial T_{ij}}{\partial x} + \frac{(\Delta x)^2}{2!} \frac{\partial^2 T_{ij}}{\partial x^2} - \frac{(\Delta x)^3}{3!} \frac{\partial^3 T_{ij}}{\partial x^3} + \ldots$$

$$T_{i,j+1} = T_{ij} + \Delta y \frac{\partial T_{ij}}{\partial y} + \frac{(\Delta y)^2}{2!} \frac{\partial^2 T_{ij}}{\partial y^2} + \frac{(\Delta y)^3}{3!} \frac{\partial^3 T_{ij}}{\partial y^3} + \ldots$$

$$T_{i,j-1} = T_{ij} - \Delta y \frac{\partial T_{ij}}{\partial y} + \frac{(\Delta y)^2}{2!} \frac{\partial^2 T_{ij}}{\partial y^2} - \frac{(\Delta y)^3}{3!} \frac{\partial^3 T_{ij}}{\partial y^3} + \ldots$$

By adding the adjacent temperature of the i and j direction, one has

$$T_{i+1,j} + T_{i-1,j} = 2\left(1 + \frac{\delta^2}{2!} + \frac{\delta^4}{4!} + \frac{\delta^6}{6!} + \ldots\right) T_{ij} \tag{2.4}$$

$$T_{i,j+1} + T_{i,j-1} = 2\left(1 + \frac{\eta^2}{2!} + \frac{\eta^4}{4!} + \frac{\eta^6}{6!} + \ldots\right) T_{ij} \tag{2.5}$$

where

$$\delta = \Delta x \frac{\partial}{\partial x} \quad , \quad \eta = \Delta y \frac{\partial}{\partial y} \quad .$$

Expanding the corner point $T_{i+1,j+1}$ about the center point T_{ij}, one has

$$T_{i+1,j+1} = T_{i,j} + \left(\Delta x \frac{\partial T_{ij}}{\partial x} + \Delta y \frac{\partial T_{ij}}{\partial y}\right) + \frac{1}{2!}\left(\Delta x \frac{\partial T_{ij}}{\partial x} + \Delta y \frac{\partial T_{ij}}{\partial y}\right)^2$$

$$+ \frac{1}{3!}\left(\Delta x \frac{\partial T_{ij}}{\partial x} + \Delta y \frac{\partial T_{ij}}{\partial y}\right)^3 + \ldots$$

$$T_{i+1,j+1} = [1 + (\delta + \eta) + \frac{1}{2!}(\delta + \eta)^2 + \frac{1}{3!}(\delta + \eta)^3 + \ldots] T_{ij}$$

Similarly an expansion of the other corner points results in

$$T_{i-1,j+1} = [1 + (-\delta + \eta) + \frac{1}{2!}(-\delta + \eta)^2 + \frac{1}{3!}(-\delta + \eta)^3 + \ldots] T_{ij}$$

$$T_{i-1,j-1} = [1 - (\delta + \eta) + \frac{1}{2!}(\delta + \eta)^2 - \frac{1}{3!}(\delta + \eta)^3 + \ldots] T_{ij}$$

$$T_{i+1,j-1} = [1 + (\delta - \eta) + \frac{1}{2!}(\delta - \eta)^2 + \frac{1}{3!}(\delta - \eta)^3 + \ldots] T_{ij} .$$

By addition, Equation (2.2) becomes

$$T_c = 4[1 + \frac{1}{2!}(\delta^2 + \eta^2) + \frac{1}{4!}(\eta^4 + 6\eta^2\delta^2 + \delta^4) + \frac{1}{6!}(\eta^6 + 15\,\eta^4\delta^2 + 15\,\eta^2\delta^4 + \delta^6) + \ldots] T_{ij} . \qquad (2.6)$$

Substitution of Equations (2.4), (2.5) and (2.6) into Equation (2.1) results in

$$\begin{aligned}
&(\tfrac{1}{\beta} - p)(T_{i+1,j} + T_{i-1,j}) + (\beta - p)(T_{i,j+1} + T_{i,j-1}) \\
&\quad + \tfrac{p}{2} T_c - 2(\tfrac{1}{\beta} + \beta - p)\, T_{ij} = [\tfrac{1}{\beta}(\delta^2 + \beta^2\eta^2) \\
&\quad + \tfrac{1}{12\beta}(\delta^4 + 6\beta p\eta^2\delta^2 + \beta^2\eta^4) + \tfrac{1}{360\beta}(\delta^6 + 15\beta p\eta^4\delta^2 \\
&\quad + 15\beta p\eta^2\delta^4 + \beta^2\eta^6) + \ldots] T_{ij} \\
&\quad = (\Delta x)(\Delta y)\,[\nabla^2 + \tfrac{(\Delta y)^2}{12}(\beta^2 D_x^4 + 6\beta p\, D_{xy}^2 + D_y^4 \\
&\quad + \tfrac{(\Delta y)^4}{360}(\beta^4 D_x^6 + 15p(\beta\, D_{xyy}^2 + \beta^3\, D_{xxy}^2 + D_y^6 + \ldots] T_{ij} \qquad (2.7)
\end{aligned}$$

where again

$$D_x = \frac{\partial}{\partial x} \ , \ D_y = \frac{\partial}{\partial y} \ , \ D_{xy} = \frac{\partial^2}{\partial x \partial y} \ , \ \text{etc.}$$

Solving Equation (2.7) for $\nabla^2 T_{ij}$, one has a general nine-point approximation to the Laplacian operator.

$$\begin{aligned} \nabla^2 T_{ij} = \frac{1}{(\Delta x)(\Delta y)} \Big[&\left(\frac{1}{\beta} - p\right)(T_{i+1,j} + T_{i-1,j}) + (\beta - p)(T_{i,j+1} + T_{i,j-1}) \\ &+ \frac{p}{2} \left(T_{i+1,j+1} + T_{i-1,j+1} + T_{i+1,j-1} + T_{i-1,j-1}\right) \\ &- 2\left(\frac{1}{\beta} + \beta - p\right) T_{ij} \Big] - \frac{(\Delta y)^2}{12} \left(\beta^2 D_x^4 + 6\beta p \, D_{xy}^2 + D_y^4\right) \\ &+ O(h^4) \ . \end{aligned} \tag{2.8}$$

The truncation error for this relation is determined by the proper choice of the parameter, p. If p = 0, the relation results in the familiar five-point approximation (Equation 4.5). To get a truncation error of $O(h^4)$, it is necessary for

$$\left(\beta^2 D_x^4 + D_y^4 + 6\beta p \, D_{xy}^2\right) T_{ij} = 0 \ . \tag{2.9}$$

Using the operator identity

$$\left(\beta^2 D_x^2 + D_y^2\right) \nabla^2 = \beta^2 D_x^4 + D_y^4 + (\beta^2 + 1) \, D_{xy}^2 \tag{2.10}$$

and solving for p, one has

$$p = \frac{\beta + \frac{1}{\beta}}{6} - \frac{\left(\beta^2 D_x^2 + D_y^2\right) \nabla^2 T_{ij}}{6\beta D_{xy}^2 \, T_{ij}} \tag{2.11}$$

where $\nabla^2 T_{ij}$ is given by the general heat conduction equation as

$$\nabla^2 T_{ij} = \frac{\rho C_p}{K} \frac{\partial T_{ij}}{\partial t} - \frac{S}{K} \quad . \tag{2.12}$$

2.2 Steady-State Analysis of the Continuous Problem

The conventional steady-state heat conduction equation deduced from Equation (1.1)

$$- \nabla . K(\bar{r},T)\ \nabla T(\bar{r},t) = S(\bar{r},t) \tag{2.13}$$

is satisfied internal to the (x,y) domain of interest, where

∇ = the gradient,

K = the thermal conductivity,

T = temperature,

S = heat generation rate, and

$\bar{r}$ = spacial vector.

At an internal interface, temperatures and heat fluxes are required to be continuous:

$$T_+ = T_- \tag{2.14}$$

$$\left(K \frac{\partial T}{\partial r}\right)_+ = \left(K \frac{\partial T}{\partial r}\right)_- \tag{2.15}$$

where $\frac{\partial T}{\partial r}$ is the normal derivative at the interface, and + and - indicate limiting values on the two sides of the interface.

At a boundary, general boundary conditions, as given by Equations (1.3), (1.4), (1.5), and (1.6) can be written in the form

$$a\ K \frac{\partial T}{\partial r} + h_c T = h_c T_f \tag{2.16}$$

where the parameter a takes the value 0 or 1. Both the film coefficients, h_c, and the fluid or sink temperature, T_f, are assumed known and h_c is assumed to be non-negative. In addition, an initial temperature distribution $T(\bar{r},o)$ is assumed given.

In the steady-state case with constant thermal properties, and constant heat generation, Equation (2.13) becomes

$$- \nabla^2 T = \frac{S}{K} = \text{const} . \tag{2.17}$$

Therefore, the parameter p given by Equation (2.11) reduces to

$$p = \frac{\beta + \frac{1}{\beta}}{6} . \tag{2.18}$$

One can use the above value for p in Equation (2.8) and solve Equation (2.17) for the temperature at node (i,j). Therefore, after rearrangement, one has

$$\begin{aligned} T_{ij} \cong \frac{1}{10(\Delta x^2 + \Delta y^2)} \Big[& \frac{S}{K} (6\ \Delta x^2 . \Delta y^2) \\ & + (5\ \Delta y^2 - \Delta x^2)\ (T_{i+1,j} + T_{i-1,j}) \\ & + (5\ \Delta x^2 - \Delta y^2)\ (T_{i,j+1} + T_{i,j-1}) \\ & + \left(\frac{\Delta x^2 + \Delta y^2}{2}\right)\ (T_{i+1,j+1} + T_{i+1,j-1} + T_{i-1,j+1} \\ & + T_{i-1,j-1}) \Big] + O(h^4) \end{aligned} \tag{2.19}$$

which is the nine-point approximation for the temperature node (i,j). This relation will be compared to the five-point approximation given by Equation (A.7) in Appendix A.

3. COMPUTATIONAL RESULTS OF THE STEADY-STATE CASE

3.1 Numerical Technique

If there are I nodes in the problem and if the heat balance equations, Equations (2.19) and (A.7), are written for each node, then there will be I equations and I unknowns, and the resulting system of equations can be solved iteratively. Since the values of the temperatures on the right-hand side of Equations (2.19) and (A.7) are yet unknown, one cannot directly solve for the temperature at node (i,j). However, if an estimate of the temperature-distribution exists, then Equations (2.19) and (A.7) can be applied again at each node, and hopefully, one will have a better estimate for the temperature distribution. The procedure can be repeated using this better estimate. This procedure can be continued until the estimates have converged to the approximation of the temperature distribution. The iterative process can be written, in the steady-state case with constant thermal properties, and heat generation for the nine-point formula as

$$
\begin{aligned}
T_{i,j}^{(m+1)} = \frac{1}{10(\Delta x^2 + \Delta y^2)} \Big[& \frac{S}{K} (6\, \Delta x^2 \cdot \Delta y^2) \\
& + (5\Delta y^2 - \Delta x^2)(T_{i+1,j}^{(m)} + T_{i-1,j}^{(m)}) + (5\, \Delta x^2 - \Delta y^2) \\
& \cdot (T_{i,j+1} + T_{i,j-1}) + \left(\frac{\Delta x^2 + \Delta y^2}{2}\right)(T_{i+1,j+1}^{(m)} \\
& + T_{i+1,j-1}^{(m)} + T_{i-1,j+1}^{(m)} + T_{i-1,j-1}^{(m)}) \Big] \\
& + O(h^4)
\end{aligned}
\tag{3.1}
$$

where m = iteration step, and for the five point as

$$T_{ij}^{(m+1)} \cong \frac{1}{2(\frac{1}{\beta} + \beta)} [\frac{1}{\beta} (T_{i+1,j}^{(m)} + T_{i-1,j}^{(m)}) + \beta(T_{i,j+1}^{(m)} + T_{i,j-1}^{(m)}) + (\Delta x)(\Delta y) \frac{S}{K}] + O(h^2) \quad . \tag{3.2}$$

The program uses a convergence criterion based on the maximum absolute error between two successive iterations. This error must be less than a program input epsilon value.

$$\text{Max} \mid T_{ij}(\text{old}) - T_{ij}(\text{new}) \mid \leq \text{EBS} \tag{3.3}$$

3.2 Definitions of Error and Speed of Convergence

To compare the accuracy of the nine-point relation developed in this chapter with the five-point relation from Appendix A for the steady-state case, one needs an exact analytical solution as a reference case. The analytical solutions can be used to evaluate the absolute and relative error of the numerical solutions. If $T_{i,j}^{*}$ is the value of the analytical solution at a point (i,j), and $T_{i,j}$ is the value of the converged numerical solution at the same point, then the absolute error at point (i,j) is defined as

$$E_{A_{i,j}} = |T_{i,j} - T_{i,j}^{*}| \tag{3.4}$$

and the relative error at point (i,j) is defined as

$$E_{R_{i,j}} = \frac{E_{A_{i,j}}}{T_{i,j}^{*}} \quad . \tag{3.5}$$

To arrive at a single overall error value for the numerical solution, the Euclidean norm [16] for the absolute and relative error matrices can be calculated. The Euclidean error norm used in this study is defined as

$$E_{L_2} = [\Sigma_i \Sigma_j (E_{Ai,j})^2]^{1/2} . \tag{3.6}$$

When solving finite difference equations with an iterative technique, one requires that the iterated function should converge to the solution as rapidly as possible. Therefore, in a comparison of two different finite difference techniques one must have an accurate method for determining the speed of convergence of the techniques. The first inclination would be to use the number of iterations to convergence as a measure of speed of convergence. However, this does not always give accurate results.

A more accurate method involves the calculation of the convergence rate defined as [17]

$$\nu = - \text{Ln } \lambda \tag{3.7}$$

where ν = the convergence rate and

λ = the largest eigenvalue of the iteration matrix.

The eigenvalue λ can be calculated using the ratio of two successive L_2 residual norms, that is,

$$\lambda = \frac{||L_2^m||}{||L_2^{m+1}||} \tag{3.8}$$

The L_2 residual norms are defined as

$$L_2 = [\Sigma_i \Sigma_j (RE_{ij})^2]^{1/2} \tag{3.9}$$

where the residue RE_{ij} is defined as

$$RE_{ij} = T_{ij}^{(m+1)} - T_{ij}^{(m)} \tag{3.10}$$

and

T_{ij} = numerical solution at node (i,j)

m = iterate number (m = 0,1,2,3,...) .

In this study, the graphical method for the convergence is also used. When the logarithm of the MAX $|T_{ij}(\text{old}) - T_{ij}(\text{new})|$ is plotted against the number of iterates, a straight or nearly straight line with a negative slope α_o results. As α_o approached its optimum value, the slopes increase with a negative magnitude.

3.3 Steady-State Results With Constant Thermal Conductivity and Heat Generation

3.3.1 General mechanical problem

Consider, for purposes of illustration and of testing the numerical techniques, that the problem region is a slab 0.61 m by 0.61 m. The temperature at the boundaries of the slab will be kept at -17.8°C. The slab is subject to a uniform internal heat generation rate of 0.103 W/cm^3. The slab has a constant thermal conductivity of 34.6 W/m·c, and equally spaced increments of $\Delta x = \Delta y = 3.8$ cm. The computational results shown in Figures 3.1 to 3.4 are for absolute and

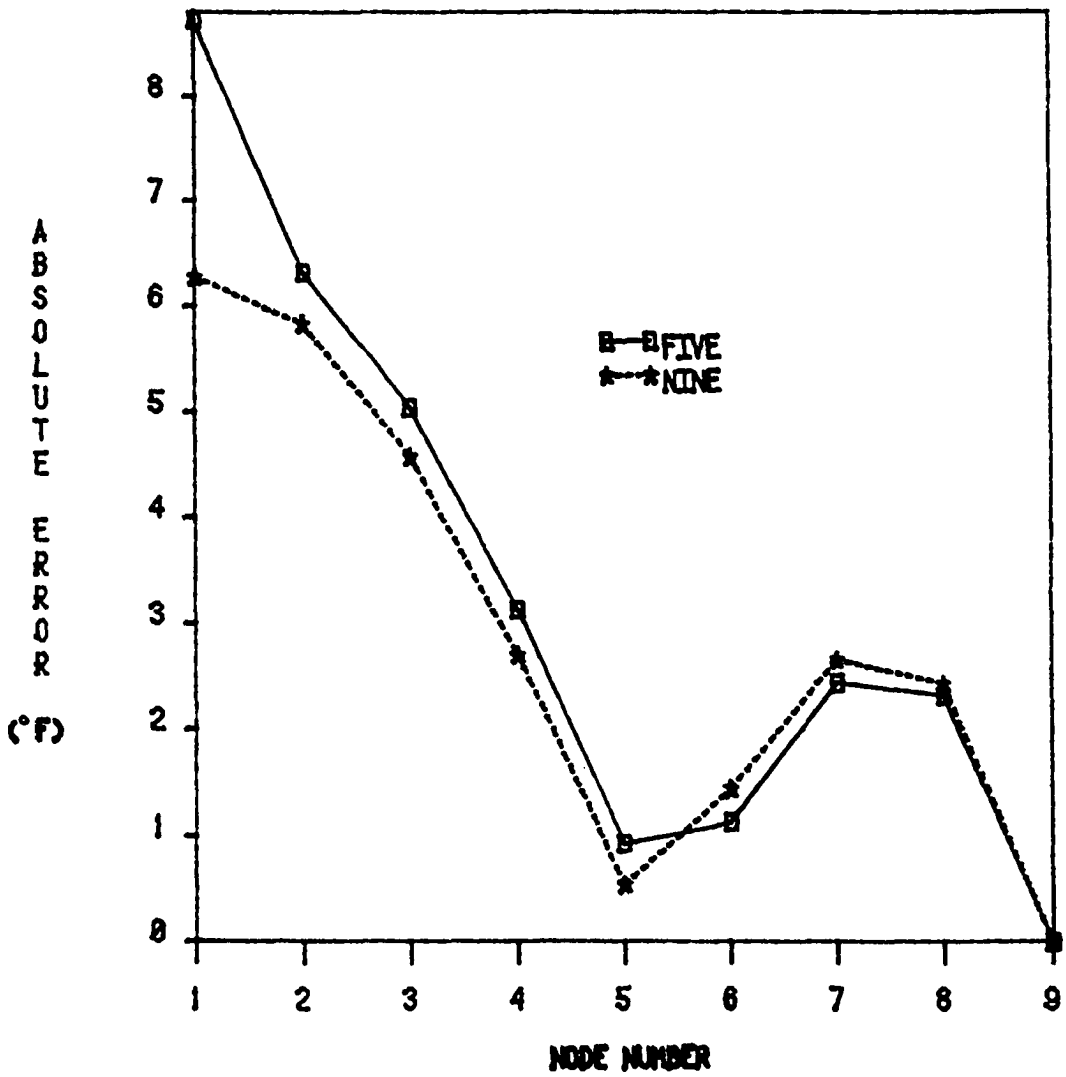

Figure 3.1. Absolute error comparison with the second-order Ritz profile along the x-axis for the centerline temperature (steady-state case, constant K and S)

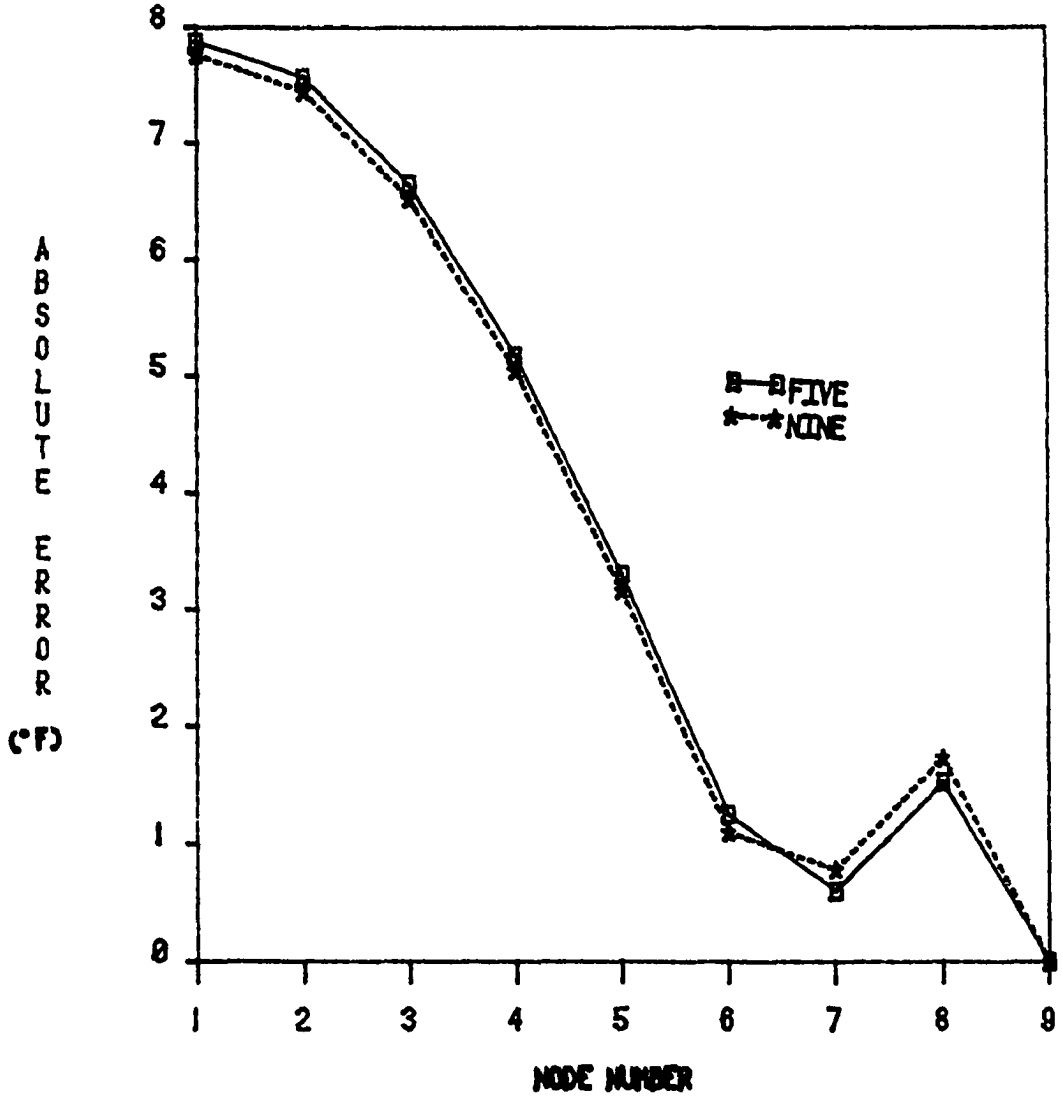

Figure 3.2. Absolute error comparison with second-order Ritz profile along the x-axis near the boundary (steady-state case with constant K and S)

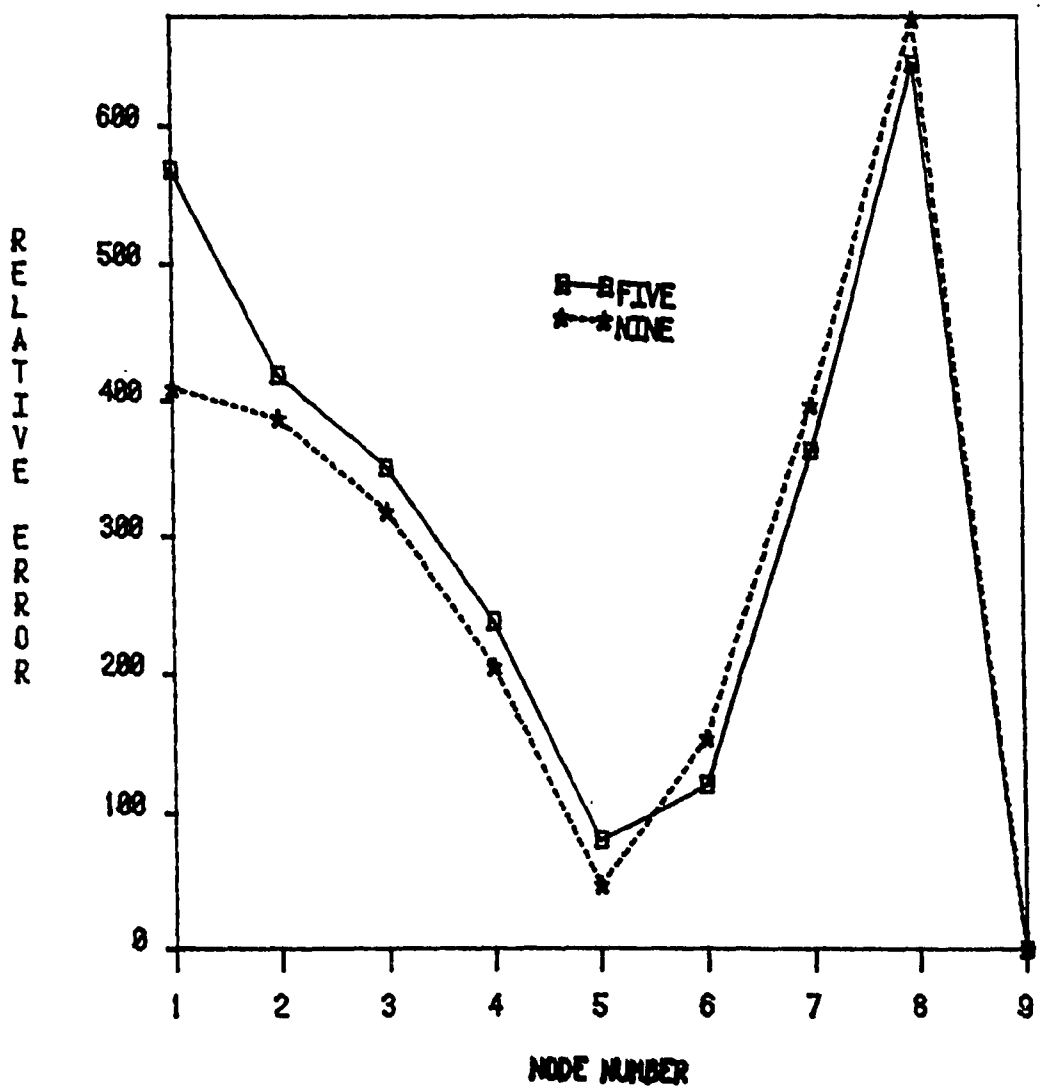

Figure 3.3. Relative error comparison with second-order Ritz profile for the centerline temperature (steady-state case with constant K and S)

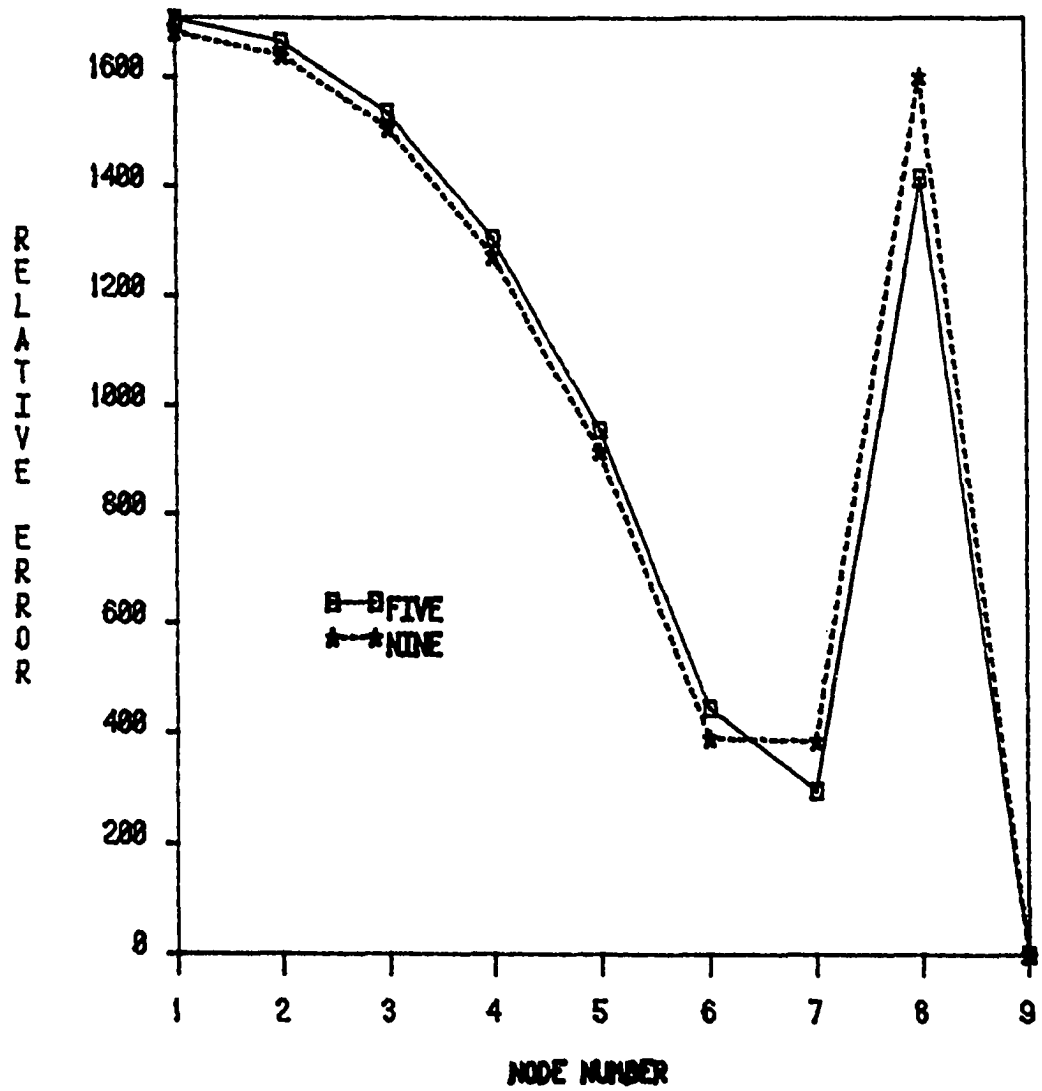

Figure 3.4. Relative error comparison with second-order Ritz profile near the boundary (steady-state case with constant K and S)

relative errors at different centerline and boundary nodes using the second-order Ritz profile. Figures 3.5 to 3.8 illustrate the results of the computations when the separation of variables method was used. The Ritz method and the separation of variables method will be used as the analytical reference cases. Figure 3.9 illustrates the cases that are used to calculate the speed of convergence for both the nine-point and five-point finite difference techniques.

It can be seen from the results that when the second-order Ritz profile is used as the reference case, the nine-point relation is more accurate than the five-point relation. Near the boundaries, the five-point relation appears to be more accurate than the nine-point relation; however, the second-order Ritz approximation is underestimating the results of the temperature distribution of these points.

The computational results using the exact analytical method of separation of variables shows that the nine-point relation is more accurate than the five-point relation for all nodes. Also, the convergence rate as given by the slopes of the curves in Figure 3.9 shows that the nine-point relation converges faster than the five-point relation.

The reason for introducing the Ritz profile method, which is an approximate analytical method, is that later in this study it will be used in some cases in a different form. In these cases, the exact analytical method of separation of variables is quite difficult to apply.

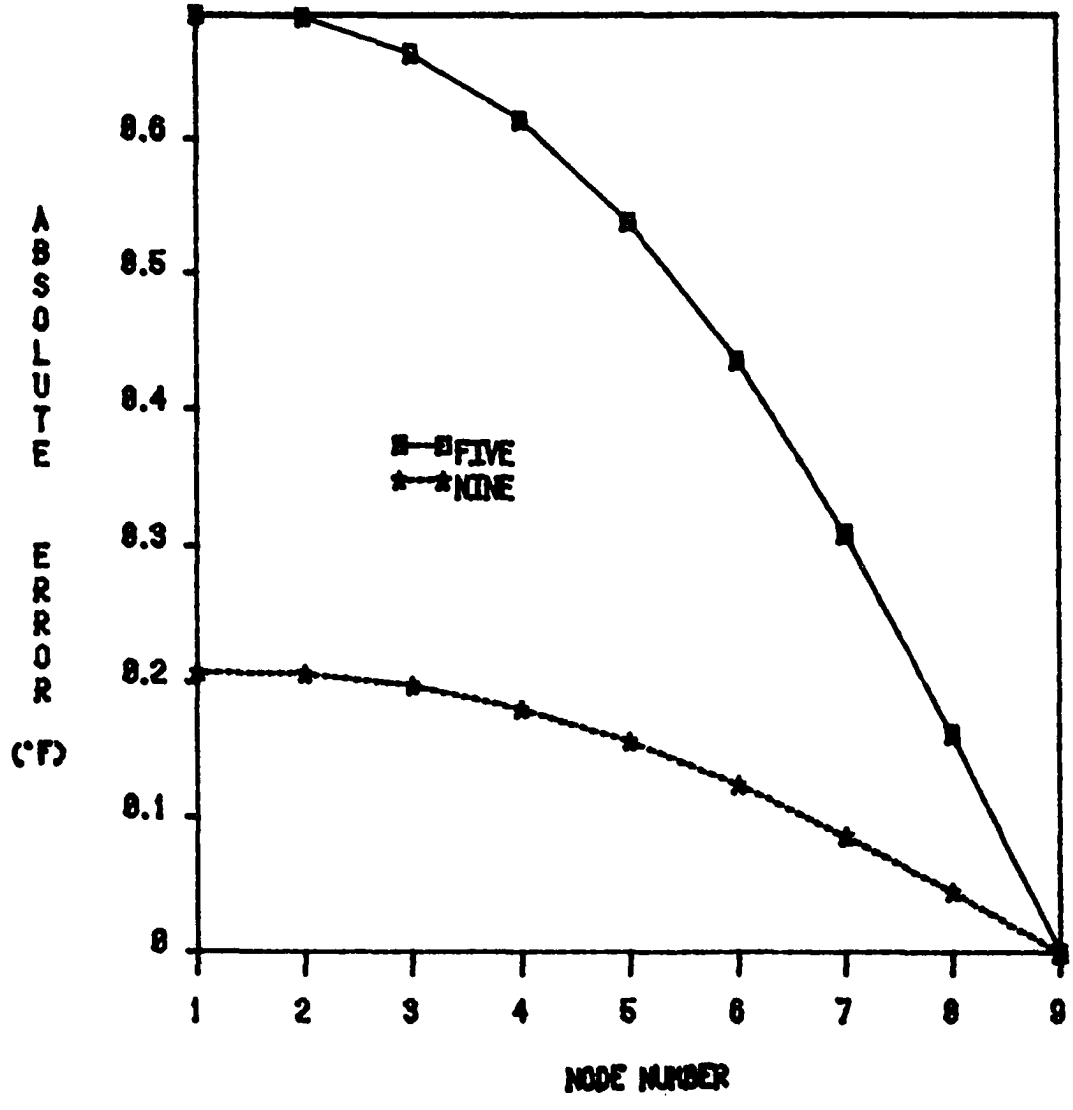

Figure 3.5. Absolute error comparison with separation of variables method for the centerline temperatures (steady-state with constant K and S)

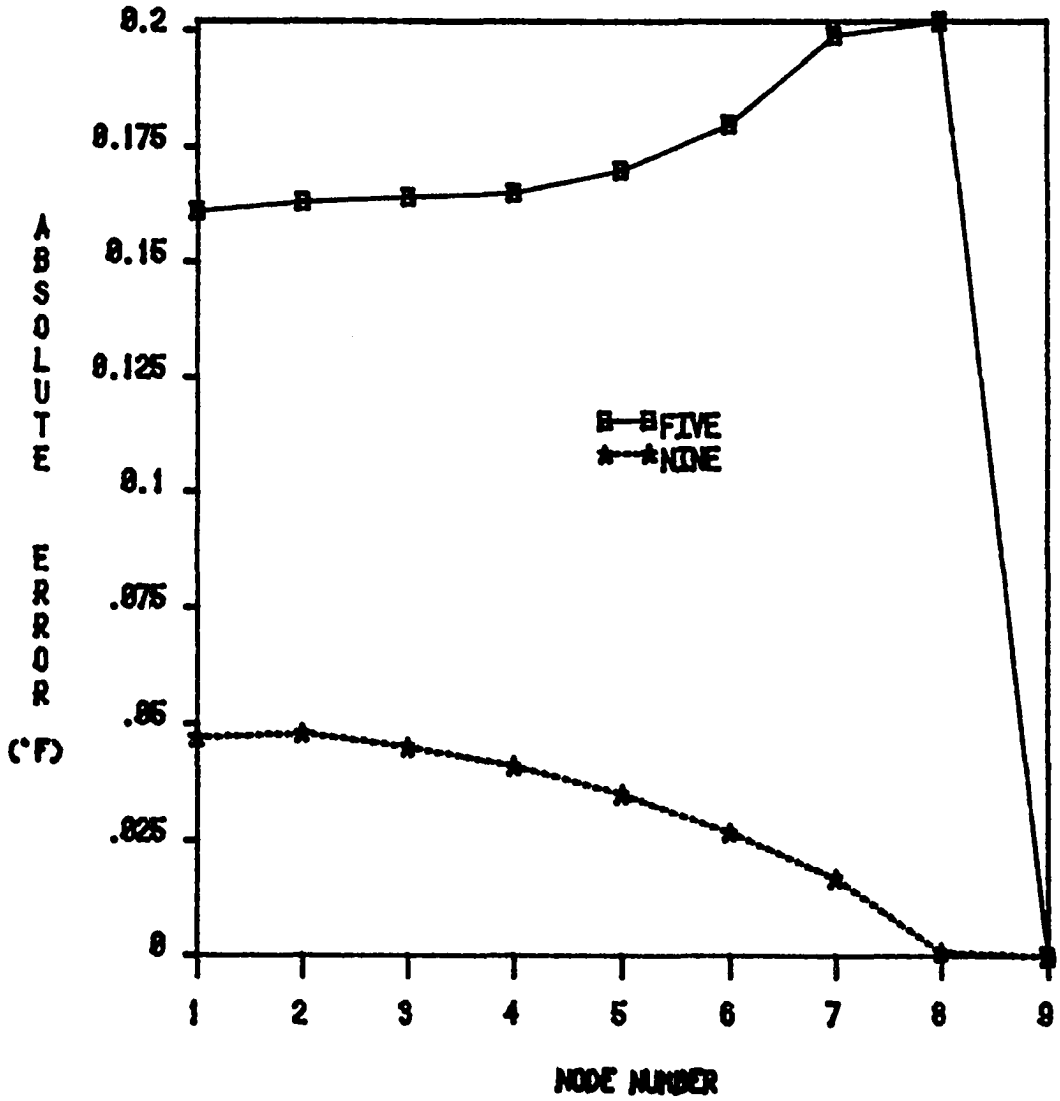

Figure 3.6. Absolute error comparison with separation of variables method near the boundary (steady-state case with constant K and S)

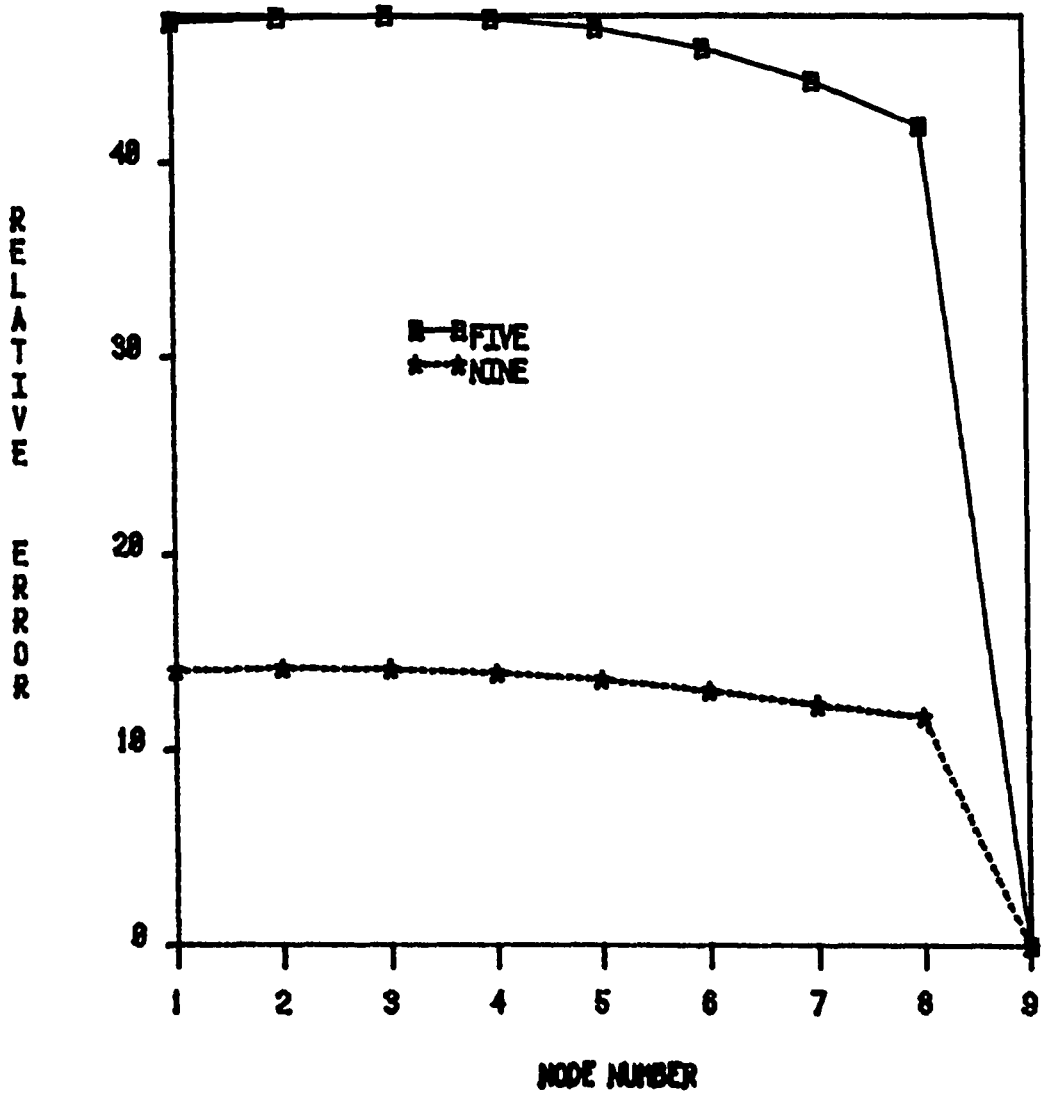

Figure 3.7. Relative error comparison with separation of variables method for the centerline temperature (steady-state case with constant K and S)

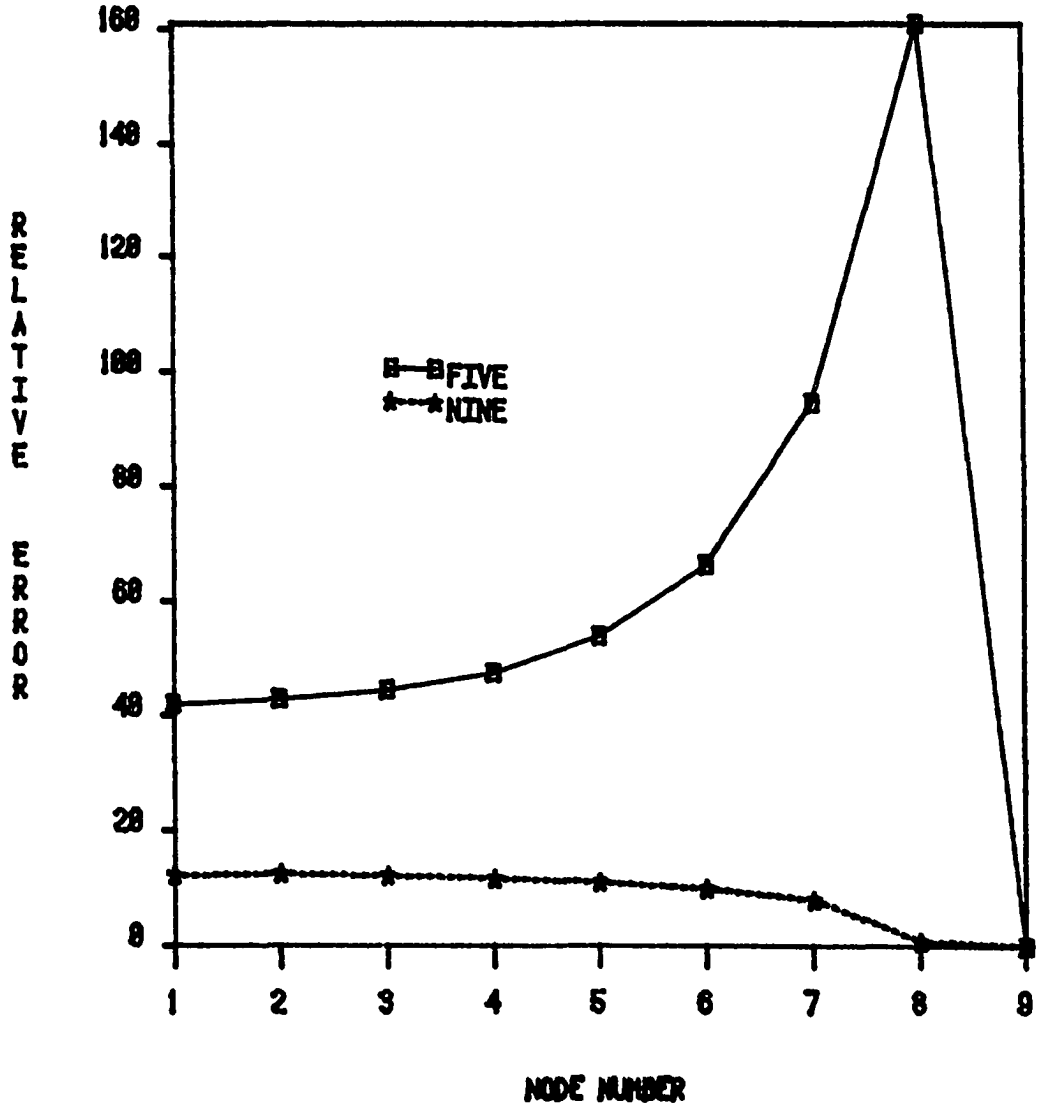

Figure 3.8. Relative error comparison with separation of variables method near the boundary (steady-state case with constant K and S)

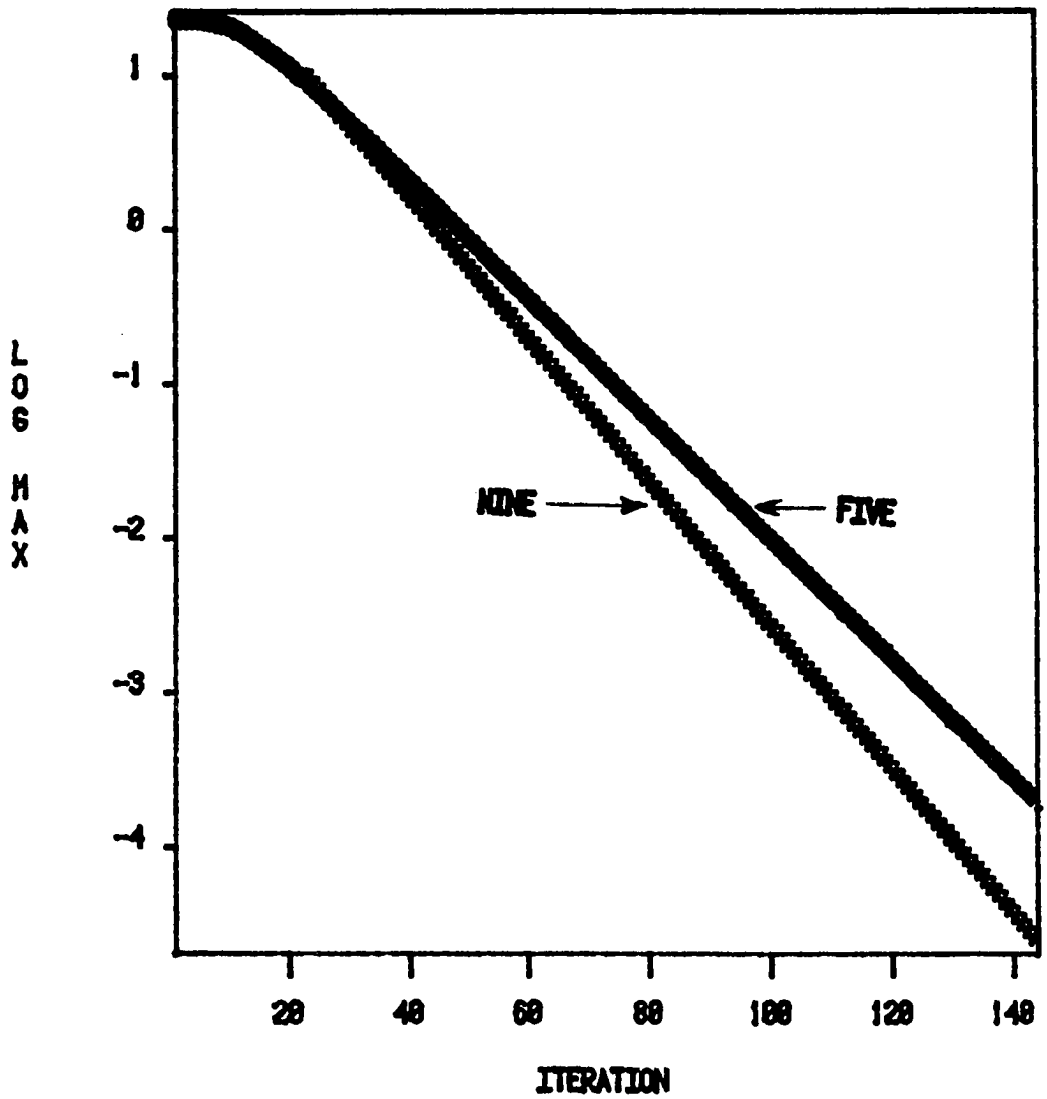

Figure 3.9. Residual norm for the nine- and five-point approximations (steady-state case with constant K and S)

3.3.2 Application to the nuclear fuel element

Consider the application of the method to a Westinghouse Pressurized Water Reactor (PWR) fuel element of outside diameter 0.94 cm (2 R_o) with a clad thickness of 0.0572 cm ($R_o - R_i$) and pellet-clad gap of 0.0082 cm. Because the model has been developed in Cartesian coordinates, the above fuel pin will be approximated by a square fuel element of cross-sectional area of 6.708×10^{-5} m^2 (see Figure 3.10).

A few assumptions that have been used in this work are:

1. There is no heat generation in the clad.
2. The fuel-clad gas gap is negligible.
3. The heat capacity and density of the fuel are constant.
4. The power generation in the fuel will be either a polynomial function of x and y or uniform.
5. The thermal conductivity in the fuel will be given either as a polynomial function of temperature or constant.
6. The axial conduction is negligible.

The following relation is used for the heat generation rate:

$$Q = A.B.L.S = 2(A + B)\ L.Q'' = L.Q' \qquad (3.11)$$

where A,B = dimensions in x and y direction of the fuel element,

L = element length,

S = volumetric power generated (w/cm^3),

Q'' = heat flux (w/cm^2), and

Q' = linear power density (w/cm).

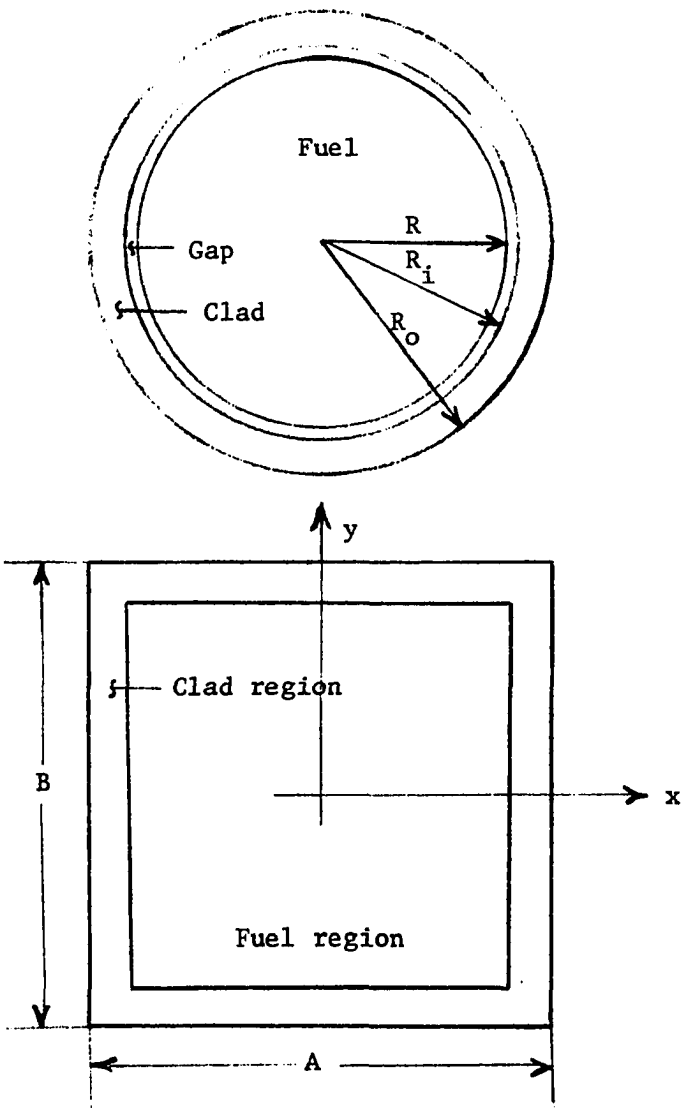

Figure 3.10. Approximation to the fuel pin cross-section

An average volumetric power of 6.351×10^8 w/cm^3 is based on a maximum linear power density of 42,600 w/m. The thermal properties of the fuel are evaluated for the specific case of constant thermal properties at the average fuel temperature, $\bar{T}_F$, given by the relation

$$\bar{T}_F = \frac{T_{F\ max} + T_{FS}}{2} \tag{3.12}$$

where $T_{F\ max}$ = maximum fuel temperature and

T_{FS} = fuel surface temperature given by

$$T_{FS} = T_{F\ max} - \frac{S(A/2)^2}{2K} \tag{3.13}$$

where K is the fuel thermal conductivity. Using these equations and Figure 3.11 [18], one can determine the thermal conductivity of the uranium dioxide at the average temperature. A value of 0.025 w/cm°C is used at a fuel surface temperature of 890°C. The computational results are shown in Figures 3.12 and 3.13 for the absolute and the relative L_2 norms as a function of the number of grids used. The reference case taken here is the five-point approximation solution given by using a region of 64 by 64 grids. The nine-point relation gives more accurate results than the five-point relation up to value of 5.3 of the logarithm of the number of grids (Figure 3.12). This is approximately a region in which a grid of 15 by 15 points is used. The behavior of the curves in Figure 3.12 is reversed after 5.3; this is because the reference case was taken as the five-point relation for the 64 by 64 grid region. The residual vector norm given by Equation (3.9) is plotted against the number of iterations to converge in Figure 3.14 for

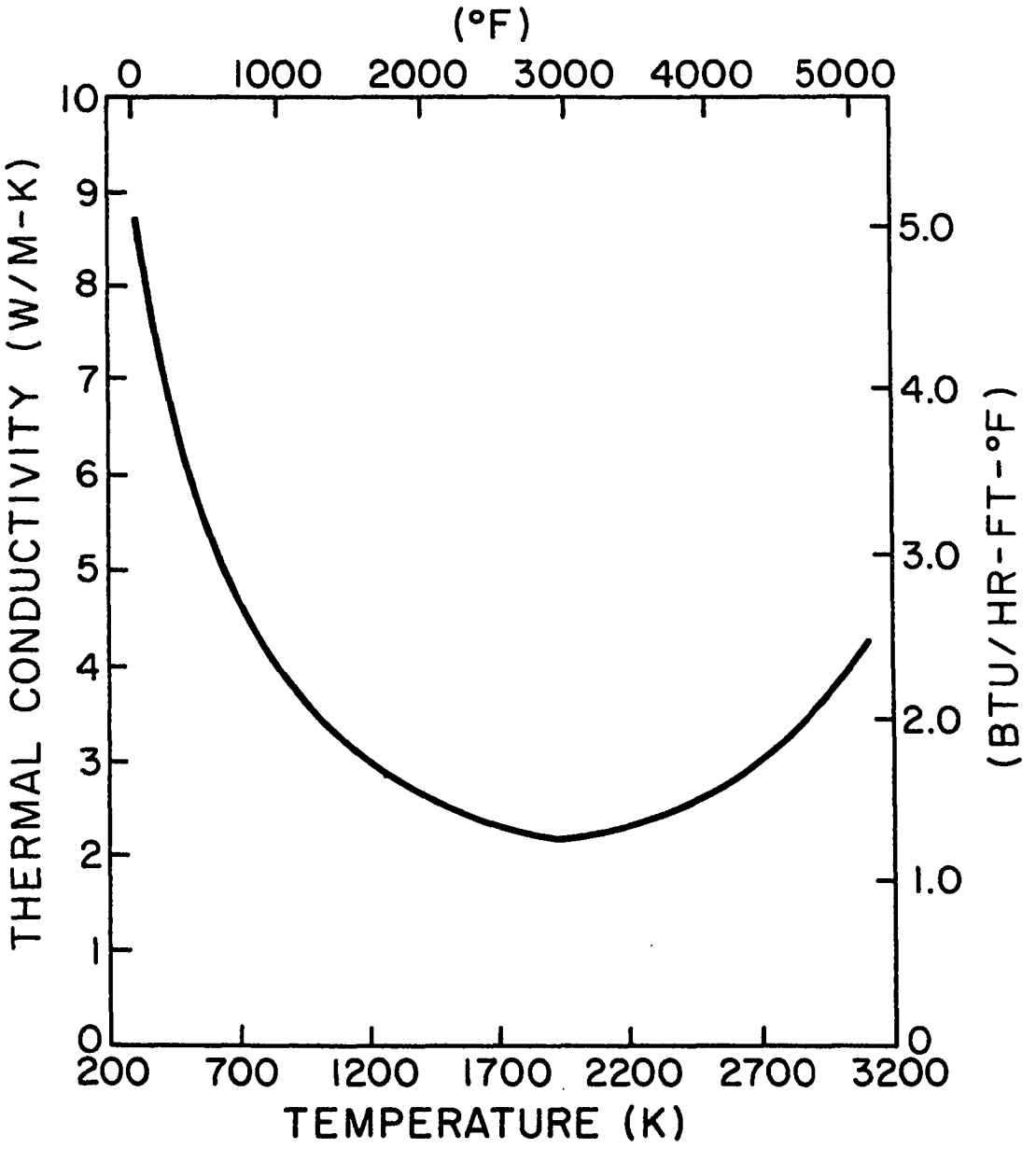

Figure 3.11. Uranium dioxide thermal conductivity as a function of temperature

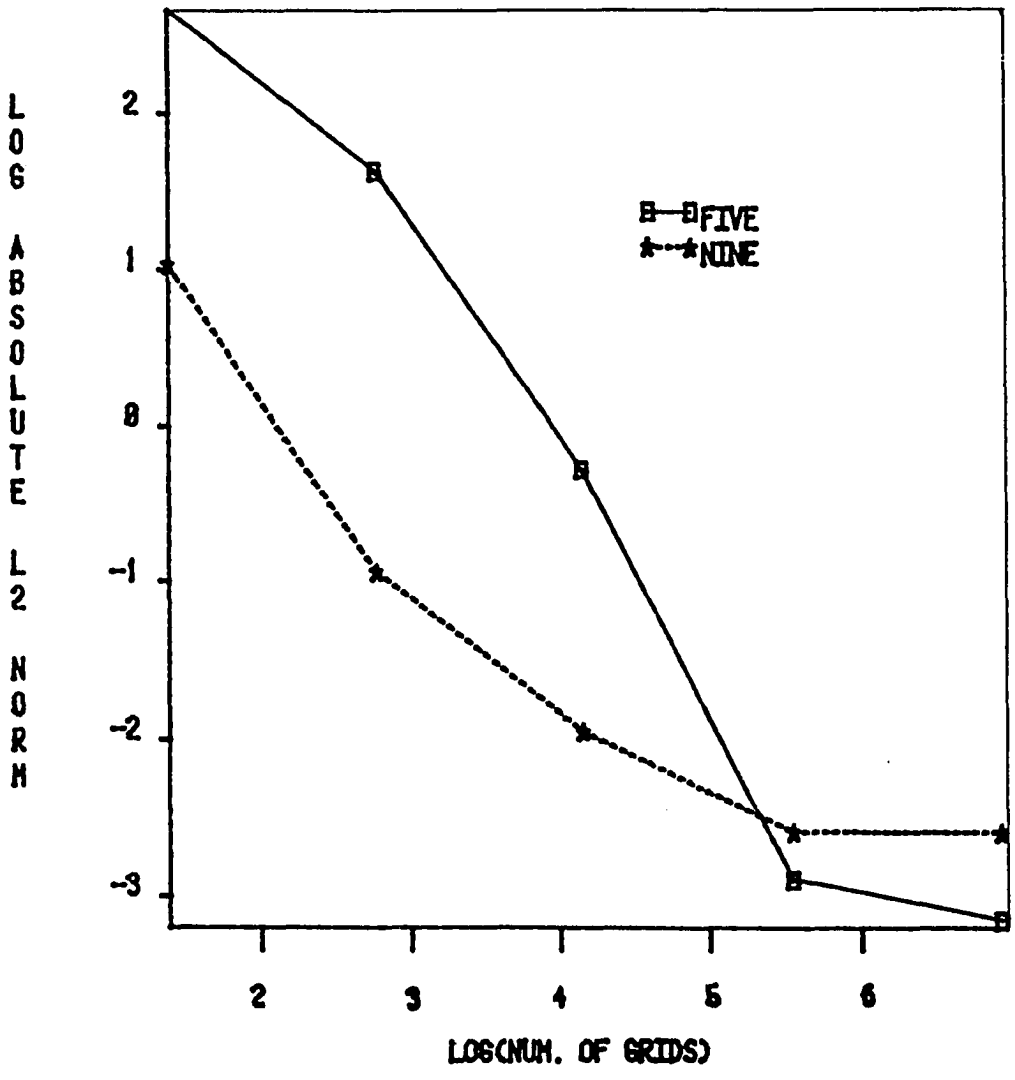

Figure 3.12. Log absolute L_2 norm versus Log (num. of grids) for the steady-state case, constant K and S for UO_2 fuel element

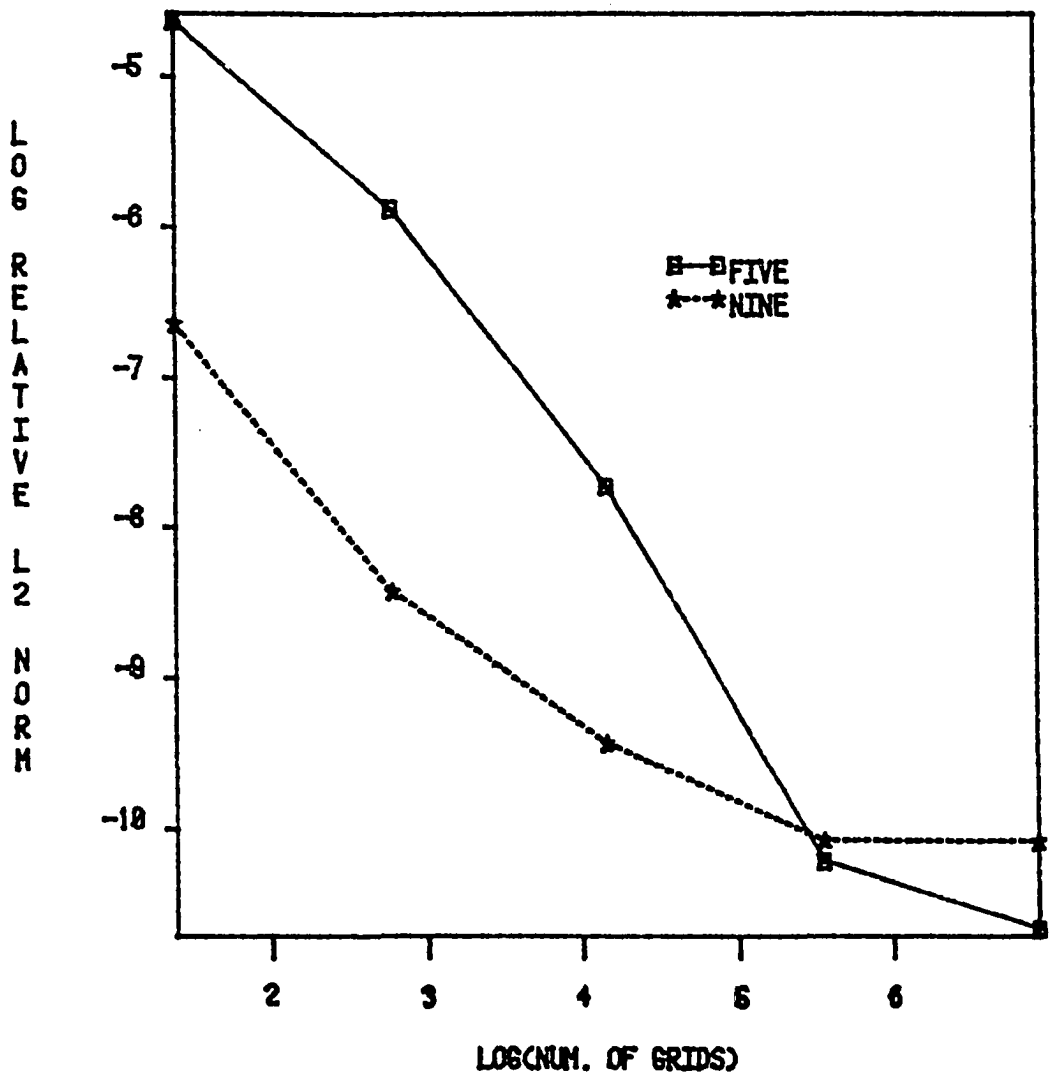

Figure 3.13. Log relative L_2 norm versus Log (num. of grids) for the steady-state case, constant K and S for UO_2 fuel element

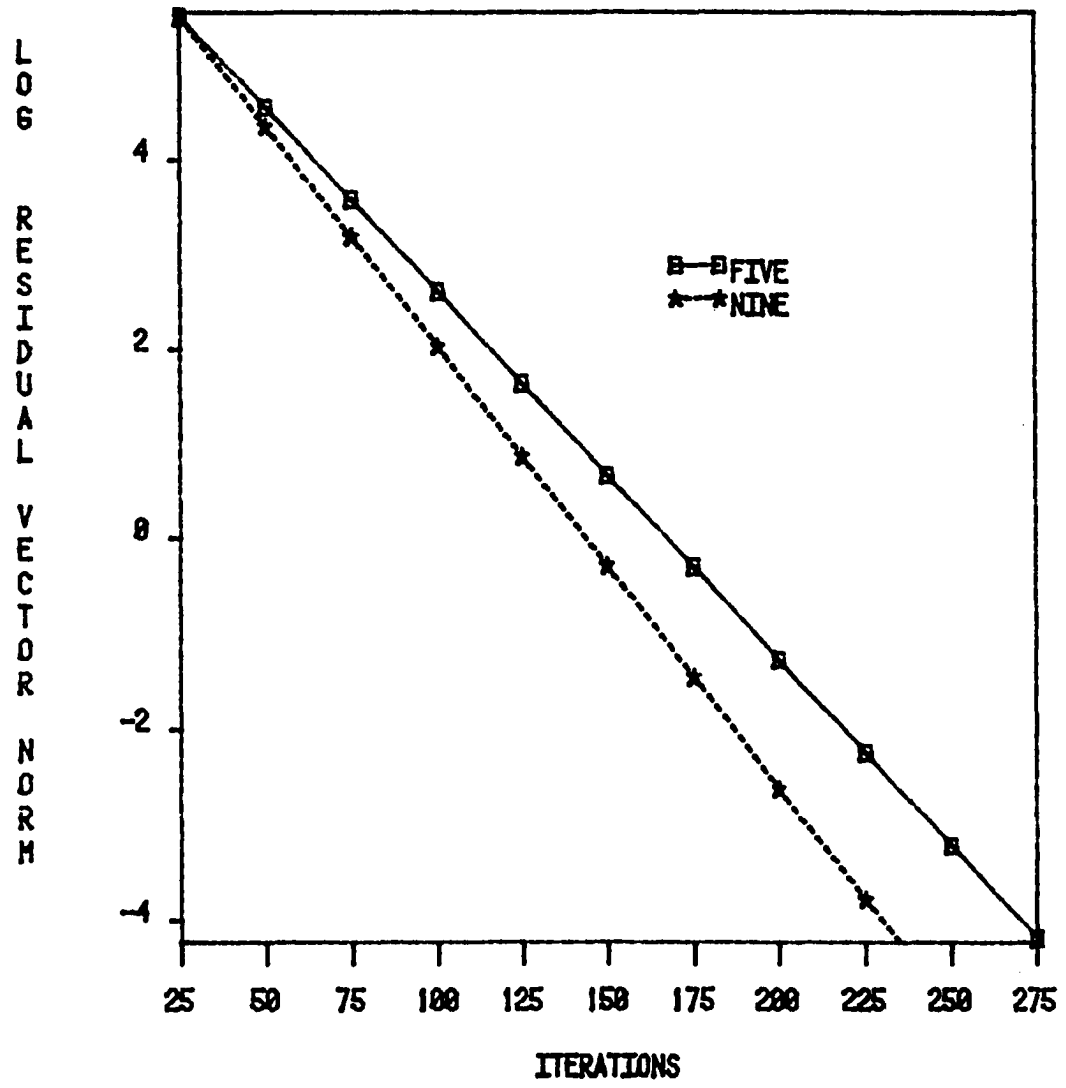

Figure 3.14. Log residual vector norm versus iterations for a 16 by 16 grid, for the steady-state case, constant K and S for UO_2 fuel element

a 16 by 16 grid for the five-point and nine-point relations. One can see that the nine-point relation has a steeper slope than the five-point relation, which means a faster convergence. The same computation was repeated for different values of the number of grids used (i.e. 2 by 2, 4 by 4, 8 by 8 and 32 by 32 grids).

One way of calculating the convergence rate as given by Equation (3.7) is to plot the slopes of the curves in Figure 3.14 as functions of the number of grids used. This will give results which are independent of the convergence criteria (EBS). The results of those calculations are shown in Figure 3.15. One can see that the nine-point formula has a higher convergence rate than the five-point formula over all ranges.

3.4 Steady-State Results With Variable Internal Heat Generation

3.4.1 Application to the nuclear fuel element

In this problem, the heat generation will be given as a function of space and taken in case of the nuclear fuel element described in Section 3.3.2 as a second-order polynomial [19] as follows:

$$S = \frac{Q'}{A.B}\,(2 - F)\,\left[1 + \frac{F - 1}{1 - \frac{F}{2}} \cdot \left\{\left(\frac{2x}{A}\right)^2 + \left(\frac{2y}{B}\right)^2\right\}\right] \qquad (3.14)$$

where Q' = linear power density (w/m),

F = peak to average fuel element power, and

A,B = fuel element dimension (m).

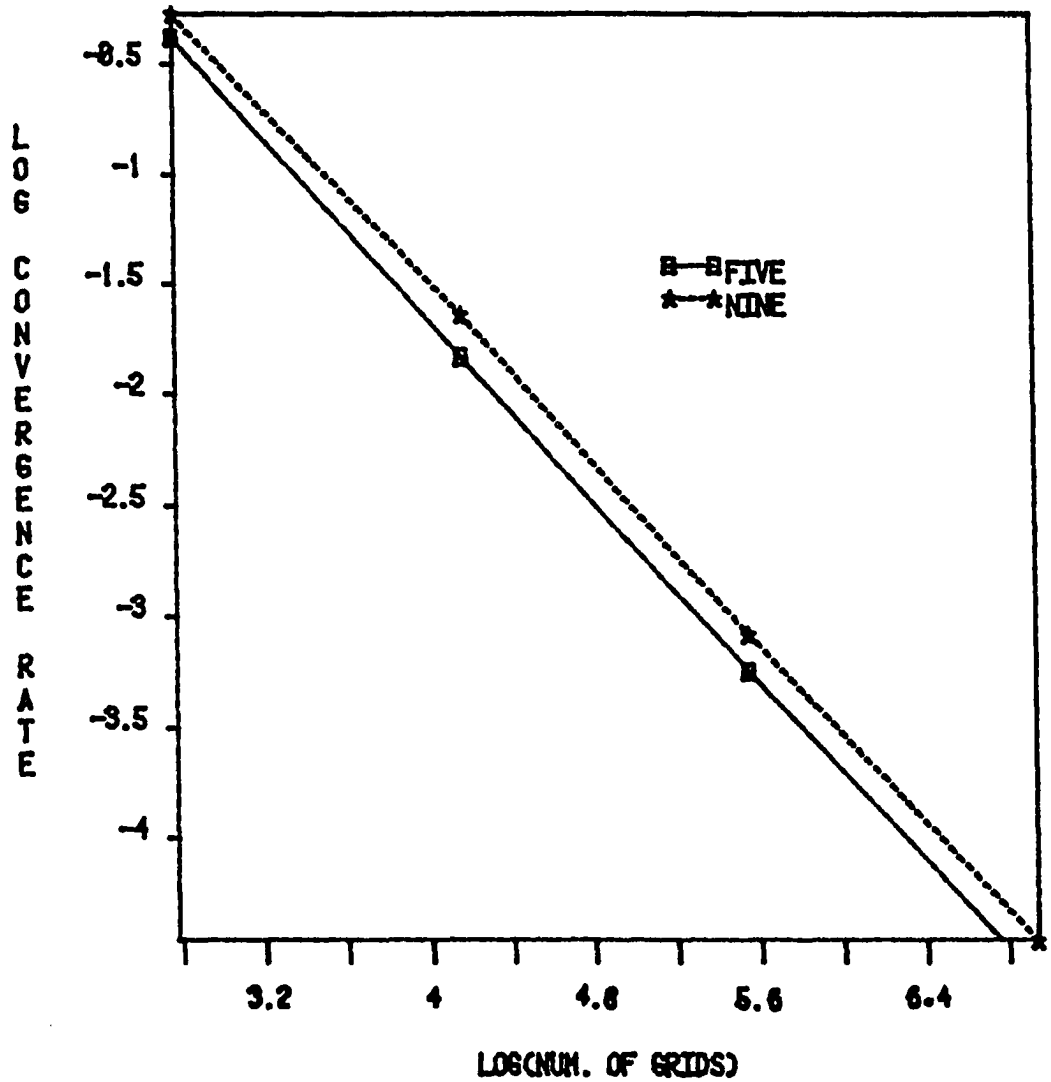

Figure 3.15. Log convergence rate versus Log (num. of grids) for the steady-state case, constant K and S for UO_2 fuel element

Only the fuel region is considered, and uniform boundary temperatures of 890°C are used. The algorithm given for the nodal temperature, T_{ij}, using the nine-point relation in this case, is no longer given by Equation (3.1). One can find the following expression for the nodal temperature

$$T_{ij} = \frac{1}{2(\beta + \frac{1}{\beta} - p)} \left[\frac{\Delta x.\Delta y.S}{K} + (\frac{1}{\beta} - p)\cdot(T_{i+1,j} + T_{i-1,j}) \right.$$

$$\left. + (\beta - p)\cdot(T_{i,j+1} + T_{i,j-1}) + \frac{p}{2} \cdot T_c\right] \qquad (3.15)$$

where the parameter p is given by

$$p = \frac{\beta + \frac{1}{\beta}}{6} + \frac{(\beta^2 D_x^2 + D_y^2) \cdot [AA]}{6\beta D_{xy}^2 T_{ij}} \qquad (3.16)$$

$$AA = \frac{Q'\cdot(2 - F)}{K.A.B.} \cdot \left[1 + \frac{(F - 1)}{(1 - \frac{F}{2})} \cdot \{(\frac{2x}{A})^2 + (\frac{2x}{B})^2\}\right] . \qquad (3.17)$$

Since D_{xy}^2 cannot be determined, a numerical approximation

$$D_{xy}^2 T_{ij} \cong \frac{1}{\Delta x^2 \Delta y^2} \cdot (T_c - 2T_A + 4\, T_{ij}) + 0(h^2) \qquad (3.18)$$

is used.

$$T_c = T_{i+1,j+1} + T_{i+1,j-1} + T_{i-1,j+1} + T_{i-1,j-1} \qquad (2.2)$$

and

$$T_A = T_{i+1,j} + T_{i-1,j} + T_{i,j+1} + T_{i,j-1} \qquad (3.19)$$

After some algebraic manipulations, parameter p becomes

$$p = \frac{\beta + \frac{1}{\beta}}{6} + \left[\frac{8Q'(2 - F)}{A.B.K.} \cdot \frac{F - 1}{1 - \frac{F}{2}} \cdot \left(\frac{\beta^2}{A^2} + \frac{1}{B^2}\right)\right] :$$

$$\frac{6\beta}{\Delta x^2 \Delta y^2} \cdot (T_c - 2T_A + 4\ T_{ij}) \ . \tag{3.20}$$

One can note a finite difference approximation of order $0(h^2)$ is used in Equation (3.18) since the error term will go into $0(h^4)$ in Equation (3.15). Therefore, p is now a sum of two terms:

$$p_1 = \frac{\beta + \frac{1}{\beta}}{6} \tag{3.21}$$

and

$$p_2 = \left[\frac{8Q'(2 - F) \cdot (F - 1)}{A.B.K.\ (1 - \frac{F}{2})} \left(\frac{\beta^2}{A^2} + \frac{1}{B^2}\right)\right] :$$

$$\frac{6\beta}{\Delta x^2 \Delta y^2} (T_c - 2T_A + 4\ T_{ij}) \ . \tag{3.22}$$

The computational results of the temperature distribution, the relative L_2 norm, the residual vector norm, and the convergence rate for the UO_2 fuel plate described in Section 3.3.2 are based on a maximum linear power density, Q'_{max}, of 426 w/cm and a peak to average power, F, of 1.23. The other data are the same as those in Section 3.3.2. Figure 3.16 shows the results of the relative L_2 norm as a function of the number of grids used for the five-point approximation. Figure 3.16 also shows both graphs of the nine-point approximation,

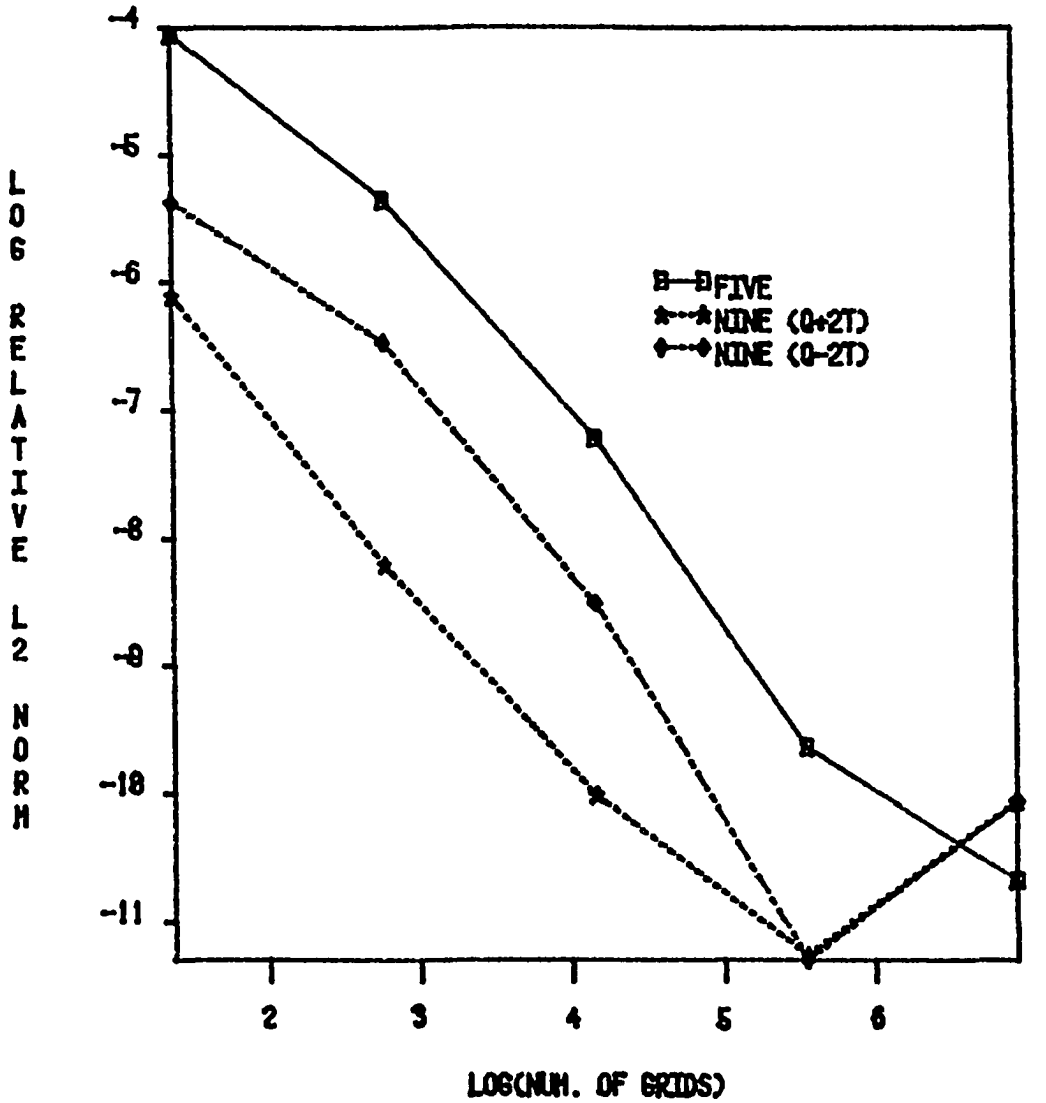

Figure 3.16. Log relative L_2 norm versus Log (num. of grids used) for the steady-state case with variable heat generation for UO_2 fuel element

one using the sum of Equations (3.21) and (3.22) for the parameter p (the graph indicated by stars (Q + 2T)); the other being the graph where p is given only by Equation (3.21) as indicated by diamond (Q - 2T).

It can be observed that the nine-point approximation in both cases discussed above is more accurate than the five-point approximation. Between the two cases of the nine-point approximation, the one using both terms (Equations (3.21) and (3.22)) for the parameter p is more accurate than the one with p being given only by Equation (3.21). This shows the importance of the second term of p given by Equation (3.22) which depends upon the solution itself. Due to the five-point approximation with the 64 by 64 grid region (small spacing) being considered as reference case, the accuracy holds up to 6.7 for the LOG (number of grids).

Figure 3.17 shows the residual vector norm versus the number of iterations for the UO_2 fuel element in a 16 by 16 grid problem. It can be inferred from this result, that by adding the second term of the parameter p, Equation (3.22), one may get a nonconverging problem or in some cases (i.e. 4 by 4 or 8 by 8 grids), oscillating solutions. One way of getting out of this problem is by damping the oscillations, but without losing the accuracy of the problem. There are different forms of damping functions that can be used. In the case of Figure 3.17, one can use the following form [20],

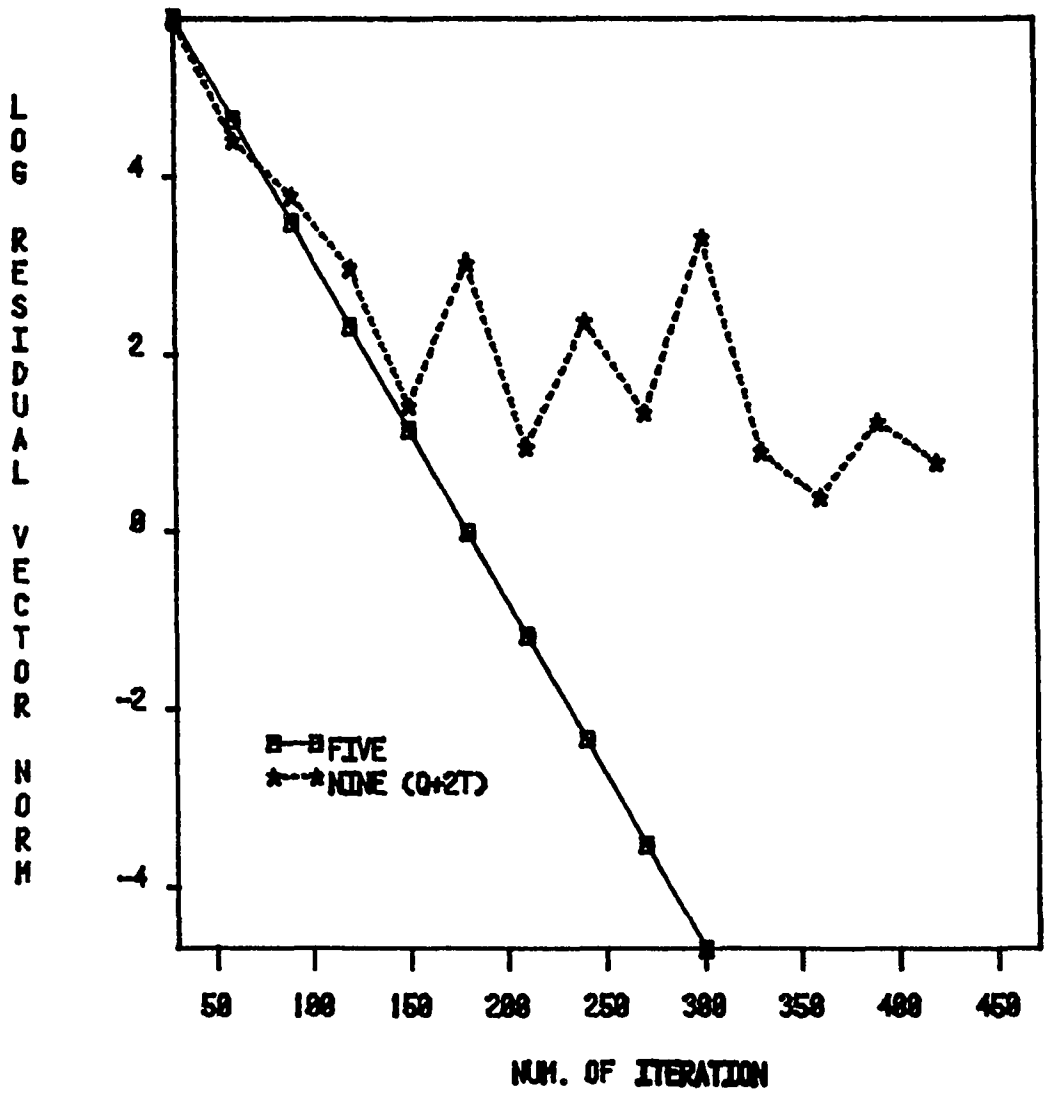

Figure 3.17. Log residual vector norm versus num. of iterations for 16 by 16 grid and steady state case with variable heat generation for UO_2 fuel element

$$DF = \frac{2 \cdot (p_2^{(n)})^2}{p_2^{(n)} + p_2^{(n+1)}} \tag{3.23}$$

where DF = damping function,

n = iteration number, and

p_2 = given by Equation (3.22).

One can note from Equation (3.23) as the solution converges, DF goes to p_2, since $p_2^{(n)}$ is the same as $p_2^{(n+1)}$.

Using Equation (3.23) to damp the oscillations, one obtains a converged solution as can be seen in Figure 3.18. Figure 3.19 shows the computational results when Equation (3.21) was used for the parameter p which is just the first term of p. This converges without using any damping function. Using the same procedure for the 2 by 2, 4 by 4 and 8 by 8 cases and calculating the slopes of the respective curves, one can get the convergence rates as shown in Figure 3.20. It can also be seen that the nine-point approximation in both cases converges faster than the five-point approximation; therefore, the nine-point approximation with the second term of p included (Equation 3.22) has the highest convergence rate.

3.4.2 Assumed analytical solution problem

More to the point to verify the correctness for the development of the parameter p analytical and numerical values of the parameter p given by Equation (2.11), one can assume an analytical solution for the temperature distribution given by

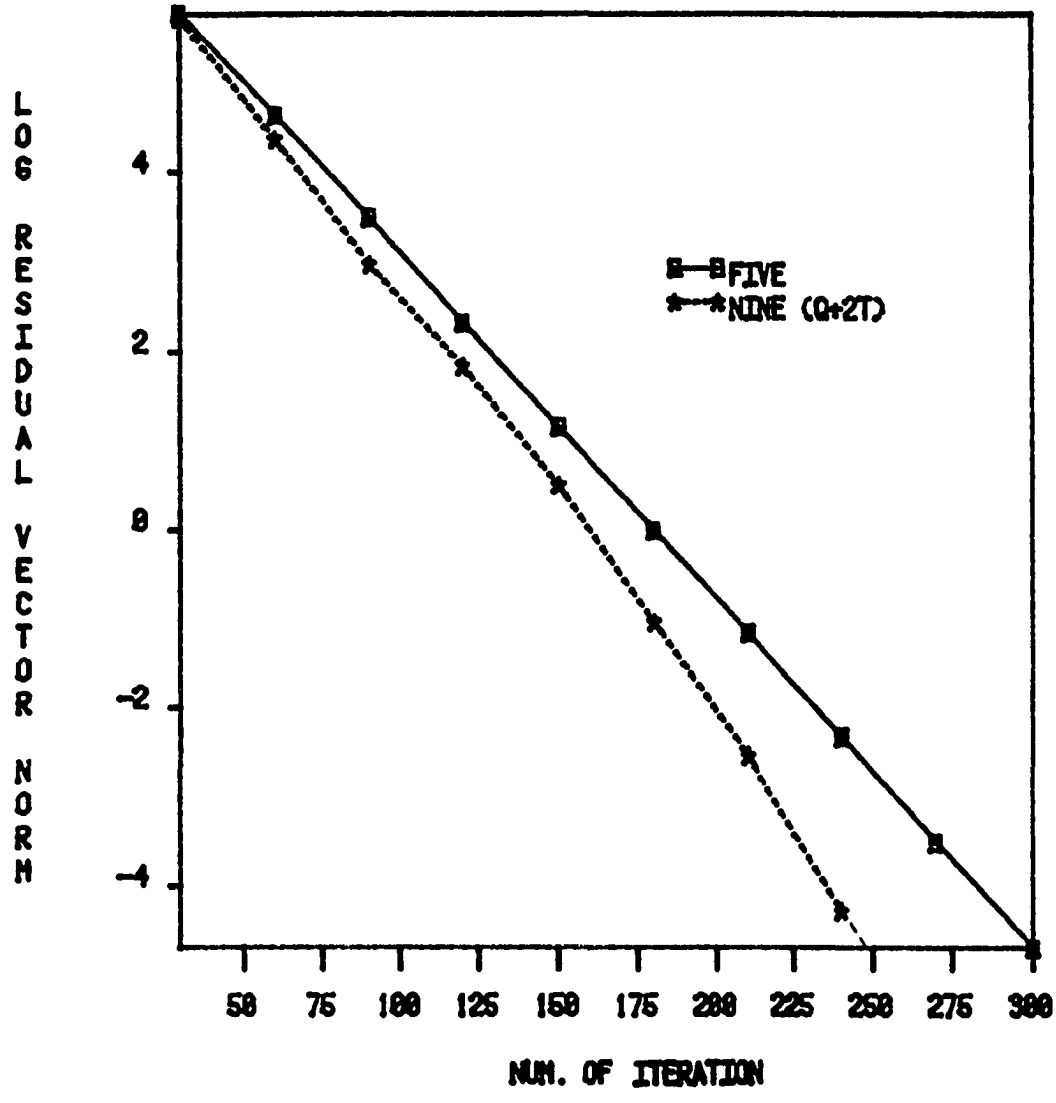

Figure 3.18. Log residual vector norm versus num. of iterations after damping oscillations for 16 by 16 grids and steady-state case with variable heat generation for UO_2 fuel element

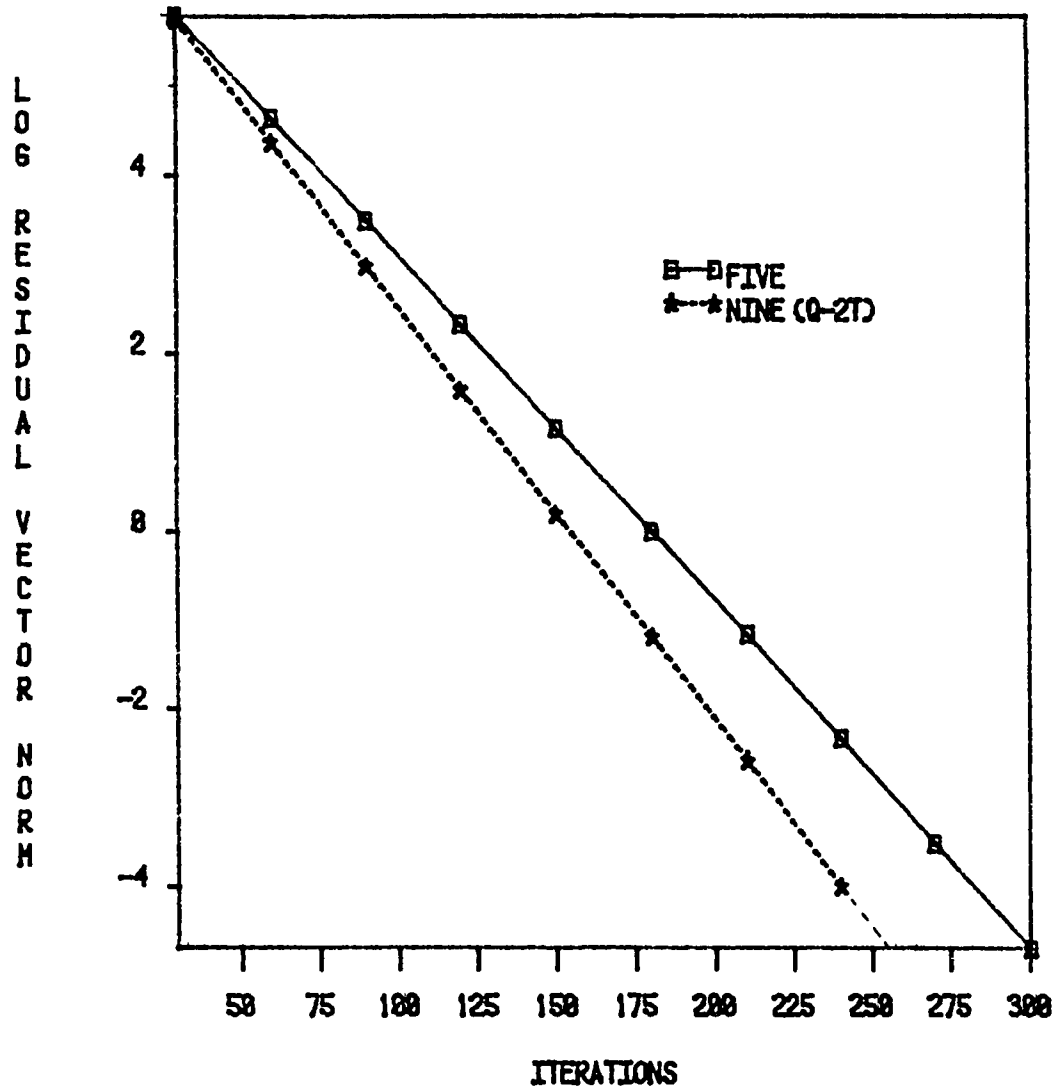

Figure 3.19. Log residual vector norm versus iterations, for 16 by 16 grids and steady-state case with variable heat generation for UO_2 fuel element

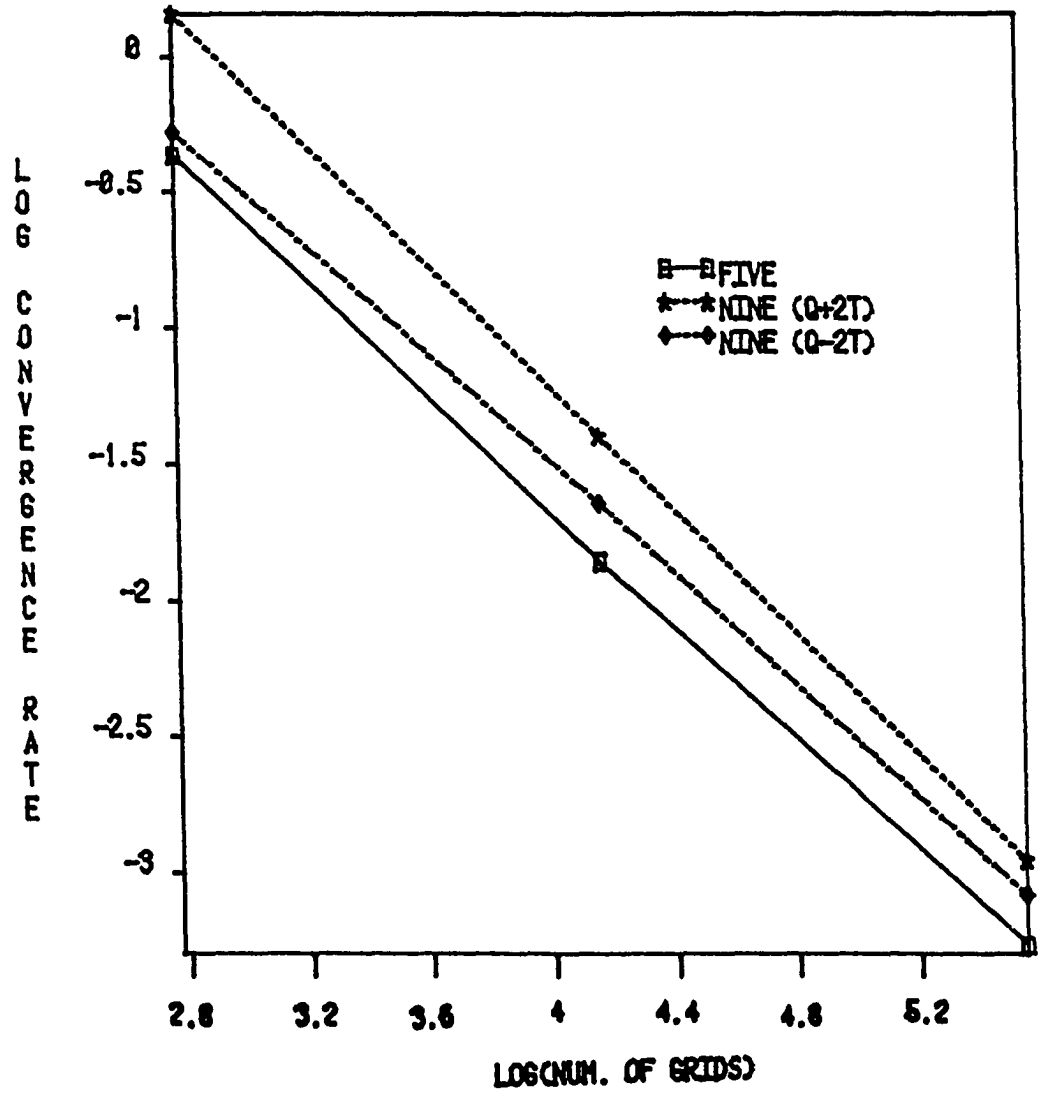

Figure 3.20. Log convergence rate versus Log (num. of grids used) for steady-state case with variable heat generation for UO_2 fuel element

$$T = T_o(A^4 - x^4)(B^4 - y^4) \tag{3.24}$$

where T_o = constant parameter and

A,B = slab dimensions.

Using Equation (3.24) in the steady-state heat conduction equation with constant thermal conductivity (Equation 2.17), one gets a source term in the form

$$S = 12\ K\ T_o\ \{x^2(B^4 - y^4) + y^2(A^4 - x^4)\} \tag{3.25}$$

Equations (3.24) and (3.25) are used in the second term of the parameter p (see Equation (2.11)) and repeated here:

$$p_2 = - \frac{(\beta^2 D_x^2 + D_y^2)\ \nabla^2 T}{6\beta\ D_{xy}^2\ T} \tag{3.26}$$

where

$$\nabla^2 T = - \frac{S}{K} . \tag{3.27}$$

For equal spacing, the first term of Equation (2.11) is constant ($p_1 = 0.333$) and $\beta = 1$. After some algebraic manipulations, one has the following analytical equation for p_2:

$$p_2 = \frac{A^4 - x^4 + B^4 - y^4 - 12\ x^2y^2}{36\ x^2y^2} . \tag{3.28}$$

It can be observed from Equation (3.28) when x and y go to zero that p_2 is infinite; however, the program, in such case, will set the parameter p equal only to the first term of Equation (2.11). The above

analytical solution for p_2 (Equation 3.28) is used by the program and can be compared with the numerical solution given by

$$p_2 = \frac{24\, T_o(A^4 - x^4 + B^4 - y^4 - 12\, x^2y^2)}{6(T_c - 2\, T_A + 4\, T_{ij})/(\Delta x^2 \Delta y^2)} \tag{3.29}$$

where T_c and T_A are given by Equations (2.2) and (3.19), respectively. The computational results given in Tables 3.1 and 3.2 for the internal nodes, show that both analytical and numerical methods have approximately the same values for p_2. In nodes where the denominator of Equation (3.26) is getting smaller, however, this makes p_2 higher which, in turn, causes oscillations of the solution. The oscillations are overcomed by the damping function (Equation 3.23).

3.4.3 General mechanical problem

For purposes of illustration, a source term of the form $S = S_oXY$ will be considered. S_o is the maximum heat generated in the slab. The second term of Equation (3.16) goes to zero for $S = S_oXY$; therefore, the parameter p is given only by Equation (3.21). The analytical method being considered as a reference case for this problem is developed in Appendix E. The results of the computations are shown in Figure 3.21 for the relative error. It can be observed that the nine-point approximation is more accurate again. This is also true for all the other nodal points. Figure 3.22 shows the larger convergence rate of the nine-point approximation with respect to the five-point approximation.

Table 3.1 Analytical[a] results of p_2 in the case of variable heat generation

13.8300	3.1040	0.9938
3.1040	0.5000	-0.01312
0.9938	-0.01312	-0.2133

[a]Equation (3.28).

Table 3.2 Numerical[a] results of p_2 in the case of variable heat generation

11.1000	3.8030	1.214
3.8010	0.4829	-0.01264
1.2114	-0.01263	-0.1862

[a]Equation (3.29).

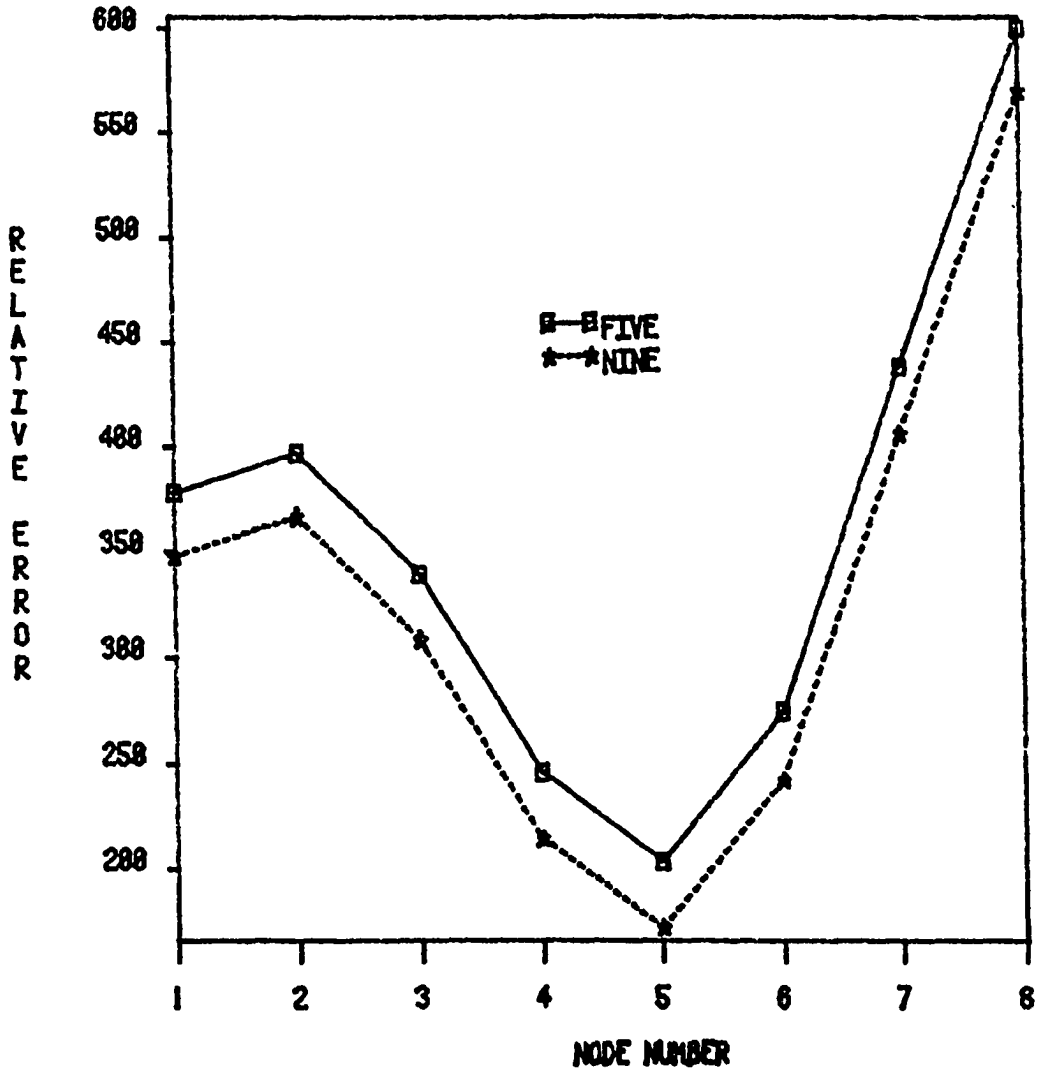

Figure 3.21. Relative error comparison along the x-axis for the steady-state case with $S = S_o XY$

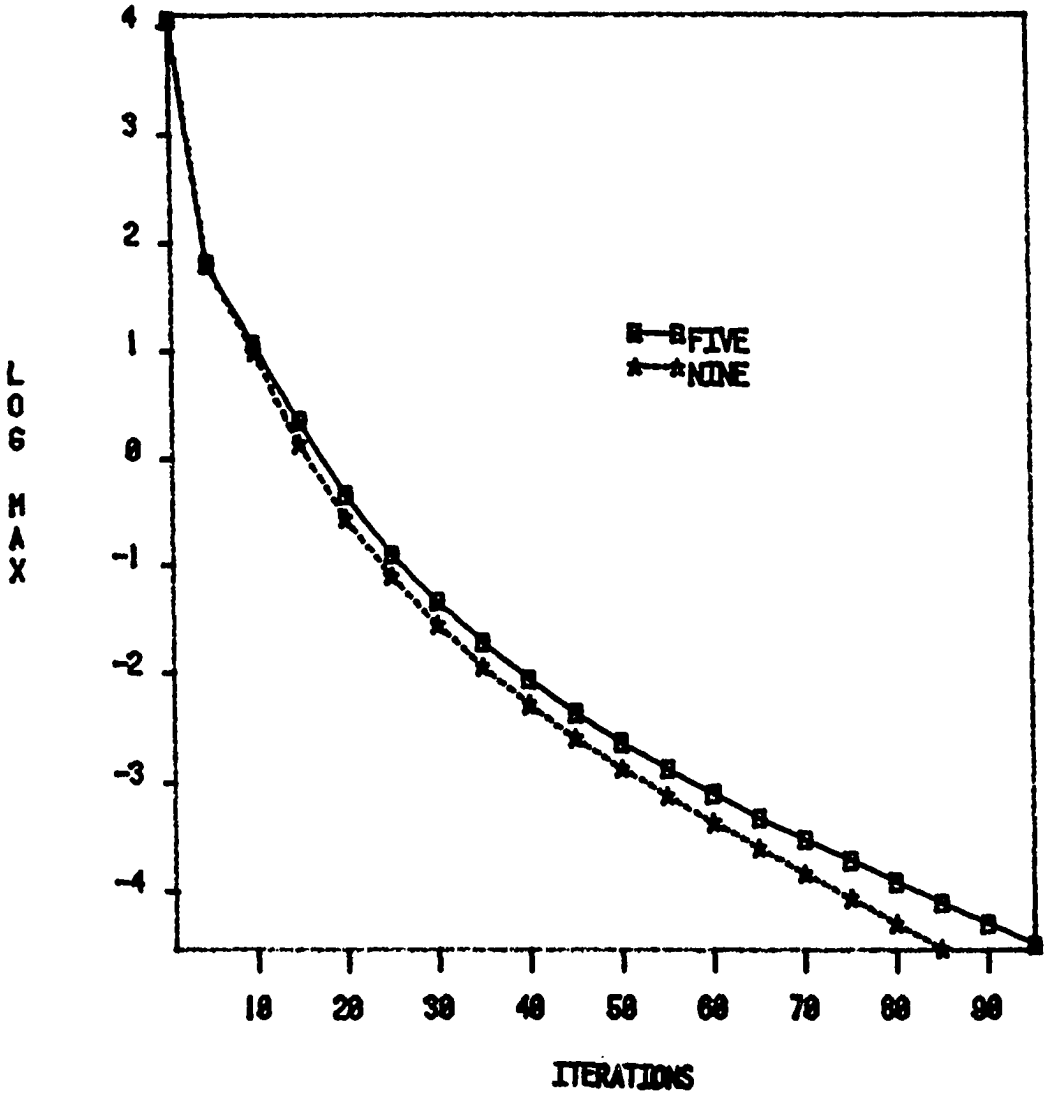

Figure 3.22. Residual norm for the nine- and five-point relations in case of steady-state and $S = S_o XY$

3.5 Steady-State Results with Variable Thermal Conductivity

3.5.1 Application to the nuclear fuel element

In this case, the thermal conductivity is taken as a function of temperature which is, in turn, a function of space (see Figure 3.11) and will be approximated by a first-order polynomial expression. The conventional steady-state heat conduction equation given by Equation (2.13) can be written as

$$(\nabla K(\bar{r},T))\cdot(\nabla T) + K(\bar{r},T)\cdot\nabla^2 T + S = 0. \tag{3.30}$$

If

$$K(T) = a + bT \ , \tag{3.31}$$

where the constants a and b are approximated from Figure 3.11 over the range (1700 - 3200 K) as

$$a = -0.85 \ w/m°C$$
$$b = 0.18.10^{-2} \ w/m°C^2 \ ,$$

the first term in Equation (3.30) is approximated as

$$b.(\nabla T)^2 \cong b[A1 - \frac{h^2}{6}(D_x^3 T + D_y^3 T)]^2 \tag{3.32}$$

where

$$A1 = \frac{T_{i+1,j} - T_{i-1,j} + T_{i,j+1} - T_{i,j-1}}{2h} \tag{3.33}$$

and

$$h = \Delta x = \Delta y \text{ (equal spacing case).}$$

Equation (3.32) becomes

$$b(\nabla T)^2 \cong b[Al^2 - 2\,Al\,\frac{h^2}{6}\,(D_x^3 T + D_y^3 T) + O(h^4)] \quad . \tag{3.34}$$

Equation (3.30), after rearrangement and using the fundamental Equation (2.8) for the Laplacian, becomes

$$b\,Al^2 + \frac{K}{h^2}\,[(1 - p)\,T_A + \frac{p}{2}\,T_c - (4 - 2p)\,T_{ij}]$$

$$+ S - h^2\,\{\frac{2b\,Al}{6}\,(D_x^3 T + D_y^3 T) + \frac{K}{12}\,(D_x^4 + D_y^4 + 6p\,D_{xy}^2 T)\} = 0 \tag{3.35}$$

where K is given by Equation (3.31), T_c by Equation (2.2) and T_A by Equation (3.19).

In Equation (3.35), the order of truncation error is determined by an appropriate choice of the parameter, p. If p = 0, the relation results in the five-point relation with error of $O(h^2)$. To get $O(h^4)$, set

$$2b\,Al\,(D_x^3 + D_y^3)\,T + \frac{K}{2}\,(D_x^4 + D_y^4 + 6p\,D_{xy}^2)\,T = 0 \quad . \tag{3.36}$$

Using the operator identities,

$$(D_x^2 + D_y^2)\,\nabla^2 = D_x^4 + D_y^4 + 2\,D_{xy}^2 \tag{3.37}$$

and

$$D_x^3 + D_y^3 = (\frac{\partial}{\partial x} + \frac{\partial}{\partial y})\,\nabla^2 - D_x^2 D_y - D_x D_y^2 \quad , \tag{3.38}$$

one has

$$p = \frac{1}{3} - \frac{(D_x^2 + D_y^2)\ \nabla^2 T}{6\ D_{xy}^2\ T} - \frac{2b\ A1}{3KD_{xy}^2\ T}$$

$$\cdot\ \{(\frac{\partial}{\partial x} + \frac{\partial}{\partial y})\ \nabla^2 T - (D_x^2 D_y + D_x D_y^2)\ T\}$$

$$p = p_1 + p_2 + p_3\ . \tag{3.39}$$

Now p is the sum of three terms. The above equations were developed for equal spacing only. The parameter p given by Equation (3.39) is a function of $\nabla^2 T$ which will be given by Equation (3.30) as

$$\nabla^2 T = -\frac{S}{K} - \frac{b}{K}\ (\nabla T)^2 \tag{3.40}$$

and

$$D_{xy}^2 T \simeq \frac{1}{h^4}\ (T_c - 2\ T_A + 4\ T_{ij}) + O(h^2)\ . \tag{3.41}$$

Also, the third-order derivative can be approximated inside the nine-point box by

$$D_x^2 D_y T \cong$$

$$\frac{(T_{i+1,j+1} - T_{i+1,j-1}) - 2(T_{i,j+1} - T_{i,j-1}) + (T_{i-1,j+1} - T_{i-1,j-1})}{2\ \Delta x^2\ \Delta y}$$

$$+ O(h^2) \tag{3.42}$$

$$D_x D_y^2 T \cong$$

$$\frac{(T_{i+1,j+1} - T_{i-1,j+1}) - 2(T_{i+1,j} - T_{i-1,j}) + (T_{i+1,j-1} - T_{i-1,j-1})}{2\,\Delta x\,\Delta y^2}$$

$$+ O(h^2) \ . \tag{3.43}$$

The second term of p is

$$p_2 = - \frac{(D_x^2 + D_y^2)\ \nabla^2 T}{6 D_{xy}^2\ T} \tag{3.44}$$

The third term of p is

$$p_3 = p_{31}\ (p_{32} - p_{33}) \tag{3.45}$$

where

$$p_{31} = (-\ 2b\ A1)/(3KD_{xy}^2 T) \tag{3.46}$$

$$p_{32} = (\frac{\partial}{\partial x} + \frac{\partial}{\partial y})\ \nabla^2 T \tag{3.47}$$

$$p_{33} = (D_x^2 D_y + D_x D_y^2)\ T \ . \tag{3.48}$$

To further simplify the equations, the thermal conductivity, K, is assumed constant, in the evaluation of p_2 and p_3 given by

$$\bar{K} = \frac{\int (a + bT)dT}{\int dT} \tag{3.49}$$

After algebraic manipulation and rearrangement, one has

$$p_{32} = -\frac{2b}{\bar{K}}\left(\frac{\partial T}{\partial x} + \frac{\partial T}{\partial y}\right)\left(\frac{\partial^2 T}{\partial x^2} + \frac{\partial^2 T}{\partial y^2} + 2\,\frac{\partial^2 T}{\partial x \partial y}\right) \tag{3.50}$$

and

$$p_2 = \frac{2b}{6\bar{K}\, D_{xy}^2 T} \cdot \left\{\left(\frac{\partial^2 T}{\partial x^2} + \frac{\partial^2 T}{\partial x \partial y}\right)^2 + \left(\frac{\partial^2 T}{\partial y^2} + \frac{\partial^2 T}{\partial x \partial y}\right)^2 + \left(\frac{\partial T}{\partial x} + \frac{\partial T}{\partial y}\right) \cdot p_{32}\right\} . \tag{3.51}$$

One can use a finite difference approximation for the derivatives in the above equations (Equations (3.50) and (3.51)) of order $0(h^2)$, since the error term goes into the $0(h^4)$ term in Equation (3.35). Once the value of p is calculated by using Equation (3.39) and updated by using the new temperature distribution, it, in turn, can be used to calculate the nodal temperature T_{ij} from Equation (3.35) as

$$T_{ij} = \frac{h^2 b\, Al^2}{K(4 - 2p)} + \frac{1}{(4 - 2p)} \cdot \left\{(1 - p)T_A + \frac{p}{2}\, T_c\right\} + \frac{h^2}{K}\,\frac{S}{(4 - 2p)} \quad . \tag{3.52}$$

Figure 3.23 shows the results of the relative L_2 norm in the case where the thermal conductivity varies linearly with temperature (Equation 3.31). One can observe that the nine-point relation in both cases gives more accurate results than the five-point relation. The nine-point relation with all p terms included (Equation 3.39) seems to have better accuracy than the nine-point relation with only the first of p as the parameter ($p = p_1$).

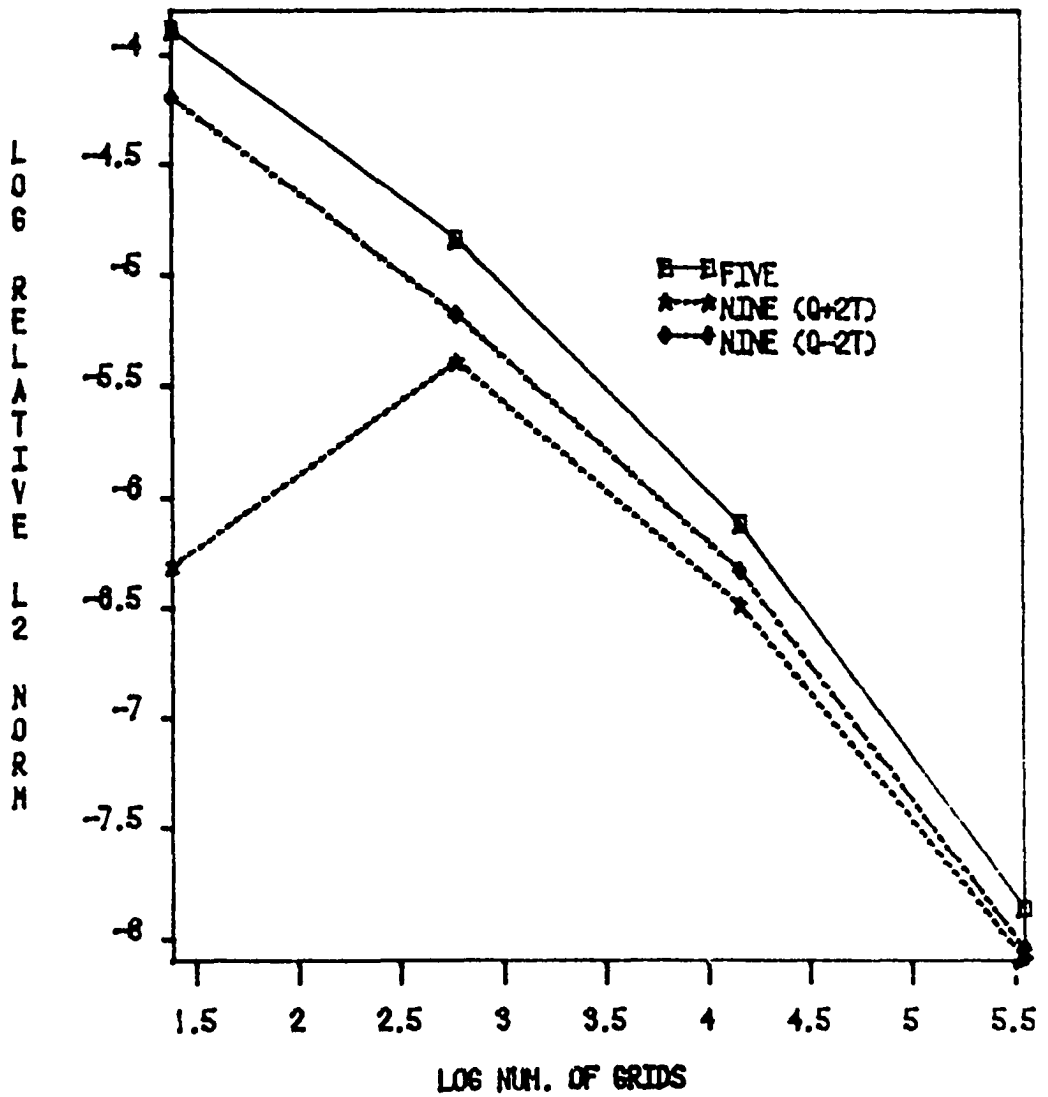

Figure 3.23. Log relative L_2 norm versus Log num. of grids for the steady-state case with $K = a + bT$ (UO_2 fuel element)

One problem with the nine-point relation, in this specific case that includes all terms of the parameter p (Equation 3.39) as Figure 3.24 shows, is that the method does not converge as fast as the nine-point relation when p equals only the first term or the five-point relation when a large number of grids is used. One way to overcome the problem is to use the successive over relation (SOR) technique.

3.5.2 Successive overrelaxation iteration method

Instead of using Equation (3.52) as the (n+1) st iterate, assume that it only yields an estimate and denote it as $\tilde{T}_{ij}^{(n+1)}$. Then define the (n+1) st iterate to be

$$T_{ij}^{(n+1)} = T_{ij}^{(n)} + \alpha[\tilde{T}_{ij}^{(n+1)} - T_{ij}^{(n)}] \tag{3.53}$$

where α = relaxation factor limited to $0 < \alpha < 2$

$\alpha > 1$ iteration is overrelaxed

$\alpha < 1$ iteration is underrelaxed.

Figure 3.25 shows the SOR computational results. One can observe that, by using an optimum SOR parameter α, the number of iterations to convergence can be reduced by one-half. In this way, the nine-point relation with all terms of p included will converge as fast as the nine-point relation with p equal only to the first term (see Equation (3.39)).

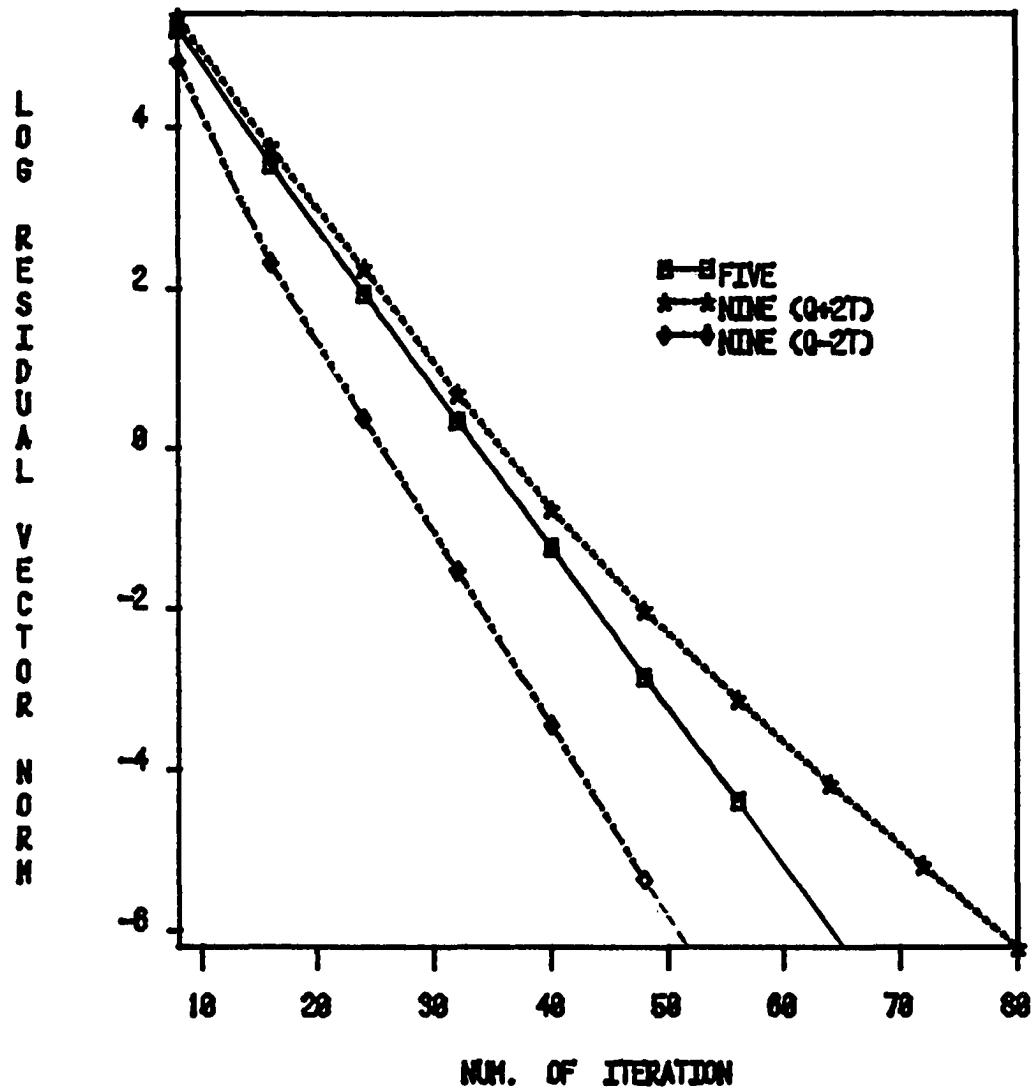

Figure 3.24. Log residual vector norm versus num. of iterations in case of K = a + bT for the steady-state and UO_2 fuel element

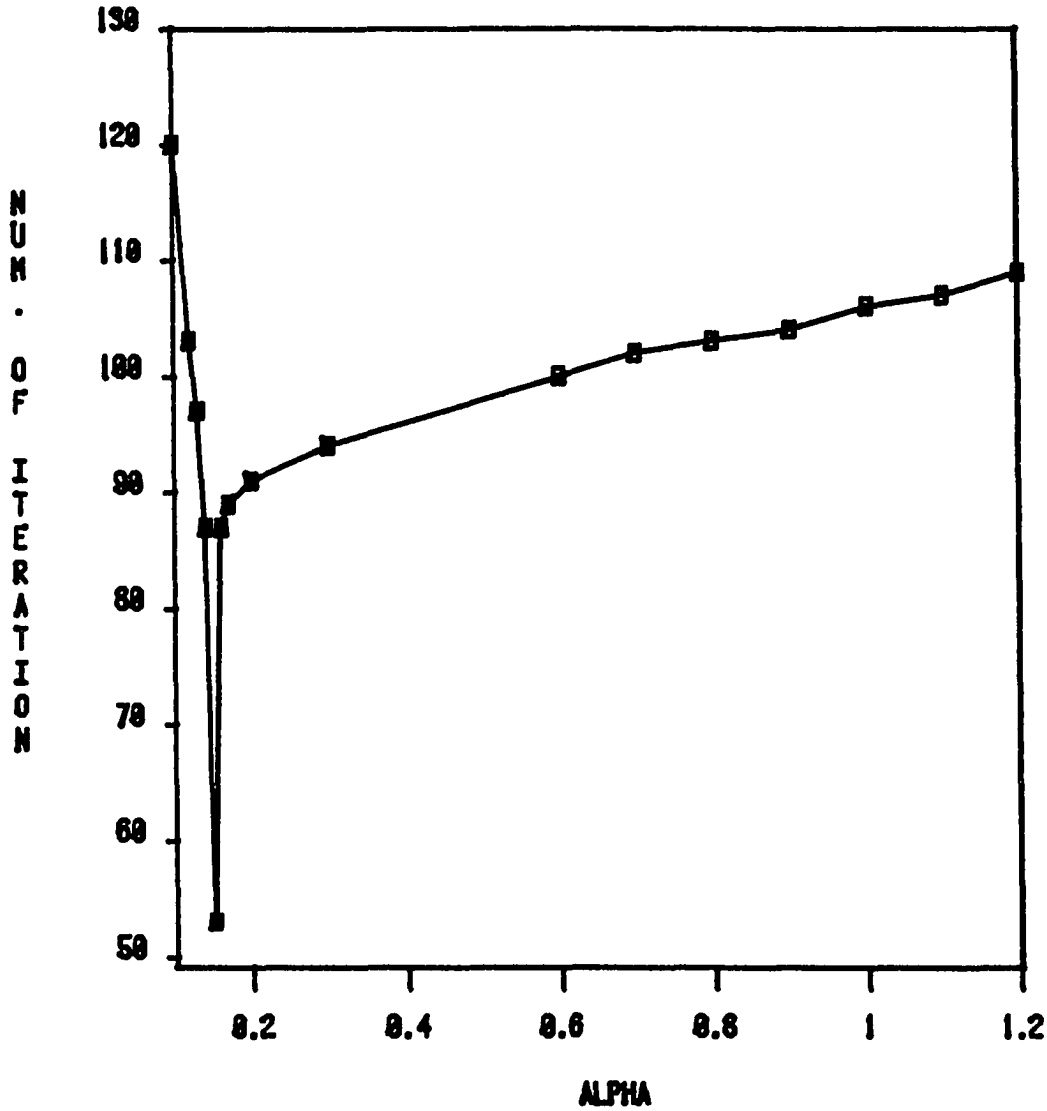

Figure 3.25. Plot of the number of iterations as a function of the SOR parameter α for optimization calculations in case of K = a + bT, steady-state, UO_2 fuel element

3.5.3 General mechanical problem

The analytical method developed in Appendix D will be used as the reference case for the purpose of illustration and testing of the program. The thermal conductivity is allowed to vary linearly with temperature in the form

$$K = K_o(1 + \xi T) \tag{3.54}$$

where K_o is the thermal conductivity at a reference temperature T_o, and ξ is the porosity coefficient. Figure 3.26 shows the results of the nine-point relation with only the first term of p as the parameter (p = 0.333) and the five-point relation. The results are approximately the same for both numerical techniques; however, the nine-point relation converges faster as Figure 3.27 shows.

3.6 Steady-State Results With Variable Heat Generation and Thermal Conductivity

3.6.1 Application to the nuclear fuel element

The thermal conductivity is allowed to vary linearly with temperature as given by Equation (3.31). The heat generation is given by Equation (3.14). Here, again, the same procedure as in Section 3.5.1 was followed to determine the different terms of the parameter p. After some algebraic manipulation, one gets

$$p_{32} = -\frac{2b}{\bar{K}}\left(\frac{\partial T}{\partial x} + \frac{\partial T}{\partial y}\right)\left(\frac{\partial^2 T}{\partial x^2} + \frac{\partial^2 T}{\partial y^2} + 2\,\frac{\partial^2 T}{\partial x \partial y}\right)$$

$$-\frac{8}{\bar{K}} \cdot \frac{Q'}{AB} \cdot \frac{(2 - F)(F - 1)}{(1 - F/2)} \cdot \left\{\frac{x}{A^2} + \frac{y}{B^2}\right\} \tag{3.55}$$

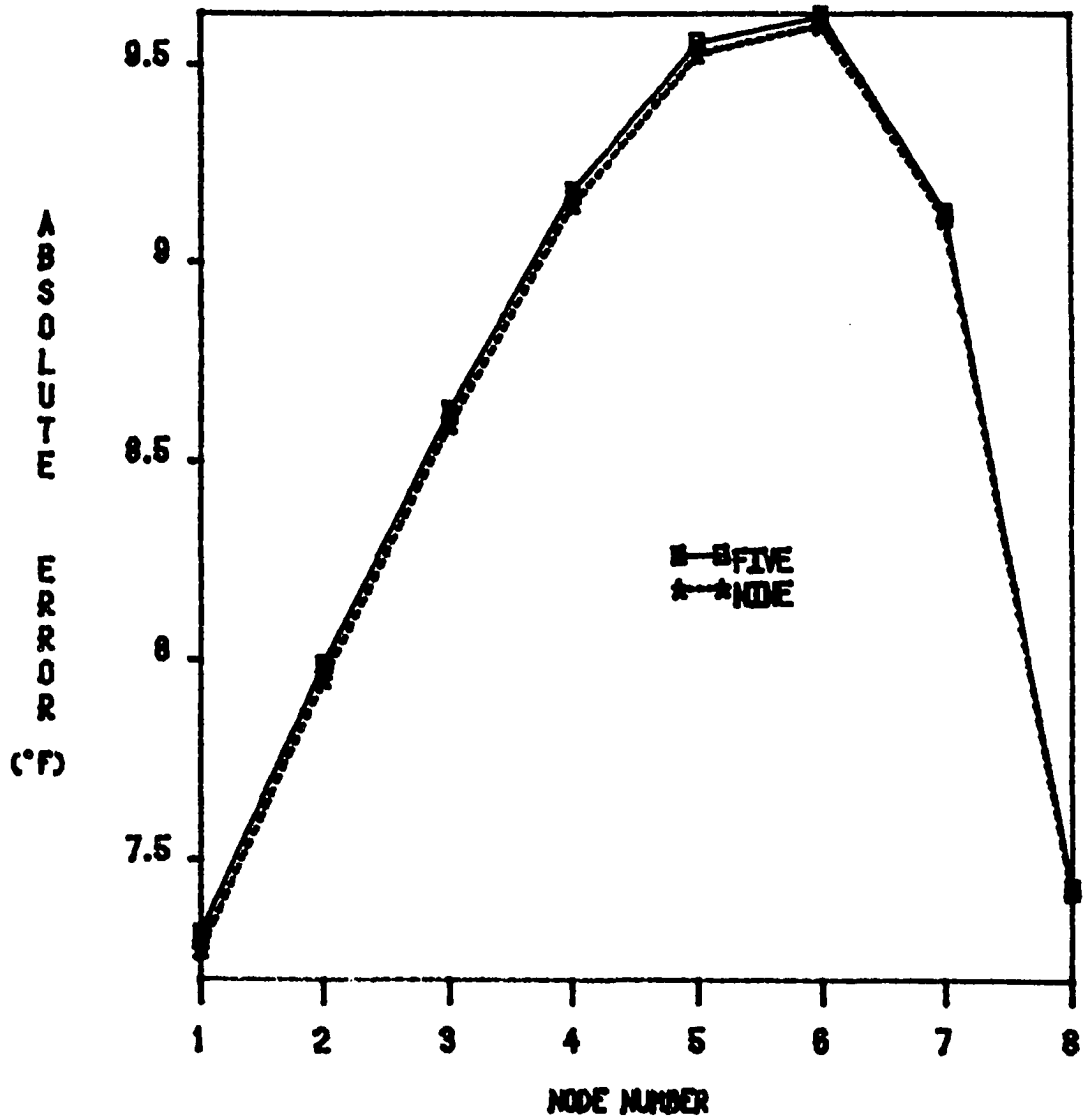

Figure 3.26. Absolute error comparison along the y-axis with $K = K_o (1 + \xi T)$ for the steady-state case

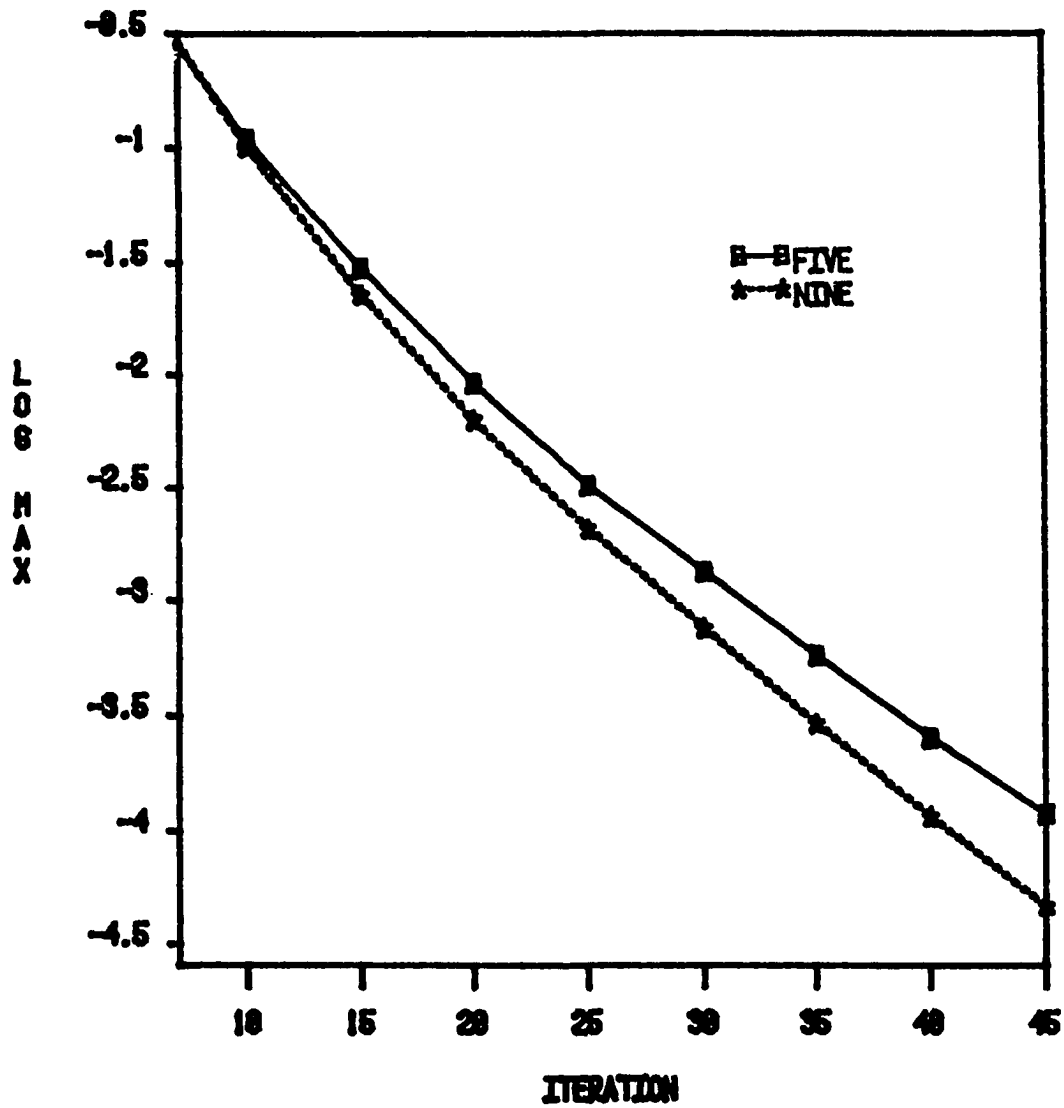

Figure 3.27. Residual norm for the nine- and five-point approximations with $K = K_o (1 + \xi T)$ and steady-state case

and

$$p_2 = \frac{2b}{6\bar{K}\, D_{xy}^2 T} \cdot \{\left(\frac{\partial^2 T}{\partial x^2} + \frac{\partial^2 T}{\partial x \partial y}\right)^2 + \left(\frac{\partial^2 T}{\partial y^2} + \frac{\partial^2 T}{\partial x \partial y}\right)^2$$

$$+ \left(\frac{\partial T}{\partial x} + \frac{\partial T}{\partial y}\right) \cdot p_{32}\} + \frac{8}{6\bar{K}\, D_{xy}^2 T} \cdot \frac{Q'}{AB} \cdot \frac{(2 - F)(F - 1)}{(1 - F/2)} \qquad (3.56)$$

$$p_3 = p_{31}\,(p_{32} - p_{33}) \qquad (3.57)$$

where p_{31} and p_{33} are given by Equations (3.46) and (3.48), respectively. It can be seen, by comparing Equations (3.50) and (3.55), that an additional term is added to Equation (3.55) due to the variable heat generation. The observation holds for p_2 given by Equations (3.51) and (3.56) of the two different problems. The computational results in Figure 3.28 show, again, a higher accuracy for the nine-point relation with p given by

$$p = \frac{1}{3} + p_2 + p_3 \qquad (3.58)$$

where p_3 and p_2 are given by Equations (3.57) and (3.56), respectively.

3.6.2 Problem with assumed analytical solution

As was done in Section 3.4.2, an analytical solution for the temperature distribution is assumed as

$$T = T_o\,(A^2 - x^2)(B^2 - y^2)\ . \qquad (3.59)$$

Using Equation (3.59) in Equation (3.30) with K given by Equation (3.31), one gets a heat source term as

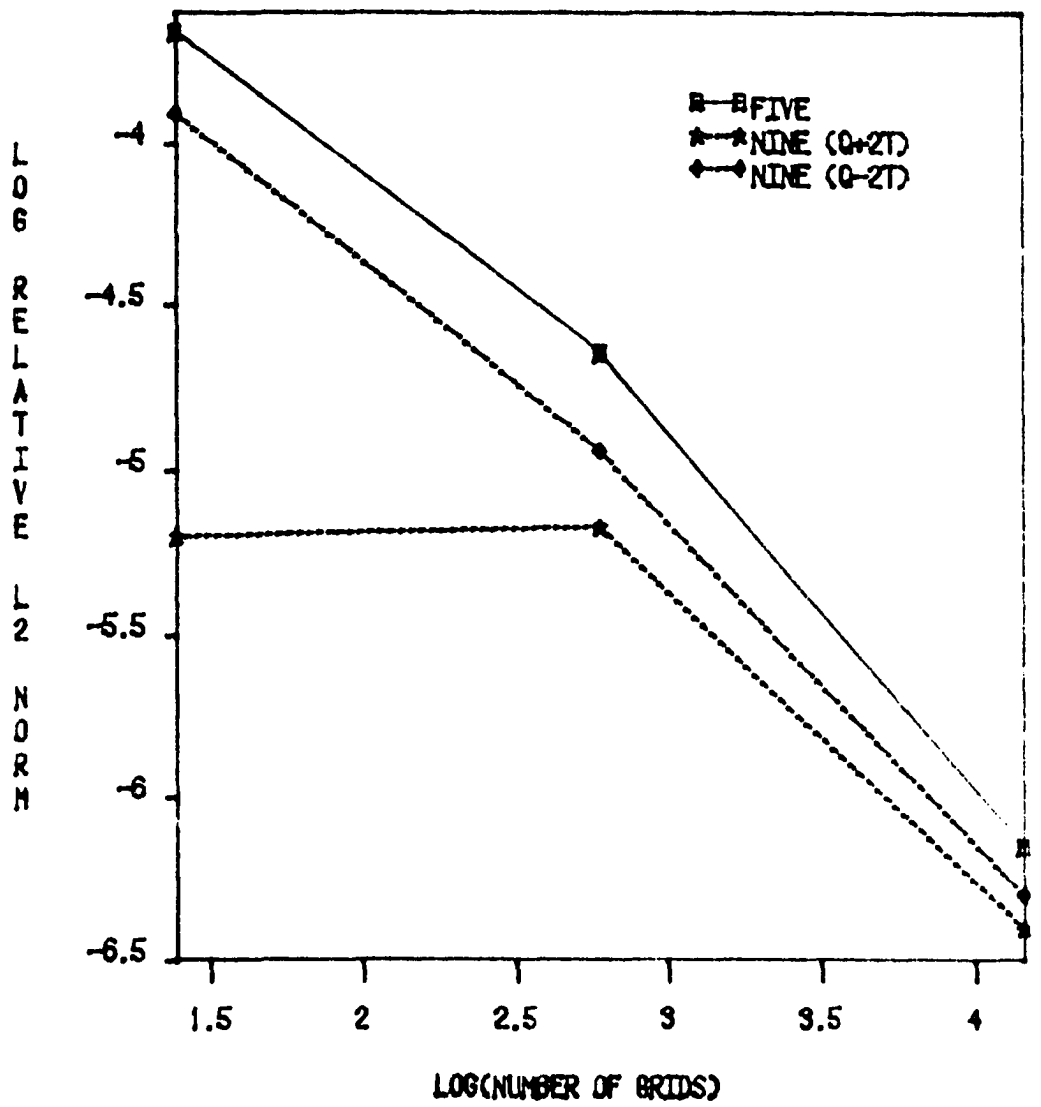

Figure 3.28. Log relative L_2 norm versus Log (num. of grids) for the steady-state case with variable heat source and thermal conductivity (UO_2 fuel element)

$$S = 2\,T_o\,[\{a + b\,T_o(A^2 - x^2)(B^2 - y^2)\} \cdot \{A^2 - x^2 + B^2 - y^2\}$$

$$- 2b\,T_o\,\{x(B^2 - y^2) + y(A^2 - x^2)\}^2\,] \,. \qquad (3.60)$$

Equations (3.59) and (3.60) are used to determine, analytically and numerically, the values of the parameter p at the internal nodes. Since the first term in Equation (3.58) is constant, only the sum of $p_2 + p_3$ will be compared. The analytical development gives a constant value for the sum of p_2 and p_3 ($p_2 + p_3 = -0.333$). The numerical solutions for p_3 and p_2 are given by the following equations.

$$p_3 = -\frac{2}{3}\frac{b\,Al}{\bar{K}\,D^2_{xy}T}\,[p_{32} - (D^2_x D_y + D_x D^2_y)\,T] \qquad (3.61)$$

where

$$p_{32} = -\frac{2b}{\bar{K}}\left(\frac{\partial T}{\partial x} + \frac{\partial T}{\partial y}\right) \cdot \left(\frac{\partial^2 T}{\partial x^2} + \frac{\partial^2 T}{\partial y^2} + 2\,\frac{\partial^2 T}{\partial x \partial y}\right)$$

$$+ \frac{4\,T_o}{K}\,[b\,T_o(A^2 - x^2 + B^2 - y^2) \cdot \{x(B^2 - y^2)$$

$$+ y(A^2 - x^2)\} + (x + y)\,\{a + b\,T_o(A^2 - x^2)(B^2 - y^2)\}$$

$$+ b\,T_o\,\{x(B^2 - y^2) + y(A^2 - x^2)\}$$

$$\cdot \{A^2 - x^2 + B^2 - y^2 - 4\,xy\}] \,. \qquad (3.62)$$

The derivatives $D^2_{xy}T$, $D^2_x D_y T$, and $D_x D^2_y T$ are given by Equations (3.41), (3.42) and (3.43), respectively.

$$p_2 = \frac{b}{3\bar{K}\, D_{xy}^2 T}\left[\left(\frac{\partial^2 T}{\partial x^2} + \frac{\partial^2 T}{\partial x \partial y}\right)^2 + \left(\frac{\partial^2 T}{\partial y^2} + \frac{\partial^2 T}{\partial x \partial y}\right)^2 + \left(\frac{\partial T}{\partial x} + \frac{\partial T}{\partial y}\right) \cdot p_{32}\right]$$

$$+ \frac{T_o}{3\bar{K}\, D_{xy}^2 T}\left[-2b\, T_o\, (A^2 - x^2 + B^2 - y^2)^2\right.$$

$$+ 8\, b\, T_o\, \{x^2(B^2 - y^2) + y^2(A^2 - x^2)\}$$

$$- 4\, \{a + b\, T_o (A^2 - x^2)(B^2 - y^2)\}$$

$$- 4\, b\, T_o\, \{(B^2 - y^2 - 2\, xy)^2 + (A^2 - x^2 - 2\, xy)^2$$

$$\left. - 2(x + y)\, [x(B^2 - y^2) + y(A^2 - x^2)]\}\right] . \qquad (3.63)$$

The computational results are given in Table 3.3 for the numerical method (Equations 3.61 and 3.63). Most nodal values of $p_2 + p_3$ in Table 3.3 are approximately the same as the analytical result (-0.333) except for a few nodes where magnitudes deviate from the analytical solutions by a significant margin. Upon further analysis, it was determined that the $D_{xy}^2 T$ term was extremely small and hence caused this large deviation (see Equation (3.41)). Therefore, this results as the numerator in Equation (3.41) gets small due to the negative term ($-2\, T_A$). Also, as mentioned before, this results in an oscillating solution that was overcome by the damping function.

Table 3.3. Numerical results of $p_2 + p_3$ in the case of variable heat generation and thermal conductivity

-0.233	-0.254	-0.353
-0.254	-0.242	0.608
-0.354	0.607	-3.300

3.7 Numerical Verification

One can also verify approximately the calculations of the parameter p by using nodes outside the nine-point box as shown in Figure 3.29.

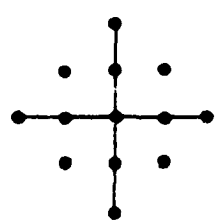

Figure 3.29. Outside nine mesh point box

Equation (3.39) can be written in the form

$$p = \frac{1}{3} - \frac{\nabla^4 T}{6D_{xy}^2 T} - \frac{2b\ A1}{3K} \frac{(D_x^3 + D_y^3)T}{D_{xy}^2 T} \tag{3.64}$$

where the following direct approximations can be made:

$$\nabla^4 T \cong \frac{1}{h^4} [20\ T_{ij} - 8\ T_A + 2\ T_c + (T_{i,j+2} + T_{i+2,j} + T_{i,j-2} + T_{i-2,j})] + O(h^2) \tag{3.65}$$

and

$$(D_x^3 + D_y^3)T \cong \frac{1}{2\ h^3} [T_{i+2,j} + T_{i,j+2} - 2(T_{i+1,j} - T_{i-1,j} + T_{i,j+1} - T_{i,j-1}) - T_{i-2,j} - T_{i,j-2}] + O(h^2)\ . \tag{3.66}$$

The approximations given by Equations (3.65) and (3.66) can be used to calculate p for the central slab node when 4 by 4 or more grids are used. The computational results for the central slab node give $p_2 = 0.158$ in case of variable heat generation with constant thermal conductivity using Equation (3.65) and $p_2 = 0.159$ when using only the inside nine-point box nodes. In case of variable thermal conductivity, the results for the central slab node are: $p_2 = 0.6369$, $p_3 = 2.046 \times 10^{-12}$ using Equations (3.65) and (3.66), whereas $p_2 = 0.5696$, $p_3 = 1.387 \times 10^{-12}$ when only the inside nine-point box nodes were used.

3.8 Steady-State Results With Convective Boundaries

3.8.1 Analytical formulation of steady-state problem

The governing equation of conduction for the problem under study with constant K is

$$\frac{\partial^2 T}{\partial x^2} + \frac{\partial^2 T}{\partial y^2} + \frac{S}{K} = 0 \tag{3.67}$$

where the boundary conditions may be written in the form (Figure 3.30)

$$\frac{\partial T(0,y)}{\partial x} = 0, \; - K \frac{\partial T(A,y)}{\partial x} = h_c[T(A,y) - T_f]$$

$$\frac{\partial T(x,0)}{\partial y} = 0, \; - K \frac{\partial T(x,B)}{\partial y} = h_c[T(x,B) - T_f] \; . \tag{3.68}$$

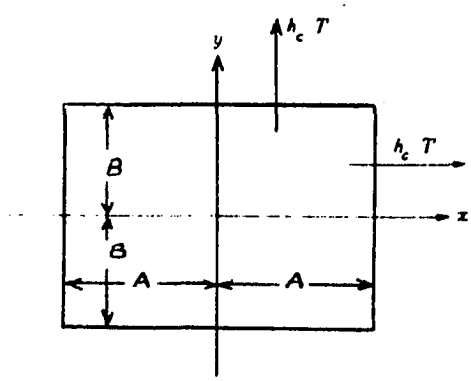

Figure 3.30. Selection of coordinate system for convective boundaries

Restricting ourselves to the case of large h_c (heat transfer coefficient) and assuming, for example, parabolic profiles in both directions such that they satisfy the boundary conditions, one can use an alternate procedure, the so-called integral method [13], for the selection of approximate profiles. This method is based on a

generalization of the Ritz procedure as developed in Appendix B. The first-order polynomial Kantorovich profile given in the form

$$T(x,y) - T_f = (B^2 - y^2)\ X(x) \tag{3.69}$$

satisfies the boundary conditions only in the y-direction.

Introducing Equation (3.69) into Equation (B.6) and integrating the latter with respect to y yields

$$\int_o^B \left(\frac{2}{3} B^2\ X'' - 2X + S/K\right)\ dx = 0\ . \tag{3.70}$$

Since Equation (3.70) is true for an arbitrary slab length A, the integrand itself must vanish everywhere in the interval (0,A). Thus, the parameter function X(x) satisfies the differential equation

$$X'' - (3/B^2)\ X = -\ 3\ S/2\ K\ B^2\ . \tag{3.71}$$

Subject to boundary conditions in the x direction,

$$T(A,y) = T_f\ . \tag{3.72}$$

In terms of the product solution, which is defined as

$$T(x,y) - T_f = X(x)\ Y(y)\ , \tag{3.73}$$

the condition (Equation 3.72) may be written in the form

$$T(A,y) - T_f = X(A)\ Y(y) = 0\ . \tag{3.74}$$

However, Equation (3.74) cannot be valid for all values of Y(y) unless X(A) = 0. Similarly, the other condition, resulting from symmetry of temperature, is found to be dX(0)/dx = 0. Thus, the boundary conditions in x are

$$\frac{dX(0)}{dx} = 0 \ , \quad X(A) = 0 \ . \tag{3.75}$$

Now the solution of Equation (3.71) which satisfies the boundary conditions (Equation 3.75) is

$$X(x) = \frac{S}{2K} \left(1 - \frac{\cosh. \ (\sqrt{3}/B)x}{\cosh. \ (\sqrt{3}/B)A}\right) \ . \tag{3.76}$$

Finally, inserting Equation (3.76) into Equation (3.69) and rearranging gives the first-order polynomial Kantorovich profile for the desired temperature distribution in the form

$$\frac{T(x,y) - T_f}{S \ B^2/K} = \frac{1}{2} \left[1 - \left(\frac{y}{B}\right)^2\right] \left(1 - \frac{\cosh. \ (\sqrt{3}/B)x}{\cosh. \ (\sqrt{3}/B)A}\right) \tag{3.77}$$

which is the equation used in the program for the analytical solution in regions with convective boundaries.

3.8.2 Difference formulation of steady-state problem

Consider a network system as shown in Figure 3.31a of squares of small, but finite size, so that the nodal points, T_{ij}, will be classified according to their location as inner and boundary (corner or side) nodal points (see Figure 3.31).

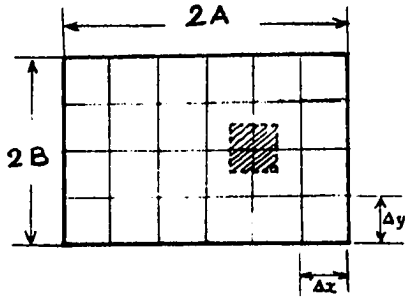

(a) Slab dimension

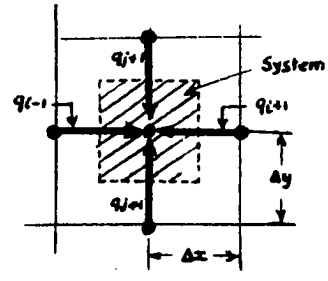

(b) System of inner nodal point

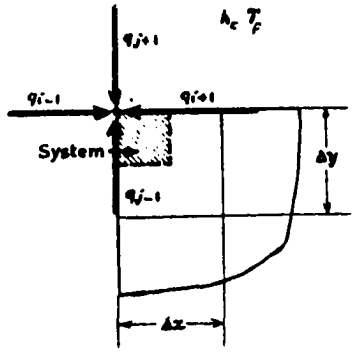

(c) System of corner nodal point

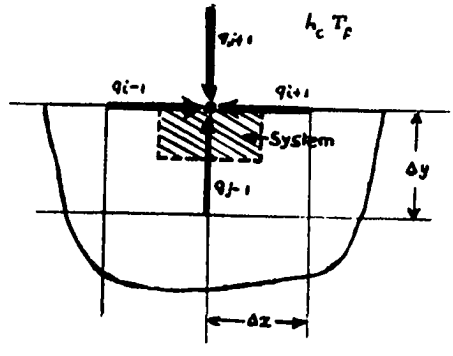

(d) System of sides nodal point

Figure 3.31. Nodal systems

The heat energy balance (the first law of thermodynamics) applied to the system of Figure 3.31(b) gives

$$q_{i-1}(\Delta y.1) + q_{j-1}(\Delta x.1) + q_{i+1}(\Delta y.1) + q_{j+1}(\Delta x.1)$$

$$+ S_{ij} (\Delta x\, \Delta y.1) = 0 \tag{3.78}$$

where 1 denotes the unit thickness. The directions of heat fluxes are arbitrarily selected toward the nodal point for algebraic convenience. Relating the q's to the temperature by using Fourier's law of conduction, one has

$$q_{i-1} = K \frac{T_{i-1,j} - T_{i,j}}{\Delta x} , \quad q_{j-1} = K \frac{T_{i,j-1} - T_{i,j}}{\Delta y}$$

$$q_{i+1} = K \frac{T_{i+1,j} - T_{i,j}}{\Delta x} , \quad q_{j+1} = K \frac{T_{i,j+1} - T_{i,j}}{\Delta y} \tag{3.79}$$

Assuming $\Delta x = \Delta y$, homogeneous material, and inserting Equations (3.79) into Equation (3.78), one gets Equation (A.8) which is repeated here:

$$T_{ij} = \frac{1}{4} [T_{i+1,j} + T_{i-1,j} + T_{i,j+1} + T_{i,j-1}$$

$$+ (\Delta x)^2 \frac{S_{ij}}{K}] = 0 . \tag{A.8}$$

This equation applies equally to all inner nodal points.

Now for the corner boundary, the first law of thermodynamics applied to the system of Figure 3.31(c) gives

$$q_{i-1}\left(\frac{\Delta y}{2}\cdot 1\right) + q_{j-1}\left(\frac{\Delta x}{2}\cdot 1\right) + q_{i+1}\left(\frac{\Delta y}{2}\cdot 1\right)$$

$$+ q_{j+1}\left(\frac{\Delta x}{2}\cdot 1\right) + S_{ij}\left(\frac{\Delta x}{2}\frac{\Delta y}{2}\cdot 1\right) = 0 \ . \qquad (3.80)$$

Relating q_{i-1} and q_{j+1} to the temperature by a Newton's Law of convection, one has

$$q_{i-1} = q_{j+1} = h_c\,(T_f - T_{ij}) \ . \qquad (3.81)$$

Using q_{j-1} and q_{i+1} from Equation (3.79), we have for $\Delta x = \Delta y$

$$T_{ij} = \left(1 - \frac{h_c(\Delta x)}{K}\right)^{-1}\left[\frac{1}{2}(T_{i,j-1} + T_{i+1,j})\right.$$

$$\left. + \frac{h_c\,\Delta x}{K}T_f + \frac{S_{ij}(\Delta x)^2}{4K}\right] \ . \qquad (3.82)$$

Equation (3.82) applies at the corners of the fuel plate. Following the foregoing procedure for the side nodal points (Figure 3.31d), one gets the following difference equation:

$$T_{ij} = \left(2 + \frac{h_c\,\Delta x}{K}\right)^{-1}\left[\frac{1}{2}(T_{i-1,j} + T_{i+1,j}) + T_{i,j-1}\right.$$

$$\left. + \frac{h_c\,\Delta x}{K}T_f + \frac{S_{ij}(\Delta x)^2}{2K}\right] \ . \qquad (3.83)$$

These equations are used in the program to solve for the temperatures at the boundaries.

3.8.3 Computational results with convective boundaries

Consider, for the purpose of illustration, the slab used in Section 3.3.1. The slab is subject to a convective heat transfer coefficient of 1135.6 w/m^2K at its boundaries, and a coolant at -6.67°C surrounding the slab. The analytical method which will be considered as a reference case is given by Equation (3.77).

The results of the computation using the nine-point relation with only the first term of p as the parameter, and the five-point relation are given for the relative error in Figure 3.32.

This shows that the nine-point relation is more accurate than the five-point relation. Also, from Figure 3.33 the infinite norm shows a steeper slope for the nine-point relation than the five-point relation.

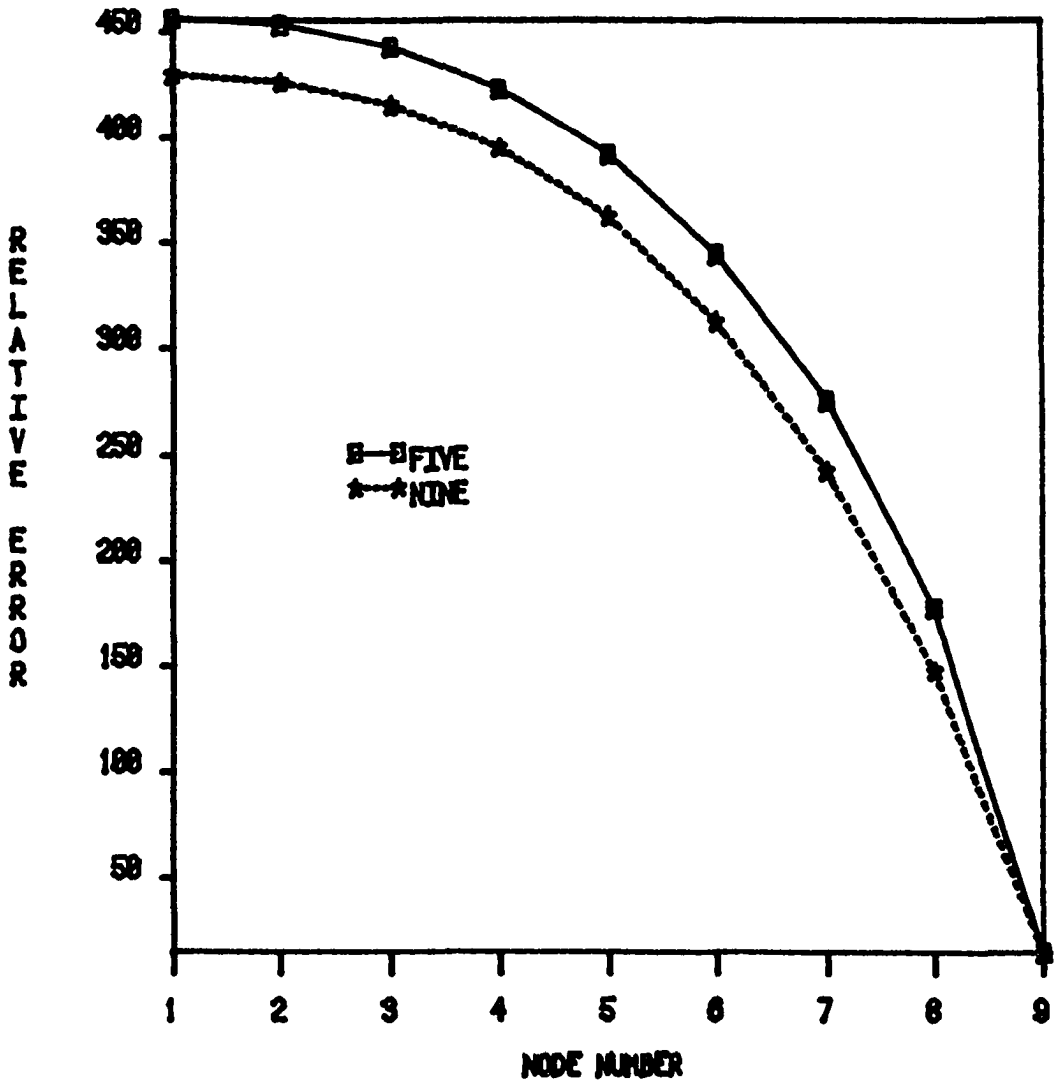

Figure 3.32. Relative error comparison along the x-axis for the steady-state case with convective boundaries

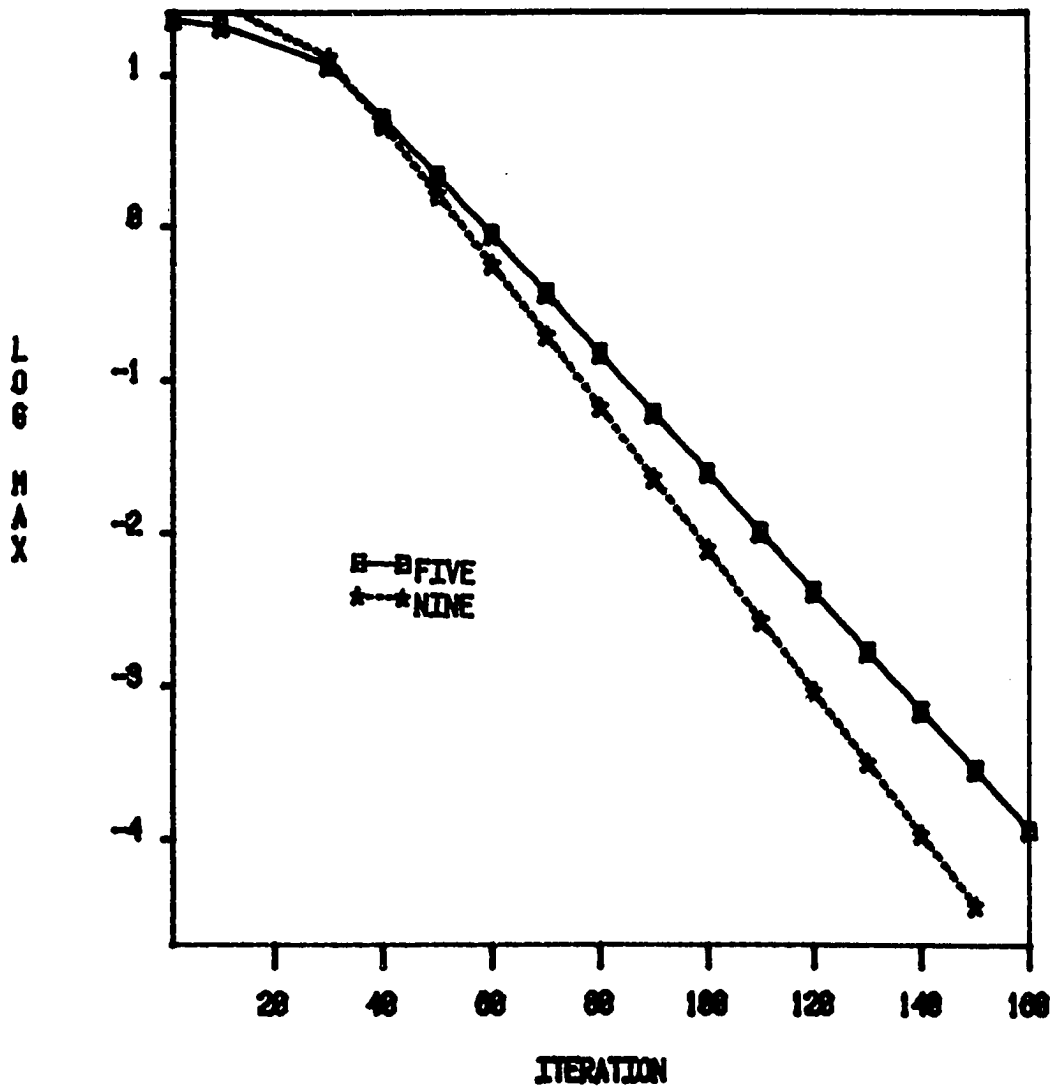

Figure 3.33. Residual norm for the nine- and five-point approximations (steady-state case with convective boundaries)

4. COMPUTATIONAL RESULTS OF THE STEADY-STATE CASE FOR THE CLAD REGION

4.1 Introduction

Consider the boundary value problem (Equation E.1) in Appendix E with S = 0. The boundary at y = 0 is kept at temperature $\phi(x,t)$ and the remaining boundaries are kept at zero (°F) temperature for purpose of illustration, that is

$$T = 0 \quad \text{at} \quad x = 0,\ x = A,\ y = B,\ t > 0$$

$$T = \phi(x,t) \quad \text{at} \quad y = 0,\ t > 0$$

$$T = F \quad \text{in} \quad 0 \leq x \leq A,\ 0 \leq y \leq B,\ t = 0\ . \tag{4.1}$$

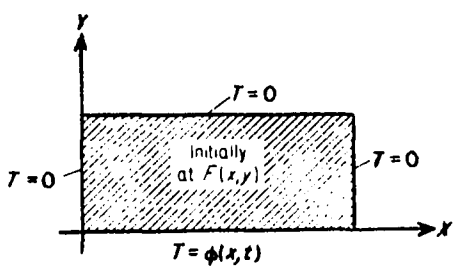

If one follows the mathematical step of Appendix E, then the solution of the present problem with the conditions in Equation (4.1) becomes

$$T(x,y,t) = \{\frac{4}{AB} \sum_{m=1}^{\infty} \sum_{n=1}^{\infty} e^{-\alpha_T(\gamma_m^2 + \eta_n^2)t} \cdot \sin \gamma_m x$$

$$\cdot \sin \eta_n y \int_{x'=0}^{A} \int_{y'=0}^{B} F \cdot \sin \gamma_m x' \cdot \sin \eta_n y' \cdot dx'dy'\}$$

$$+ \{\frac{4}{AB} \sum_{m=1}^{\infty} \sum_{n=1}^{\infty} e^{-\alpha_T(\gamma_m^2 + \eta_n^2)t} \cdot \sin \gamma_m x \cdot \sin \eta_n y$$

$$\cdot \int_{t'=0}^{t} e^{\alpha_T(\gamma_m^2 + \eta_n^2)t'} dt' \cdot \int_{x'=0}^{A} \int_{y'=0}^{B} \frac{\alpha_T}{K} \sin \gamma_m x'$$

$$\sin \eta_n y' \cdot g(x',y',t') \cdot dx'dy'\}$$

$$+ \{\frac{4}{AB} \sum_{m=1}^{\infty} \sum_{n=1}^{\infty} e^{-\alpha_T(\gamma_m^2 + \eta_n^2)t}$$

$$\cdot \sin \gamma_m x \sin \eta_n y \int_{t'=0}^{t} e^{\alpha_T(\gamma_m^2 + \eta_n^2)t'} dt'$$

$$\cdot \int_{x'=0}^{A} \alpha_T \cdot \phi(x',t') \cdot \eta_n \cdot \sin \gamma_m x' \cdot dx'\} \qquad (4.2)$$

where again

$$\gamma_m = \frac{m\pi}{A} \qquad m = 1,2,3 \ldots.$$

$$\eta_n = \frac{n\pi}{B} \qquad n = 1,2,3 \ldots.$$

and summation is taken over all eigenvalues.

It is to be noted that the analytic solution (Equation 4.2) includes three different terms. The first term on the right-hand side is for the effects of the initial condition in the slab, the second term for the effects of heat generation, and the third term for the effects of prescribed temperature distribution at the boundary y = 0. Now if one examines the special case of the clad region where there is no heat generation within the region (S ≡ 0) and if one assumes further that the clad region is initially at zero temperature (i.e. F ≡ 0) and the boundary condition at y = 0 is at the fuel surface temperature (i.e. $\phi(x)$), Equation (4.2) simplifies to

$$T(x,y,t) = \frac{4}{AB} \sum_{m=1}^{\infty} \sum_{n=1}^{\infty} \frac{\eta_n}{\gamma_m^2 + \eta_n^2} \sin \gamma_m x \cdot \sin \eta_n y \, (1 - e^{-\alpha_T(\gamma_m^2 + \eta_n^2)t}) \cdot \int_{x'=0}^{A} \phi(x') \cdot \sin \gamma_m x' \cdot dx' \, . \tag{4.3}$$

The steady-state temperature distribution is obtainable from Equation (4.3) by letting $t \to \infty$. Then,

$$T(x,y,\infty) = \frac{4}{AB} \sum_{m=1}^{\infty} \sum_{n=1}^{\infty} \frac{\eta_n}{\gamma_m^2 + \eta_n^2} \sin \gamma_m x \cdot \sin \eta_n y \cdot \int_{x'=0}^{A} \phi(x') \sin \gamma_m x' \cdot dx' \, . \tag{4.4}$$

If one makes use of the following relation,

$$\frac{2}{B} \sum_{n=1}^{\infty} \frac{\eta_n}{\gamma_m^2 + \eta_n^2} \sin \eta_n y = \frac{\sinh \gamma_m(B - y)}{\sinh \gamma_m B} \quad . \tag{4.5}$$

The double summation of Equation (4.4) is reduced to a single summation:

$$T(x,y,\infty) = \frac{2}{A} \sum_{m=1}^{\infty} \frac{\sinh \gamma_m(B - y)}{\sinh \gamma_m B} \cdot \sin \gamma_m x$$

$$\cdot \int_{x'=0}^{A} \phi(x') \cdot \sin \gamma_m x' \, dx' \quad . \tag{4.6}$$

The above equation will be used as the analytical reference case for different surface profile $\phi(x)$.

4.2 Computational Results of the Temperature Distribution in the Clad Region

Calculations to this point were done only for the fuel region where the clad regions were neglected. Consider now the application of the nine- and five-point numerical techniques in a region where there is no heat generation such as an aluminum slab of dimensions 61 cm by 30.5 cm whose thermal conductivity is 218.1 w/m °C. The slab is subjected at one of its boundaries to a uniform temperature of $\phi(x)$ = 37.8°C. The slab is also divided into 16 by 8 grids; its initial temperature is 17.8°C. The results of the computations for the relative error of the nine- and five-point approximations using as a reference case the analytical solution of Equation (4.6), are plotted in Figure 4.1. The nine-point relation gives more accurate results than the five-point

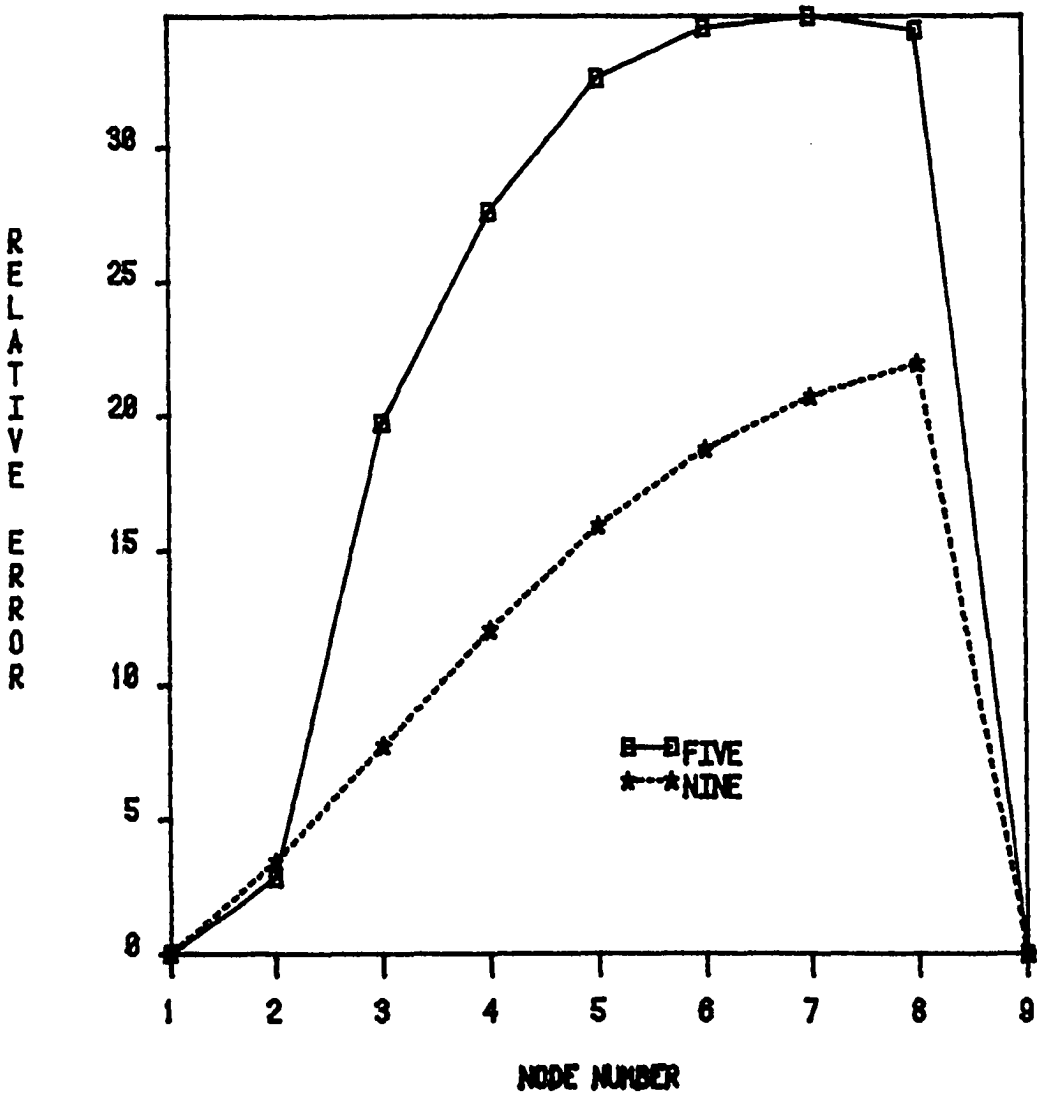

Figure 4.1. Relative error comparison along the x-axis for the centerline temperature in case of uniform $\phi(x)$, aluminum clad region (steady-state case)

relation. Also, it converges faster as it can be seen in Figure 4.2.

One can also take any other functional profile for $\phi(x)$ for example, in the case where $\phi(x)$ is given by

$$\phi(x) = 10 \exp (3x) \tag{4.7}$$

and a zirconium material for the slab described above. The results in Figures 4.3 and 4.4 show a higher and faster convergence of the nine-point relation than for the five-point relation.

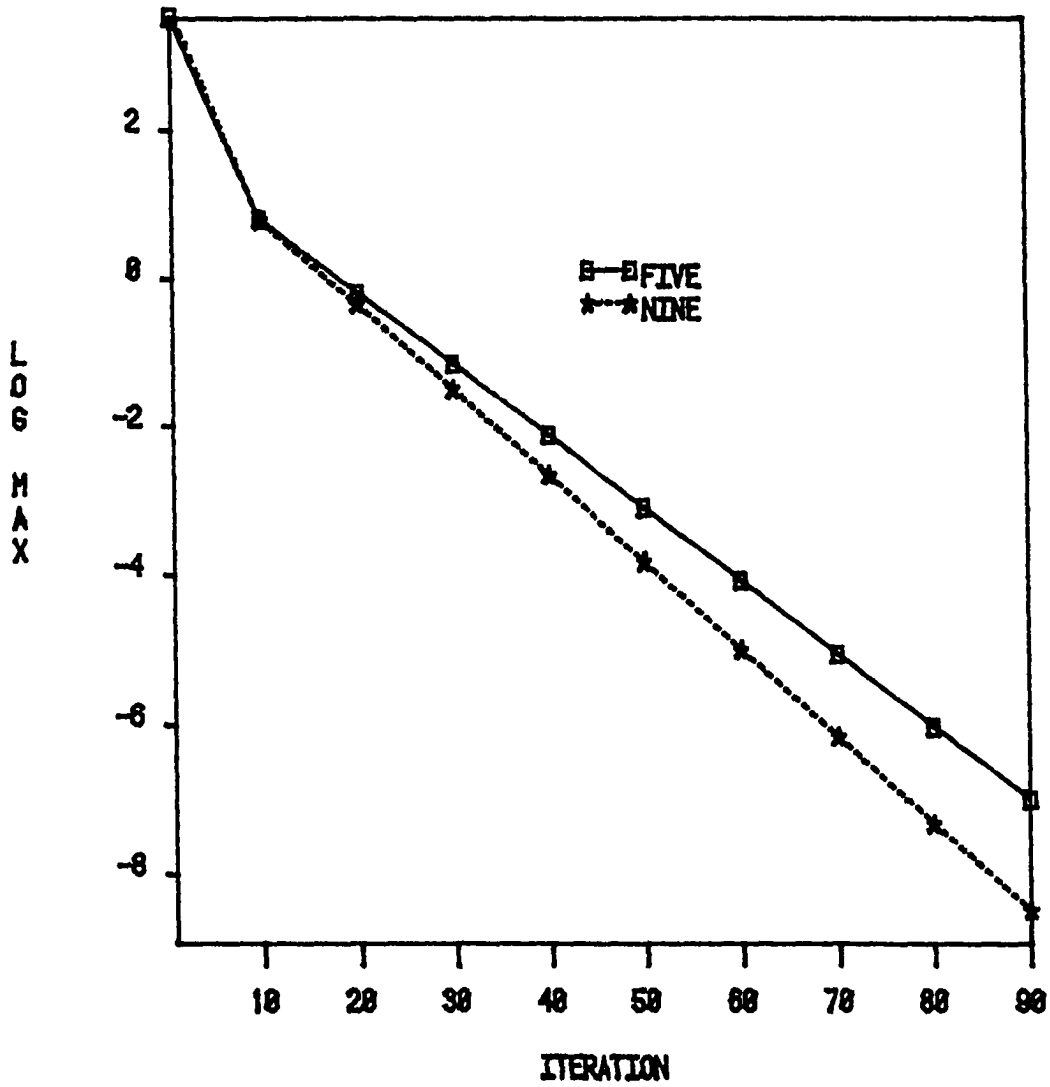

Figure 4.2. Residual norm for the nine- and five-point approximations in case of uniform $\phi(x)$, aluminum clad region (steady-state case)

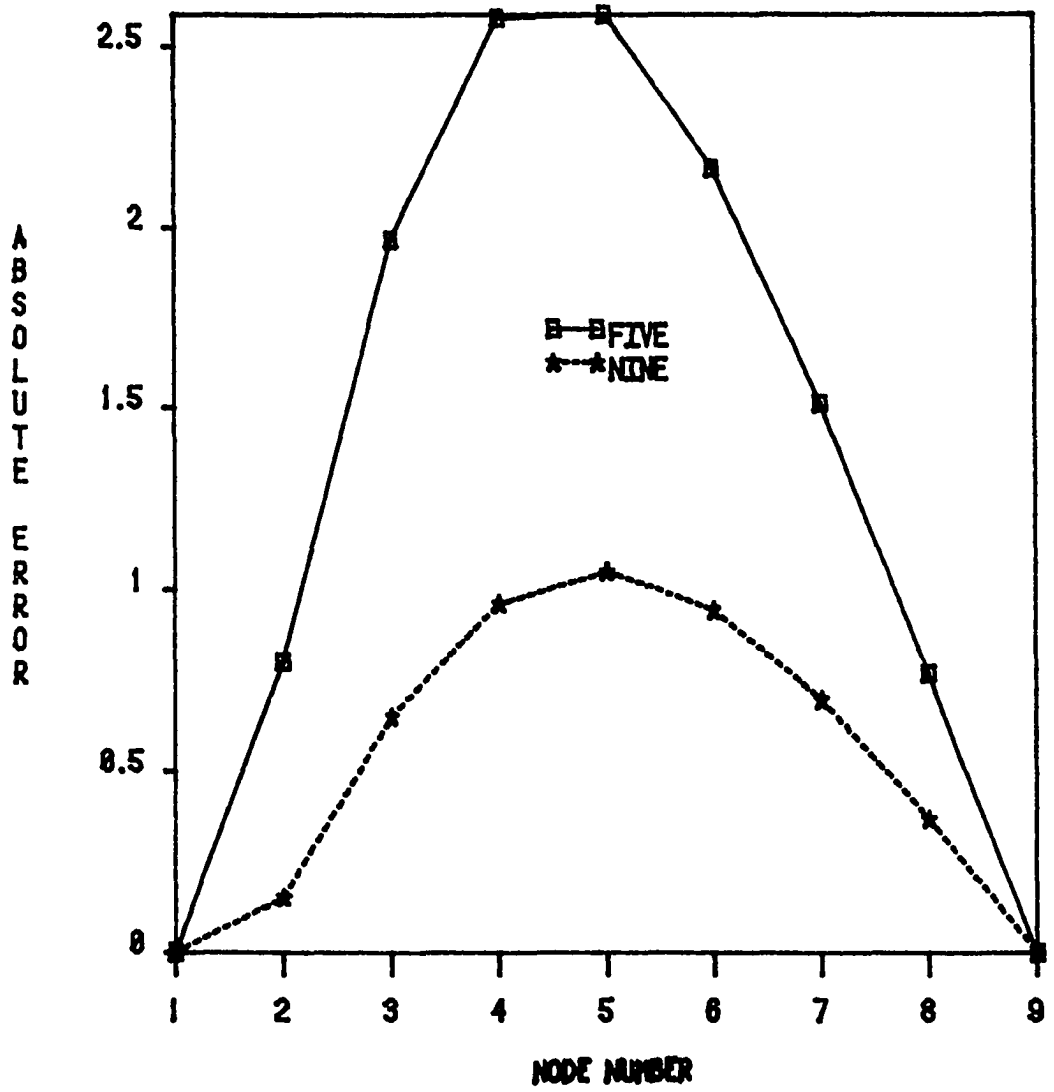

Figure 4.3. Absolute error comparison along the y-axis for the centerline temperatures with $\phi(x) = 10 \exp(3x)$, zirconium clad region (steady-state case)

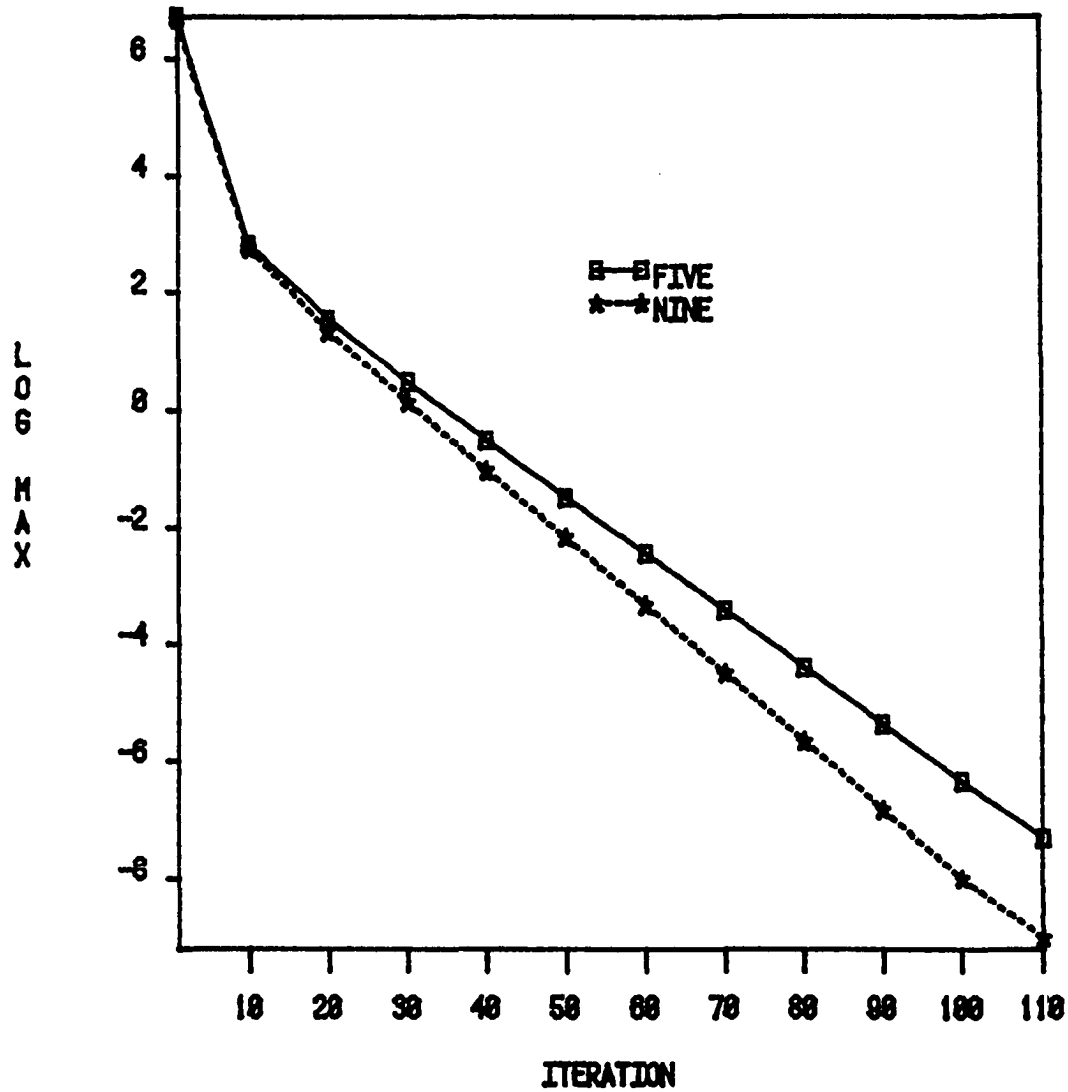

Figure 4.4. Residual vector norm for the nine- and five-point approximations with $\phi(x) = 10 \exp(3x)$, zirconium clad region (steady-state case)

5. FORMULATION AND COMPUTATIONS FOR THE UNSTEADY-STATE CASES

5.1 Introduction

The unsteady heat conduction equation which is found by an energy balance over the control volume of unit thickness ($\Delta z = 1$) and negligible axial conduction, Figure 5.1, is [21]

[Net energy conducted into the element]

+ [Energy generated within the element]

= [Change in stored energy within the element] .

Thus,

$$\nabla.(K\ \nabla T) + S = \rho\ C_p\ \frac{\partial T}{\partial t} \tag{5.1}$$

where t is the time. The development of the nine-point and five-point relationships will be based on the same assumptions mentioned in Section 3.3.2. Figure 5.2 will be considered for the material region.

5.2 Constant Thermal Properties and Heat Generation

In case of constant thermal conductivity, Equation (5.1) can be written as

$$K\ \nabla^2 T + S = \rho\ C_p\ \frac{\partial T}{\partial t}\ . \tag{5.2}$$

5.2.1 Five-point relation

Equation (5.2) can be used to develop the five-point relation if one approximates the first and second derivatives in x and y with an error of $O(h^2)$ as

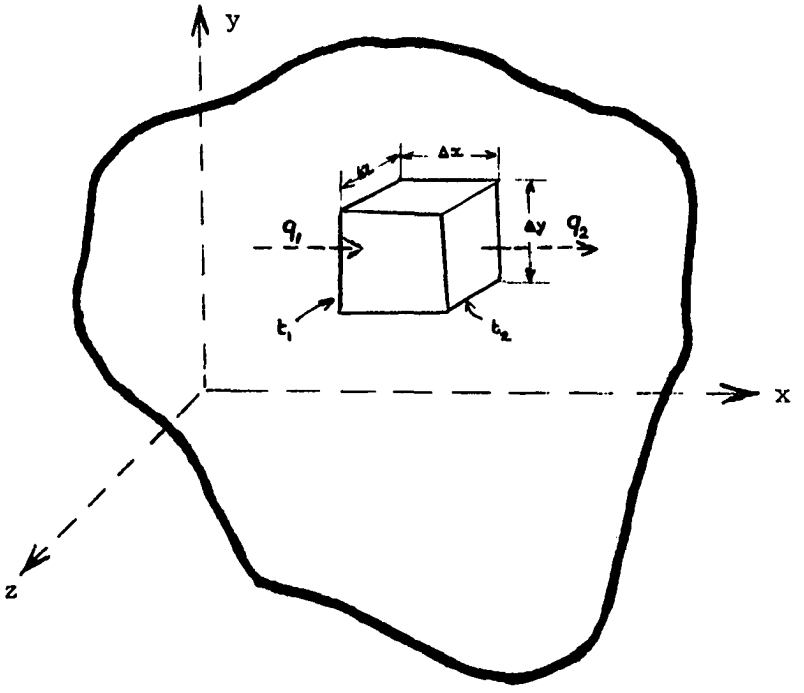

Figure 5.1. Control volume for energy balance

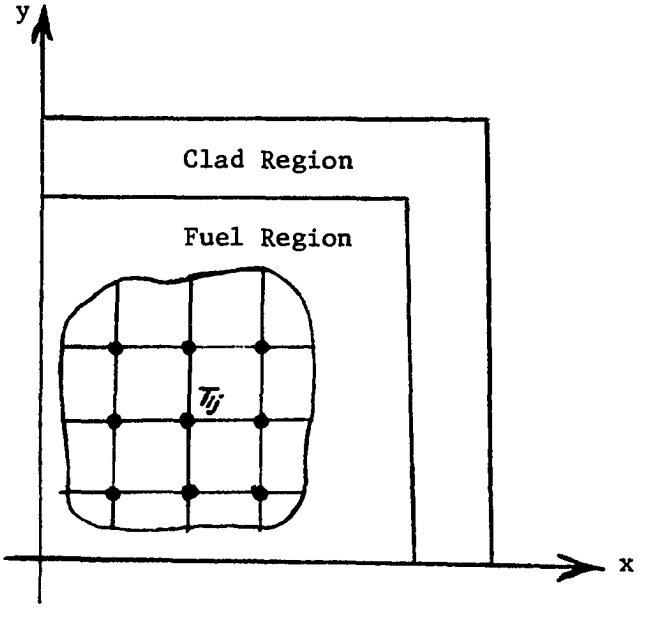

Figure 5.2. The different material regions of the fuel element

$$K\left[\frac{T_{i+1,j} - 2T_{ij} + T_{i-1,j}}{\Delta x^2} + \frac{T_{i,j+1} - 2T_{ij} + T_{i,j-1}}{\Delta y^2}\right]$$

$$+ S = \rho C_p \frac{\partial T}{\partial t} \quad . \tag{5.3}$$

5.2.2 Explicit method

This method uses the forward-difference formula for the left side of Equation (5.3) as

$$\left.\frac{\partial T}{\partial t}\right|_{i,j,k} = \frac{T^{k+1}_{i,j} - T^{k}_{i,j}}{\Delta t} + O(\Delta t) \tag{5.4}$$

where k is the time step, $T^{k}_{i,j}$ is the nodal temperature at the present time, $T^{k+1}_{i,j}$ is the temperature at the advanced time, and Δt is the time increment.

Introducing Equation (5.4) into Equation (5.3), and solving for the five-point nodal temperature in the advanced time ($T^{k+1}_{i,j}$), one gets

$$T^{k+1}_{ij} = T^{k}_{ij}\left[1 - \frac{2K\,\Delta t}{\rho C_p}\left(\frac{\Delta x^2 + \Delta y^2}{\Delta x^2 \cdot \Delta y^2}\right)\right]$$

$$+ \frac{\Delta t}{\rho C_p} K\left[\frac{T^{k}_{i+1,j} + T^{k}_{i-1,j}}{\Delta x^2} + \frac{T^{k}_{i,j+1} + T^{k}_{i,j-1}}{\Delta y^2}\right]$$

$$+ \frac{S\,\Delta t}{\rho C_p} \quad . \tag{5.5}$$

In Equation (5.5), which is the five-point relation, the unknown temperature T^{k+1}_{ij} at the time step (k+1) can be directly determined from

the knowledge of the five-point temperatures (adjacents and central, see Figure 5.2) at the previous time step, k.

Equation (5.5) provides a relatively straight forward expression for the determination of the unknowns T_{ij}^{k+1}, i = 1,2....N; j = 1,2,.... M, at the time step k + 1. The only disadvantage of this method is that once the thermal properties and the step sizes Δx, and Δy are fixed, there is a maximum permissible step size Δt, which must not be exceeded because of instability considerations. For the case of five-point relation, the stability criterion is given by

$$\Delta t \leq \gamma \frac{\rho C_p \Delta x^2 \Delta y^2}{2K(\Delta x^2 + \Delta y^2)} \quad . \tag{5.6}$$

A parameter γ can be inserted into Equation (5.6) for optimization purposes.

5.2.3 Nine-point relation

Considering Equation (5.2) and Equation (2.8) for the Laplacian Operator, one has

$$\frac{K}{h_1 h_2}\left[\left(\frac{1}{\beta} - p\right)\left(T_{i+1,j}^k + T_{i-1,j}^k\right) + (\beta - p)\left(T_{i,j+1}^k + T_{i,j-1}^k\right)\right.$$

$$\left. + \frac{p}{2} T_c - 2\left(\frac{1}{\beta} + \beta - p\right) T_{ij}^k\right] - \frac{K h_2^2}{12}\left[\beta^2 D_x^4 + D_y^4 + 6\beta p D_{xy}^2\right] T_{ij}^k$$

$$+ S = \rho C_p \left(\frac{T_{ij}^{k+1} - T_{ij}^k}{\Delta t}\right) \tag{5.7}$$

where

$$h_1 = \Delta x,$$

$$h_2 = \Delta y \text{ and}$$

$$\beta = \Delta x/\Delta y \ .$$

As in the steady-state case, the order of truncation error is determined by an appropriate choice of the parameter, p. If p = 0, one gets the five-point relation given by Equation (5.5). To get $0(h^4)$ for the spatial part of the calculation set

$$\frac{K\, h_2^2}{12} \left(\beta^2\, D_x^4 + D_y^4 + 6\beta p D_{xy}^2\right) T_{ij} = 0 \tag{5.8}$$

one has

$$p = \frac{\frac{1}{\beta} + \beta}{6} - \frac{(\beta^2 D_x^2 + D_y^2)\ \nabla^2 T}{6\beta D_{xy}^2\ T} \tag{5.9}$$

where $\nabla^2 T$ is given by

$$\nabla^2 T = \frac{\rho\, C_p}{K} \frac{\partial T}{\partial t} - \frac{S}{K} \ . \tag{5.10}$$

The numerator of the second term in Equation (5.9) becomes

$$p_{N_2} = (\beta^2 D_x^2 + D_y^2)\ \nabla^2 T = \frac{\beta^2\ \rho\ C_p}{K} \frac{\partial}{\partial x} \cdot \left[\frac{\partial}{\partial x}\left(\frac{T_{ij}^{k+1} - T_{ij}^{k}}{\Delta t}\right)\right]$$

$$+ \left\{D_y \cdot \left[D_y \cdot \left(\frac{T_{ij}^{k+1} - T_{ij}^{k}}{\Delta t}\right)\right]\right\} \cdot \frac{\rho\ C_p}{K} \tag{5.11}$$

Since the temperature is given, one can use the separation of variables to get

$$T(x,y,t) = f(x,y) \cdot g(t) \ . \tag{5.12}$$

Thus, using the chain rule one has

$$D_t \ T(x,y,t) = f(x,y) \cdot g_t(t) \tag{5.13}$$

$$D_x^2 \ D_t T(x,y,t) = f_{xx}(x,y) \cdot g_t(t) \ . \tag{5.14}$$

Again using the chain rule, one gets

$$D_x^2 \ D_t T = D_t \ D_x^2 T \tag{5.15}$$

so that

$$p_{21} = \frac{\partial}{\partial t} \left(\frac{\partial^2 T}{\partial x^2}\right) = \frac{\partial}{\partial t} \left[\frac{T_{i+1,j} - 2T_{ij} + T_{i-1,j}}{h_1^2}\right]$$

$$= \frac{1}{h_1^2 \ \Delta t} \left[T_{i+1,j}^{k+1} - T_{i+1,j}^{k} - 2(T_{ij}^{k+1} - T_{ij}^{k})\right.$$

$$\left. + T_{i-1,j}^{k+1} - T_{i-1,j}^{k}\right] \tag{5.16}$$

and

$$p_{22} = D_t \cdot (D_y^2 T) = \frac{1}{h_2^2 \ \Delta t} \left[T_{i,j+1}^{k+1} - T_{i,j+1}^{k} - 2(T_{ij}^{k+1} - T_{ij}^{k})\right.$$

$$\left. + T_{i,j-1}^{k+1} - T_{i,j-1}^{k}\right] \ . \tag{5.17}$$

Equation (5.9) becomes

$$p = \frac{\frac{1}{\beta} + \beta}{6} - \frac{(\beta^2 p_{21} + p_{22})}{6\beta D_{xy}^2 \ T} \cdot \left(\frac{\rho \ C_p}{K}\right) \tag{5.18}$$

where $D^2_{xy}T$ is given by Equation (3.18).

From Equation (5.7), one gets the nodal temperature at the advanced time for the nine-point relation as

$$T^{k+1}_{ij} = T^k_{ij} \left[1 - \frac{2\,K\,\Delta t}{\rho\, C_p\, h_1 h_2} \left(\beta + \frac{1}{\beta} - p\right)\right]$$

$$+ \frac{\Delta t\, K}{\rho\, C_p\, h_1 h_2} \left[\left(\frac{1}{\beta} - p\right)\left(T^k_{i+1,j} + T^k_{i-1,j}\right)\right.$$

$$\left. + (\beta - p)\left(T^k_{i,j+1} + T^k_{i,j-1}\right) + \frac{p}{2}\, T_c\right] + \frac{\Delta t\, S}{\rho\, C_p} \quad . \tag{5.19}$$

It can be seen that the stability criteria, in this case, is a function of the parameter p which is itself a function of the solution, and given as

$$\Delta t = \gamma(\rho\, C_p\, h_1 h_2)/\left[2\,K\left(\beta + \frac{1}{\beta} - p\right)\right] \quad . \tag{5.20}$$

5.3 Unsteady-State Results with Constant Thermal Properties and Heat Generation

5.3.1 UO_2 fuel element

The UO_2 fuel element at the steady-state case is considered to have a specific heat capacity of 0.32 KJ/Kg°C and a density of 10,400 Kg/m^3. As the computational results show in Figures 5.3 and 5.4, the absolute and the relative L_2 norm errors for the nine-point relation for both cases (i.e. for the parameter p being equal only to the first term and for the parameter p to include all terms) are more accurate than the five-point relation. One can note that the nine-point relation which

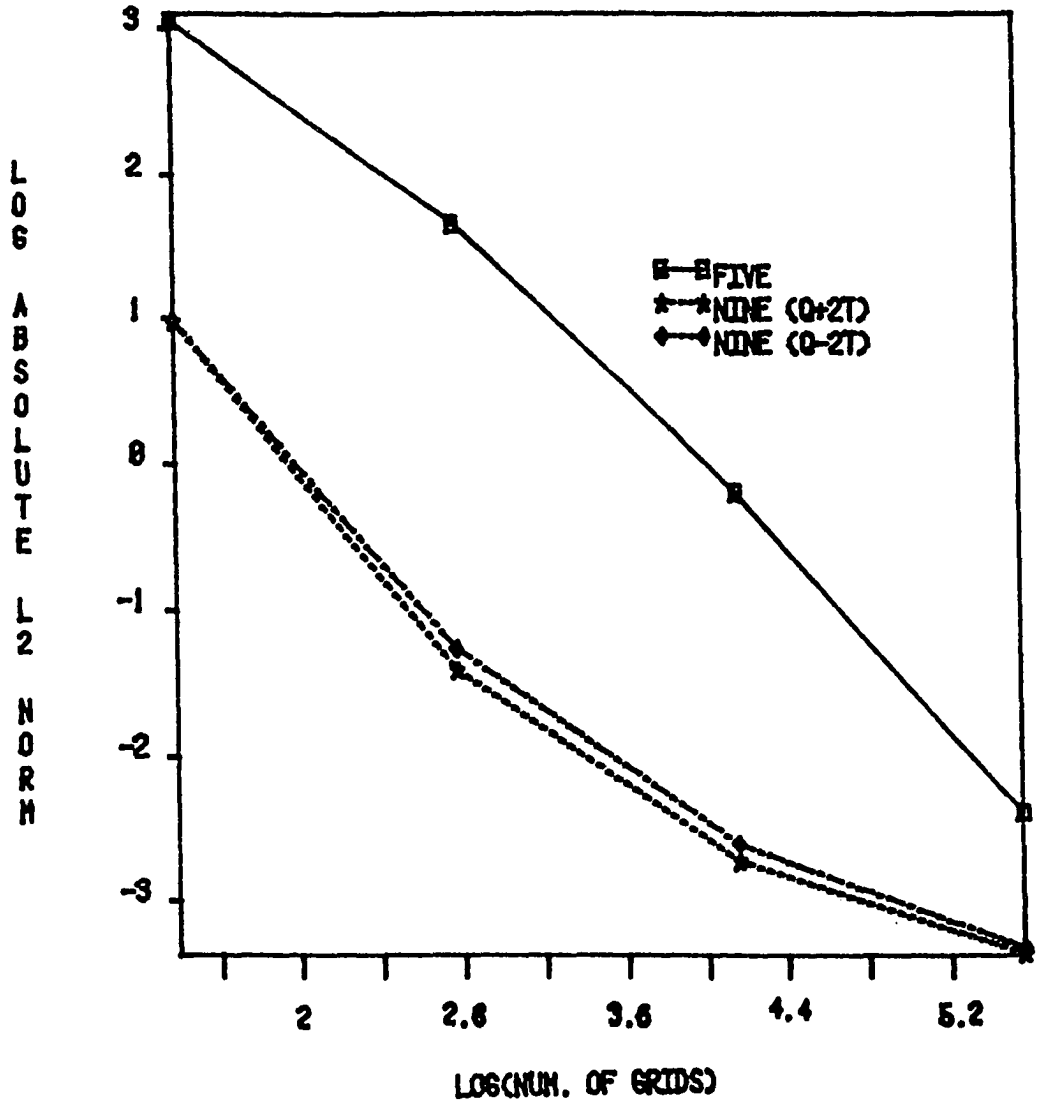

Figure 5.3. Log absolute L_2 norm versus Log (num. of grids) for unsteady-state case, constant K and S for UO_2 fuel element

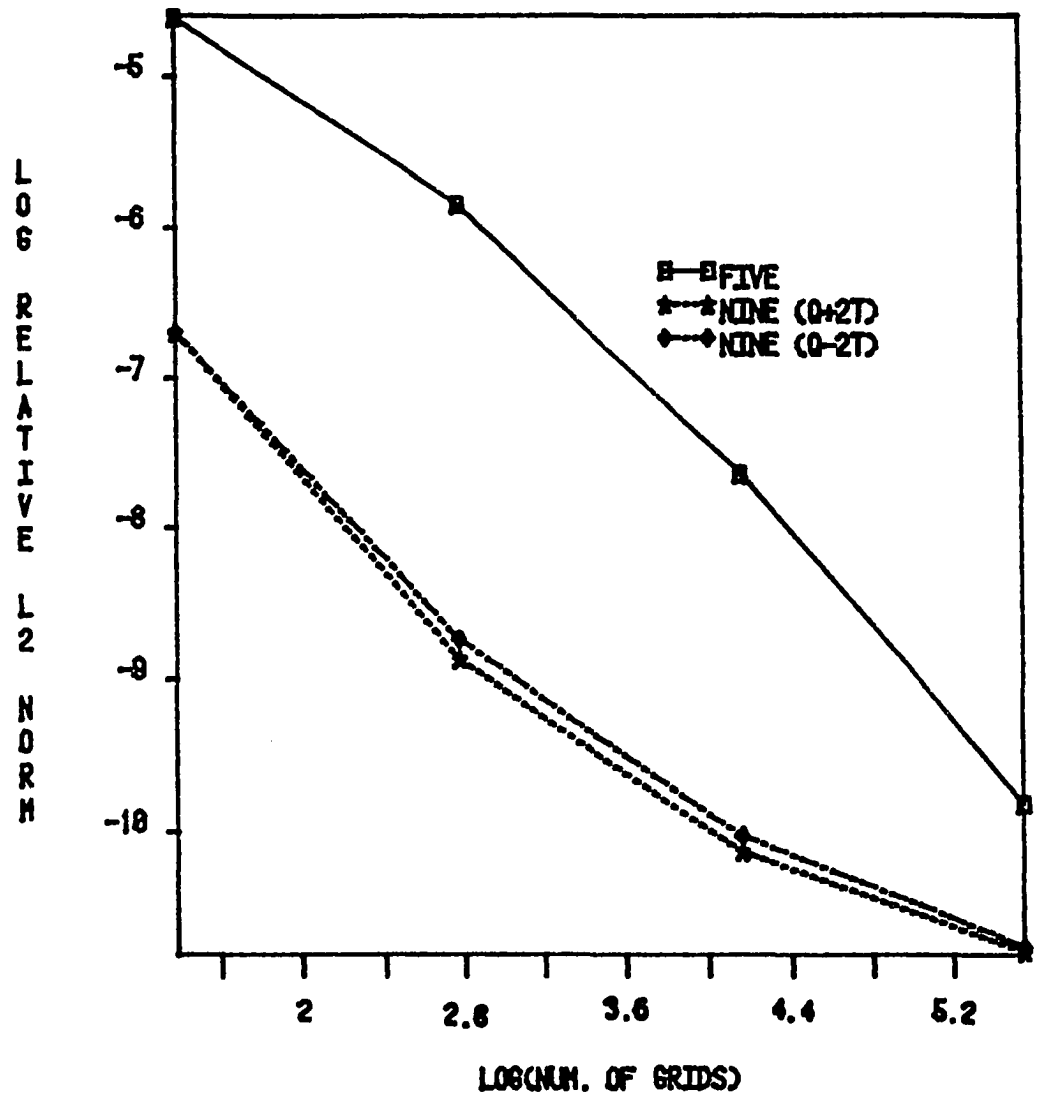

Figure 5.4. Log relative L_2 norm versus Log (num. of grids) for unsteady-state case, constant K and S for UO_2 fuel element

includes all terms for p turns out to be slightly more accurate than the relation which includes only the first term for p (see Equation (5.9)). Figures 5.5 through 5.8 show that the nine-point relation converges faster than the five-point relation.

5.3.2 General mechanical problem

The general mechanical problem in the slab at steady-state conditions is considered to have a specific heat capacity of 167 J/Kg °K and a density of 3×10^4 Kg/m^3. The exact analytical method which is considered as a reference case is given using the separation of variable by [22]

$$T(x,y,t) = \frac{S\,A^2}{K} \cdot \{\frac{1}{2}(1 - \frac{x^2}{A^2}) - \frac{16}{\pi^3} \sum_{m=0}^{\infty} (-1)^m [\cos (\frac{2m+1}{2})\pi \frac{x}{A}]$$

$$\cdot [\cosh. (\frac{2m+1}{2})\pi \frac{y}{B}]/(2m+1)^3 [\cosh. (\frac{2m+1}{2}) \frac{\pi B}{A}]$$

$$- \frac{64}{\pi^4} \sum_{m=0}^{\infty} \sum_{n=0}^{\infty} (-1)^{m+n} [\cos \frac{2m+1}{2} \pi \frac{x}{A}]$$

$$\cdot [\cos \frac{2n+1}{2} \pi \frac{A}{B} \frac{y}{B}]$$

$$- \alpha_T t/A^2 [\frac{(2n+1)^2\pi^2A^2}{4B^2} + \frac{(2m+1)^2\pi^2}{4}]$$

$$\cdot e$$

$$/(2m+1)(2n+1) [(2n+1)^2 A^2/B^2 + (2m+1)^2]\} \qquad (5.21)$$

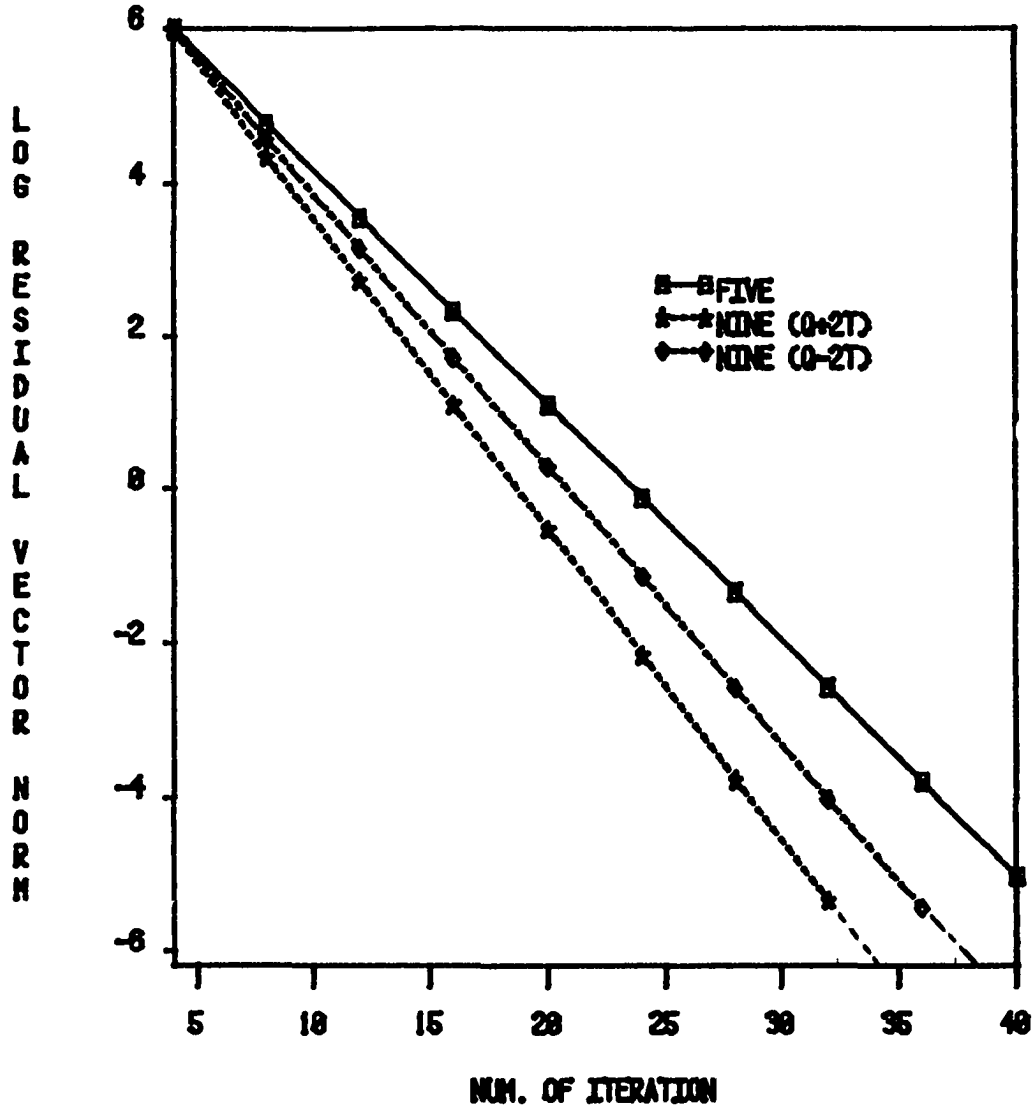

Figure 5.5. Log residual vector norm versus num. of iterations for the case of a 4 by 4 grid region, unsteady-state, constant K and S, for a UO_2 fuel element

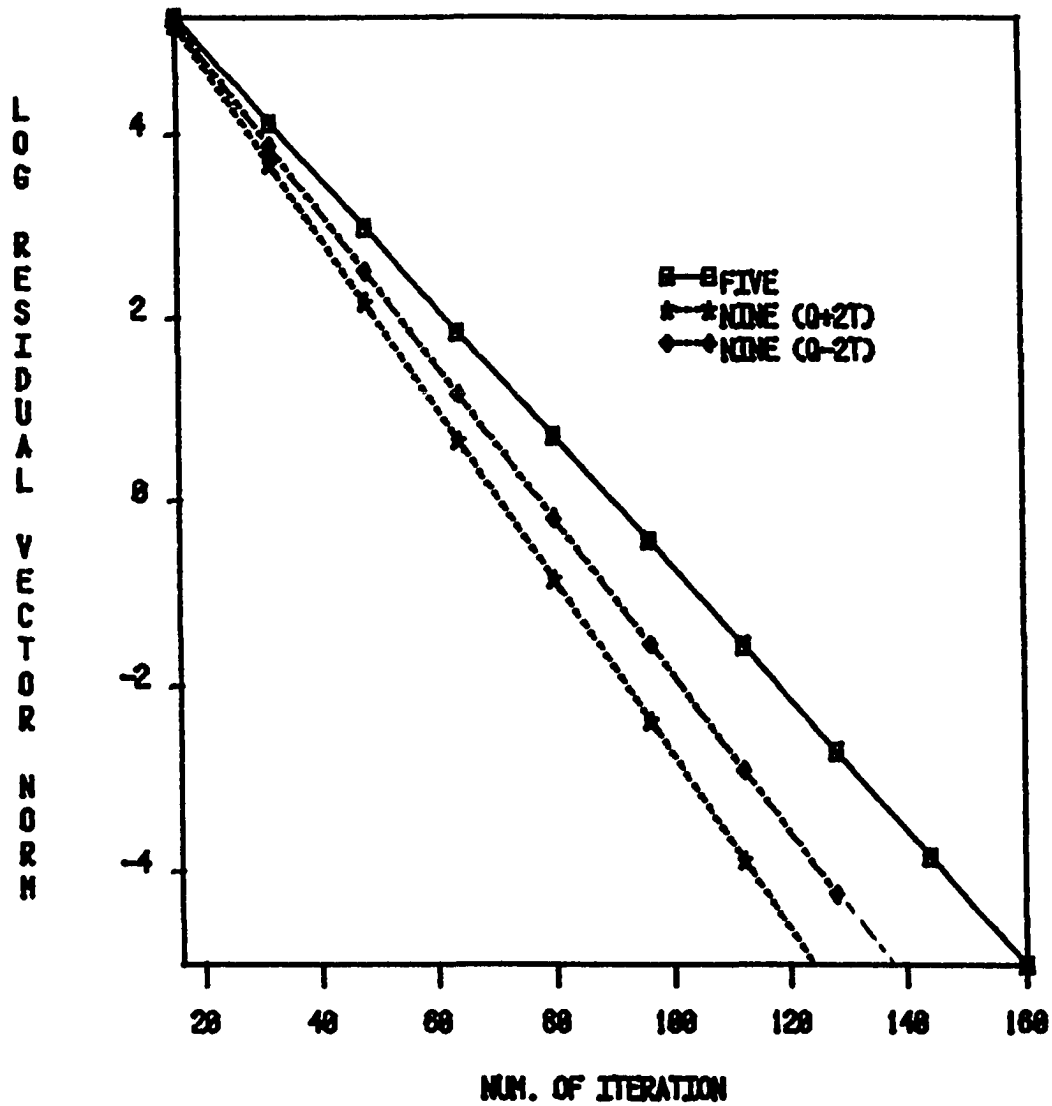

Figure 5.6. Log residual vector norm versus num. of iteration for the case of a 8 by 8 grid, unsteady-state, constant K and S, for UO_2 fuel element

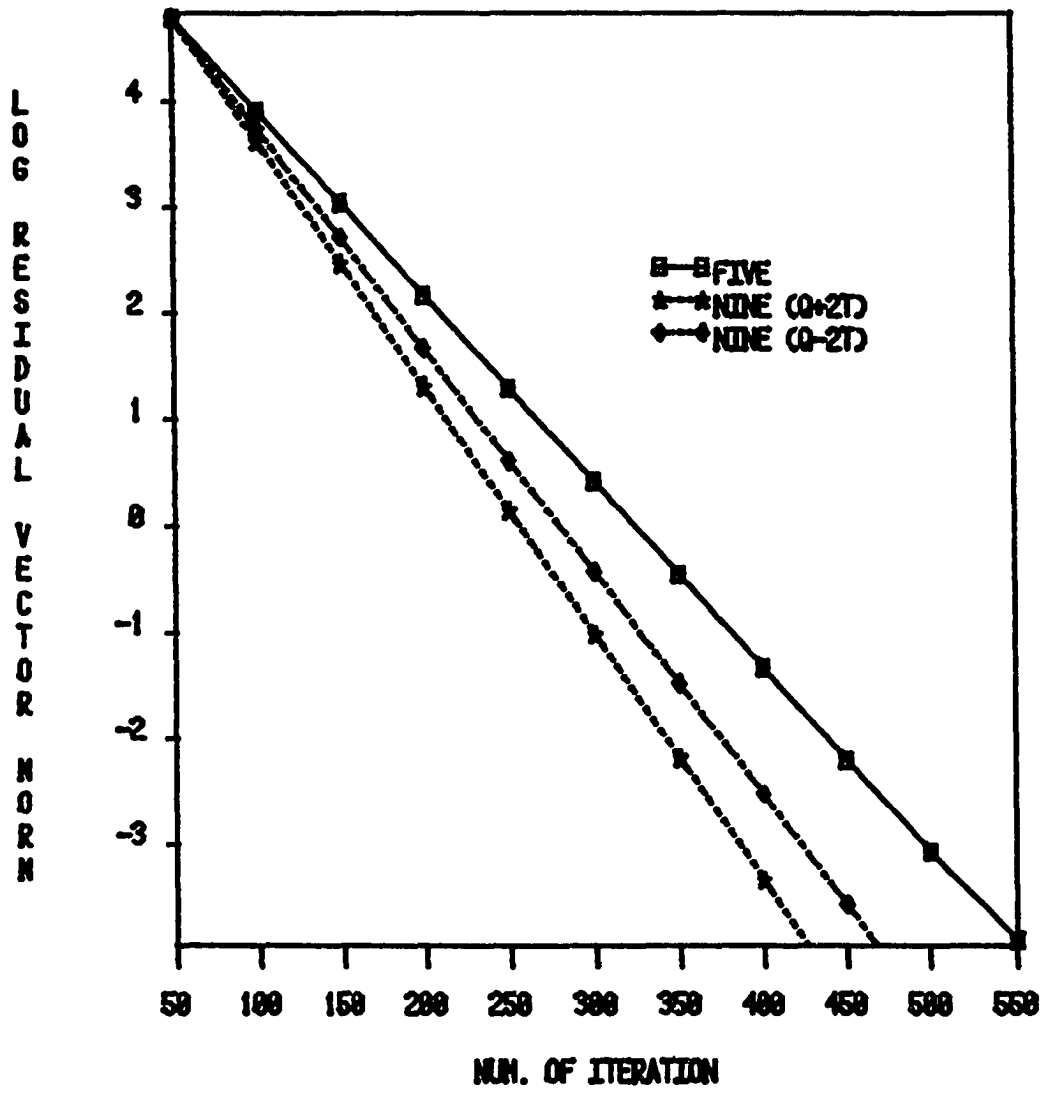

Figure 5.7. Log residual vector norm versus num. of iteration in case of a 16 by 16 grid, unsteady-state, constant K and S, for UO_2 fuel element

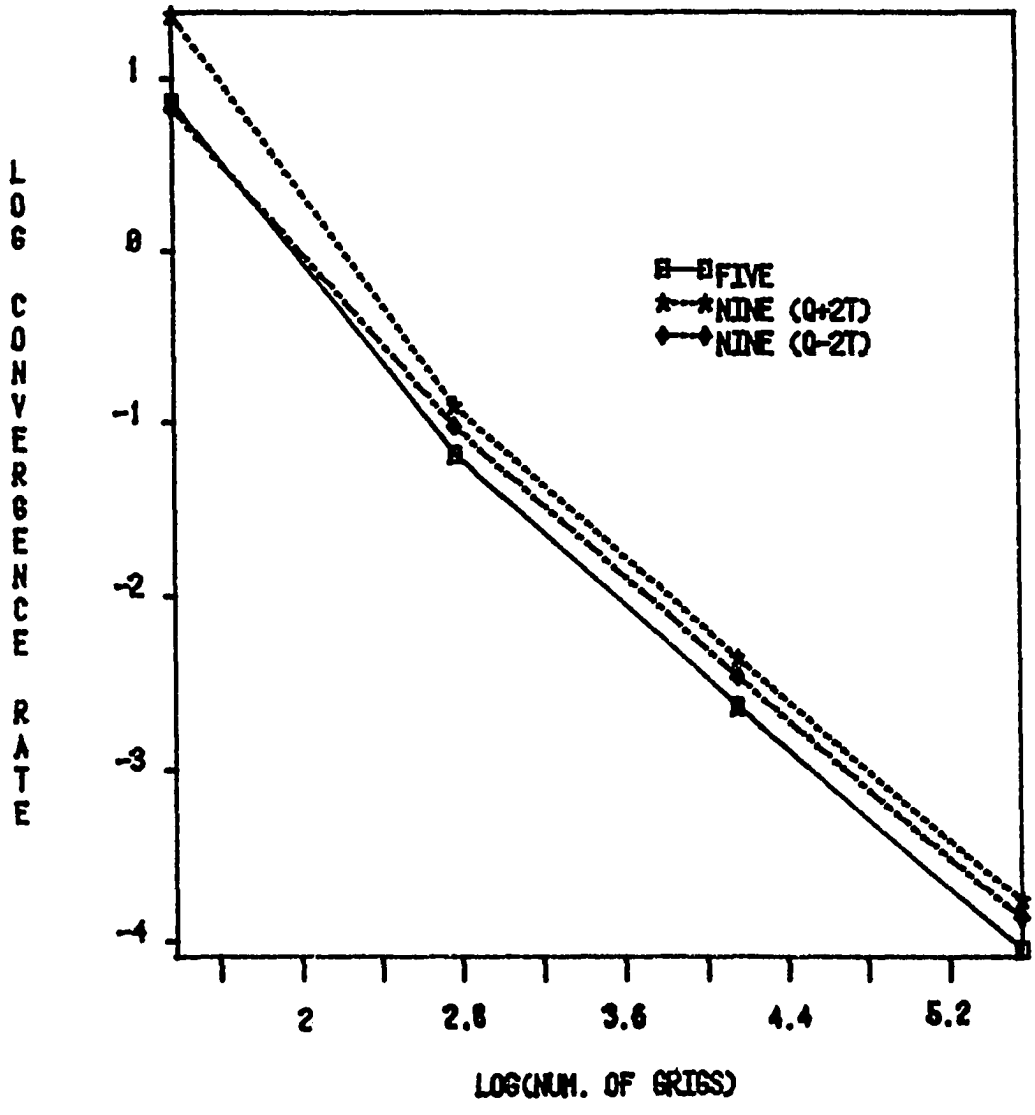

Figure 5.8. Log convergence rate versus Log (num. of grids) in case of steady-state, constant K and S, for UO_2 fuel element

where α_T is the thermal diffusivity given by

$$\alpha_T = \frac{K}{\rho C_p} . \tag{5.22}$$

The computational results of the absolute and relative errors are shown in Figures 5.9 and 5.10, and Figure 5.11 shows the convergence rate. As a result, the nine-point relation that used p as the first term of the Equation (5.9) is more accurate and converges faster than the five-point relation.

5.3.3 Optimization of the errors

Again, consider the slab of the steady-state general mechanical problem case. As mentioned before, a parameter (γ) was inserted into the stability criterion equations (Equation (5.6) corresponds to the five-point relation, and Equation (5.20) corresponds to the nine-point relation) in order to increase or decrease the step size Δt. By changing the parameters (γ) for a given thermal property and space size, one can optimize the absolute and relative errors. Figures 5.12 and 5.13 correspond to the nine-point and five-point relations, respectively. Figures 5.12 and 5.13 show the decrease in the absolute errors as the step size increases from 10% to 100% of its original value; after 100%, the solution becomes unstable.

5.4 Variable Thermal Conductivity

Taking the analytical method developed in Appendix D as the reference case, the computational results of the nine-point (p being only the first term) and the five-point relations are given in

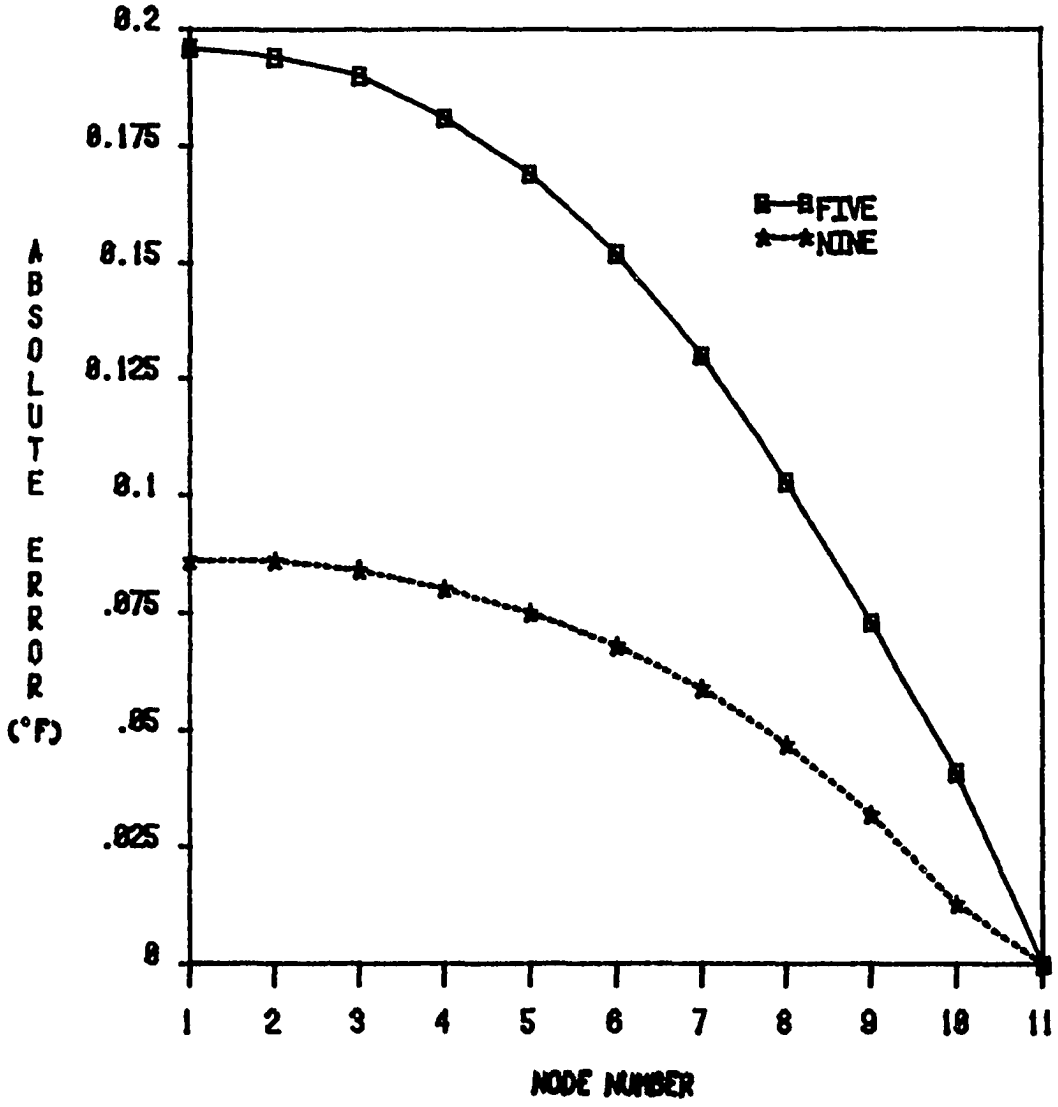

Figure 5.9. Absolute error comparison along the y-axis for the centerline temperature (unsteady-state case with constant thermal properties and heat source)

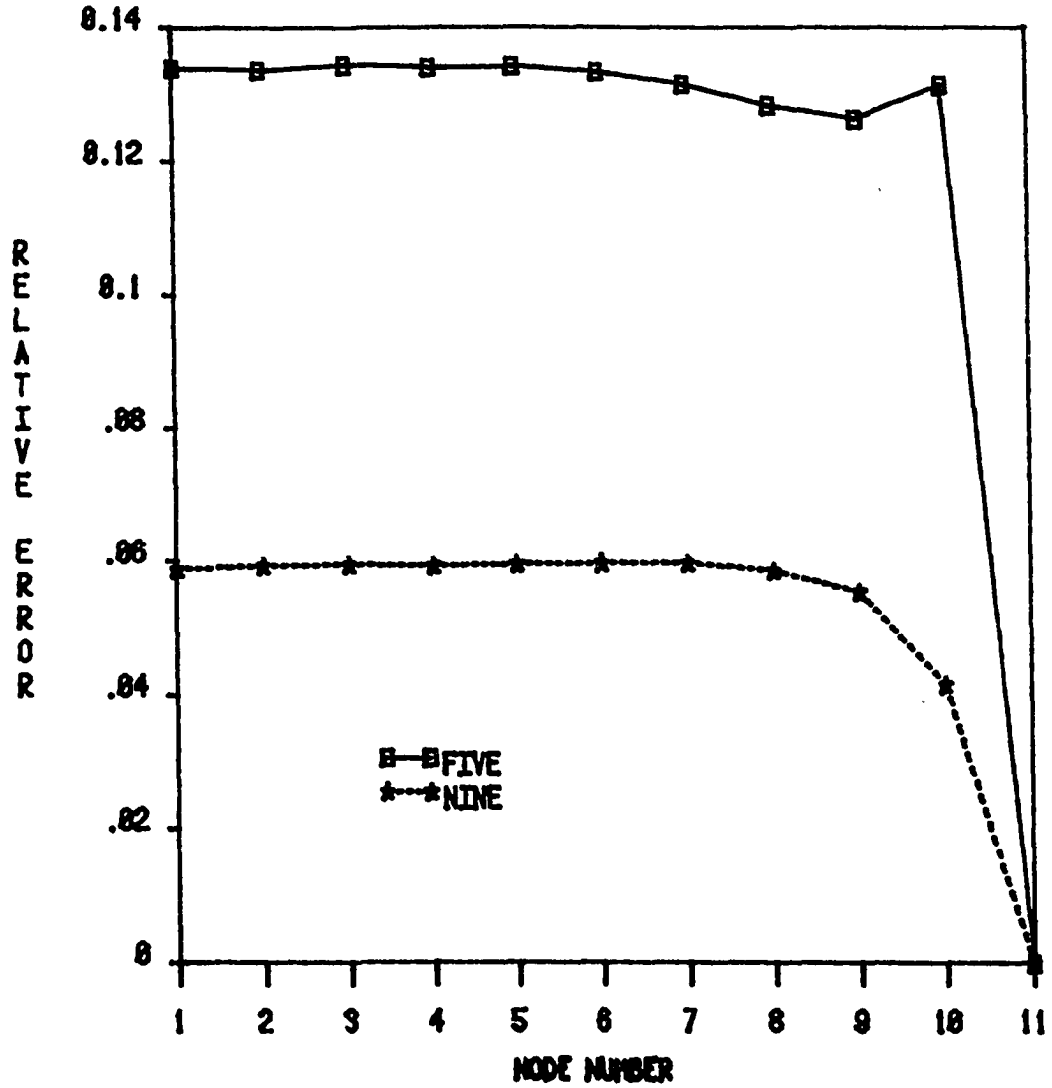

Figure 5.10. Relative error comparison along the y-axis for the centerline temperatures (unsteady-state case with constant thermal properties and heat source)

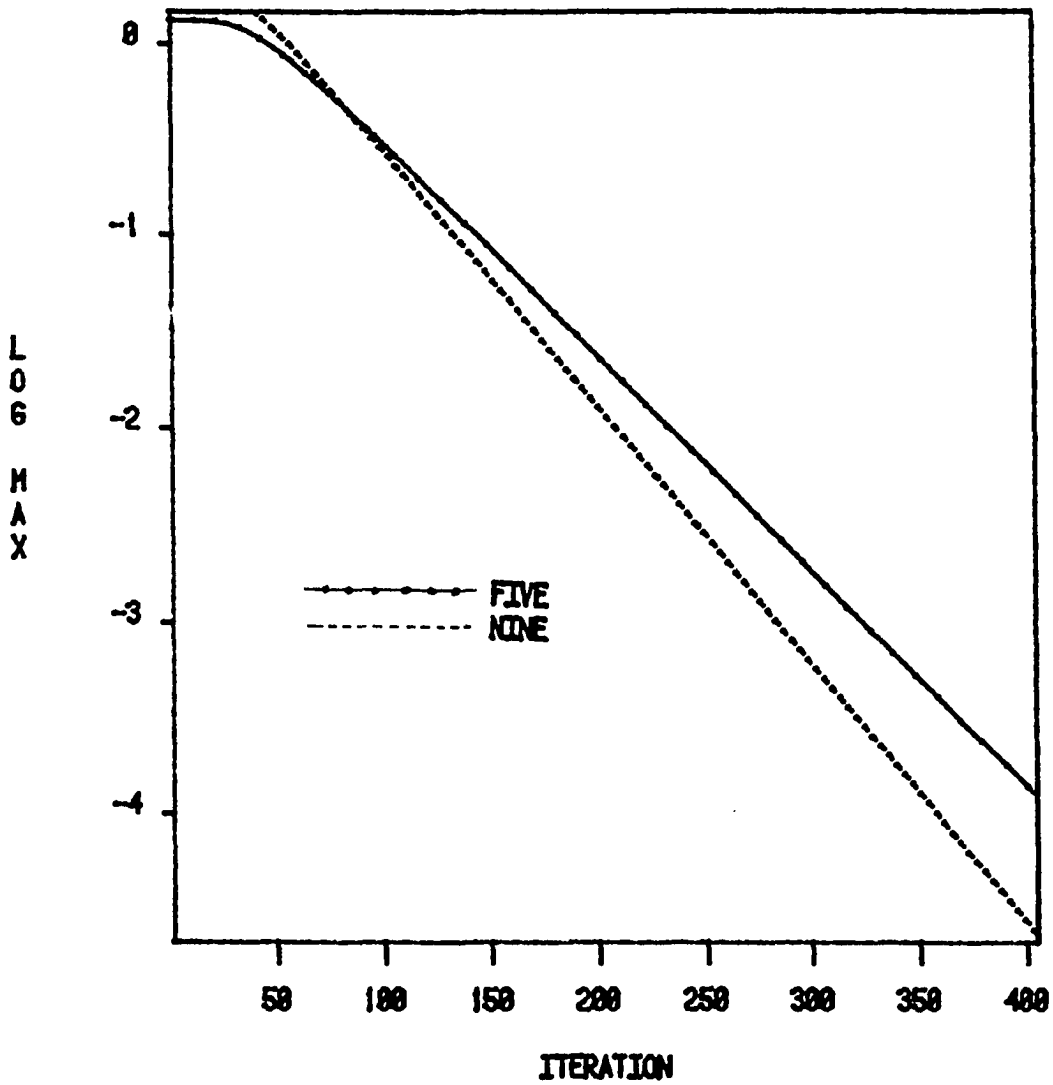

Figure 5.11. Residual norm for the nine- and five-point approximations (unsteady-state case with constant thermal properties and heat source)

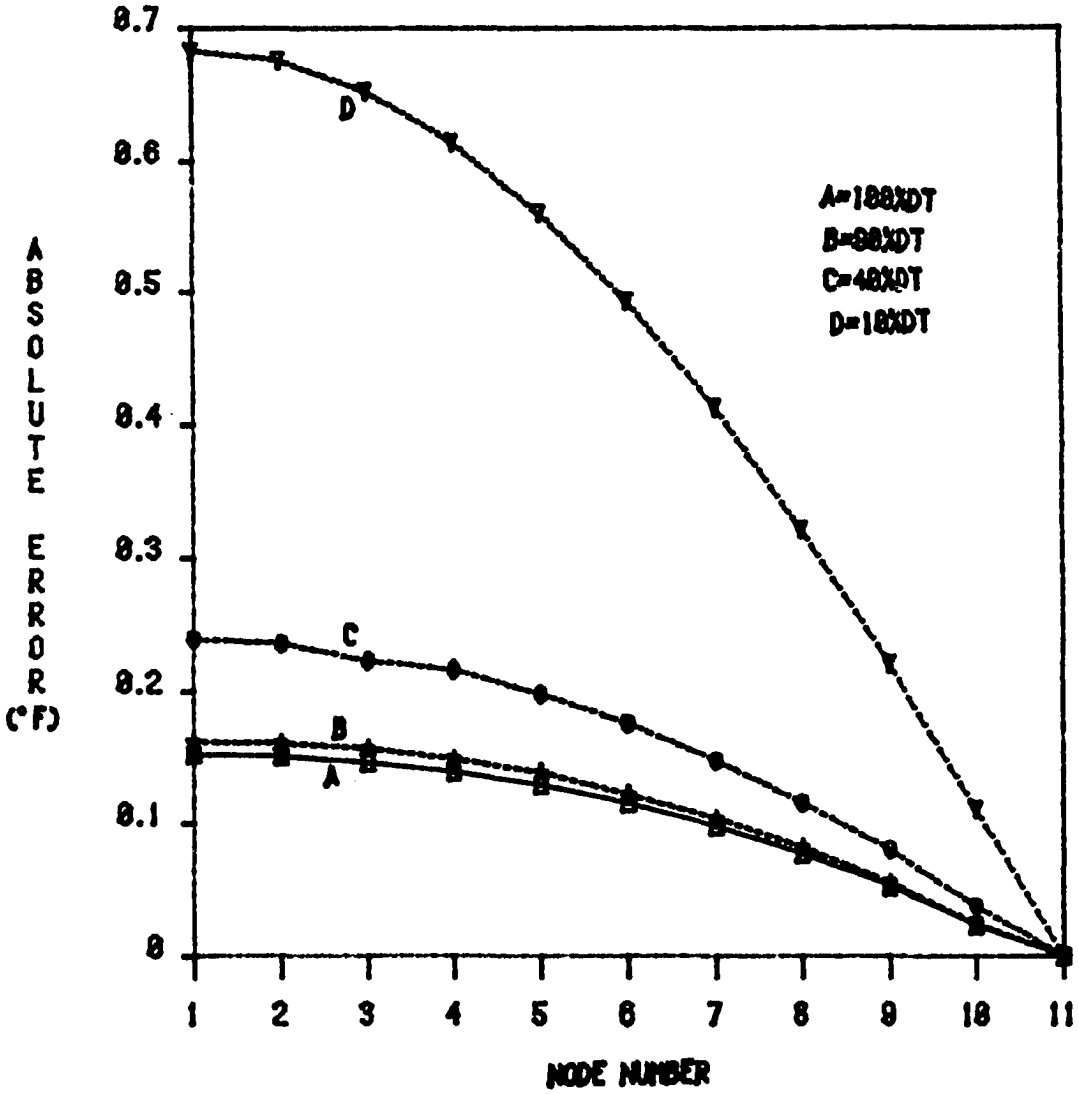

Figure 5.12. Absolute error comparison along the y-axis for the centerline temperatures of the nine-point relation (unsteady-state case with constant K and S)

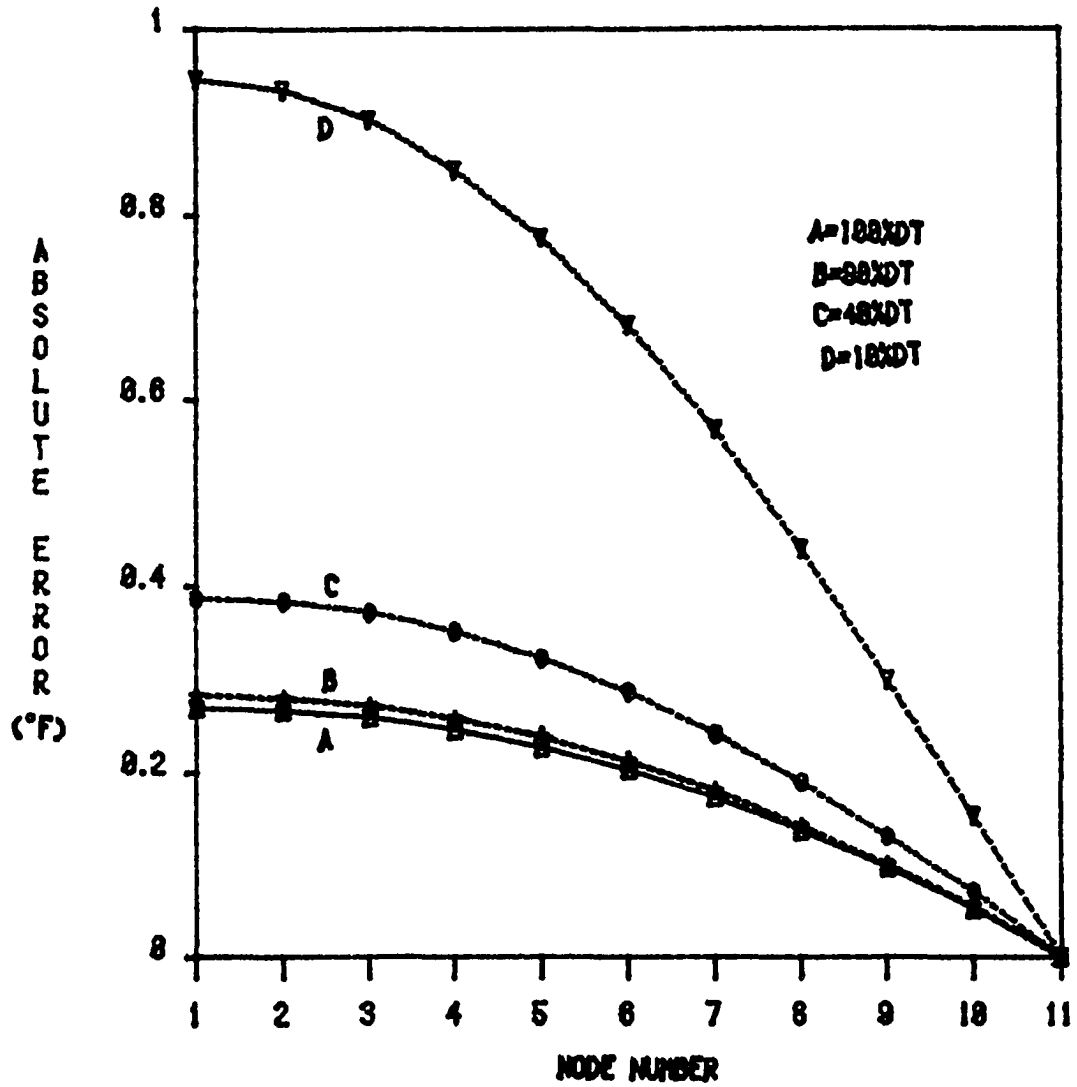

Figure 5.13. Absolute error comparison along the y-axis for the centerline temperatures of the five-point relation (unsteady-state case with constant K and S)

Figure 5.14. Therefore, the nine-point relation is more accurate than the five-point relation, and also from Figure 5.15 it can be observed that the nine-point relation converges faster than the five-point relation.

5.5 Variable Internal Heat Generation

As it was done in the slab for the steady-state case, the heat generation (S) is in the form $S = S_o XY$. Here again, one comes to the same conclusions of higher accuracy and faster convergence for the nine-point relation as compared to the five-point relation. This can be observed in Figures 5.16 and 5.17.

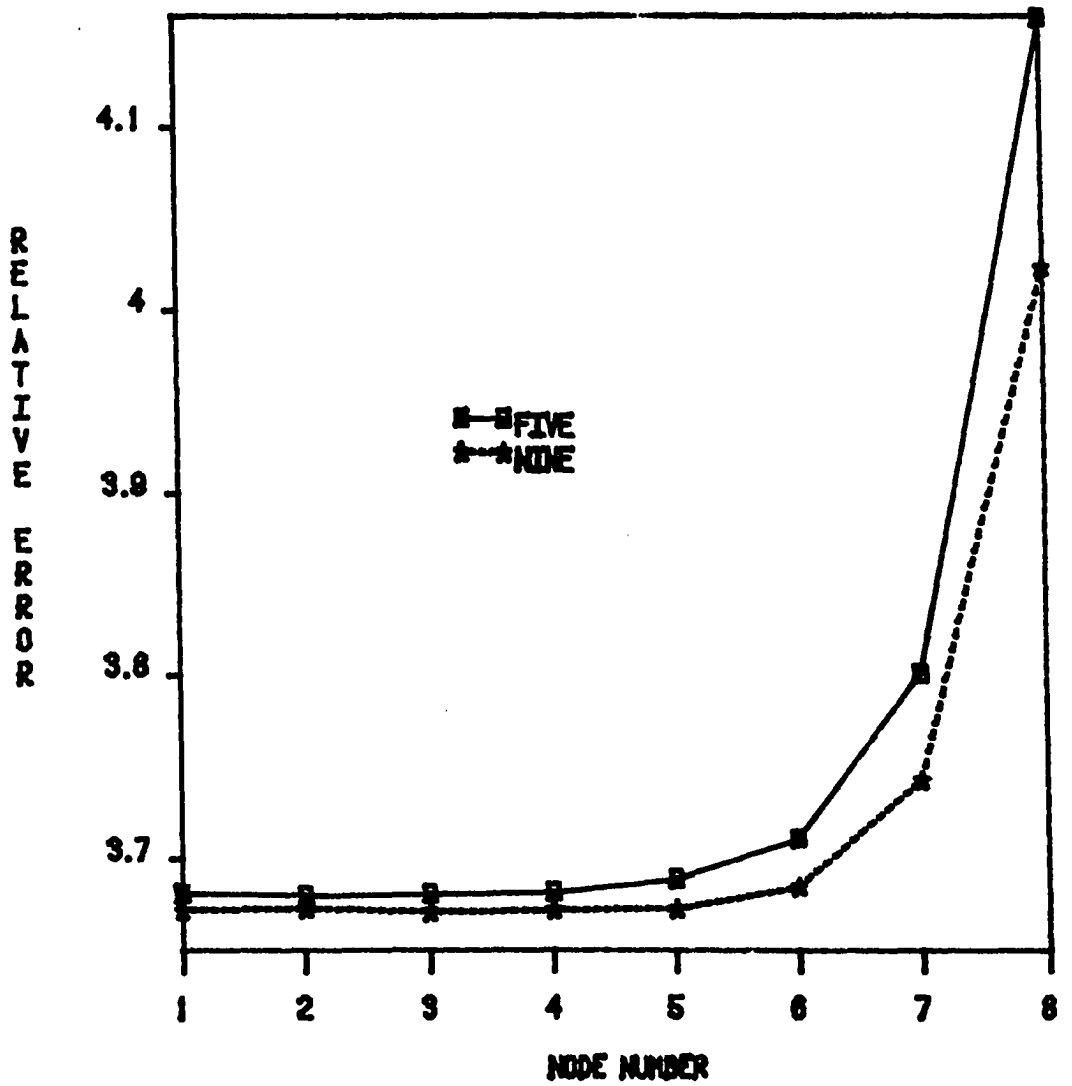

Figure 5.14. Relative error comparison along the y-axis for the unsteady-state case with $K = K_o (1 + \xi T)$

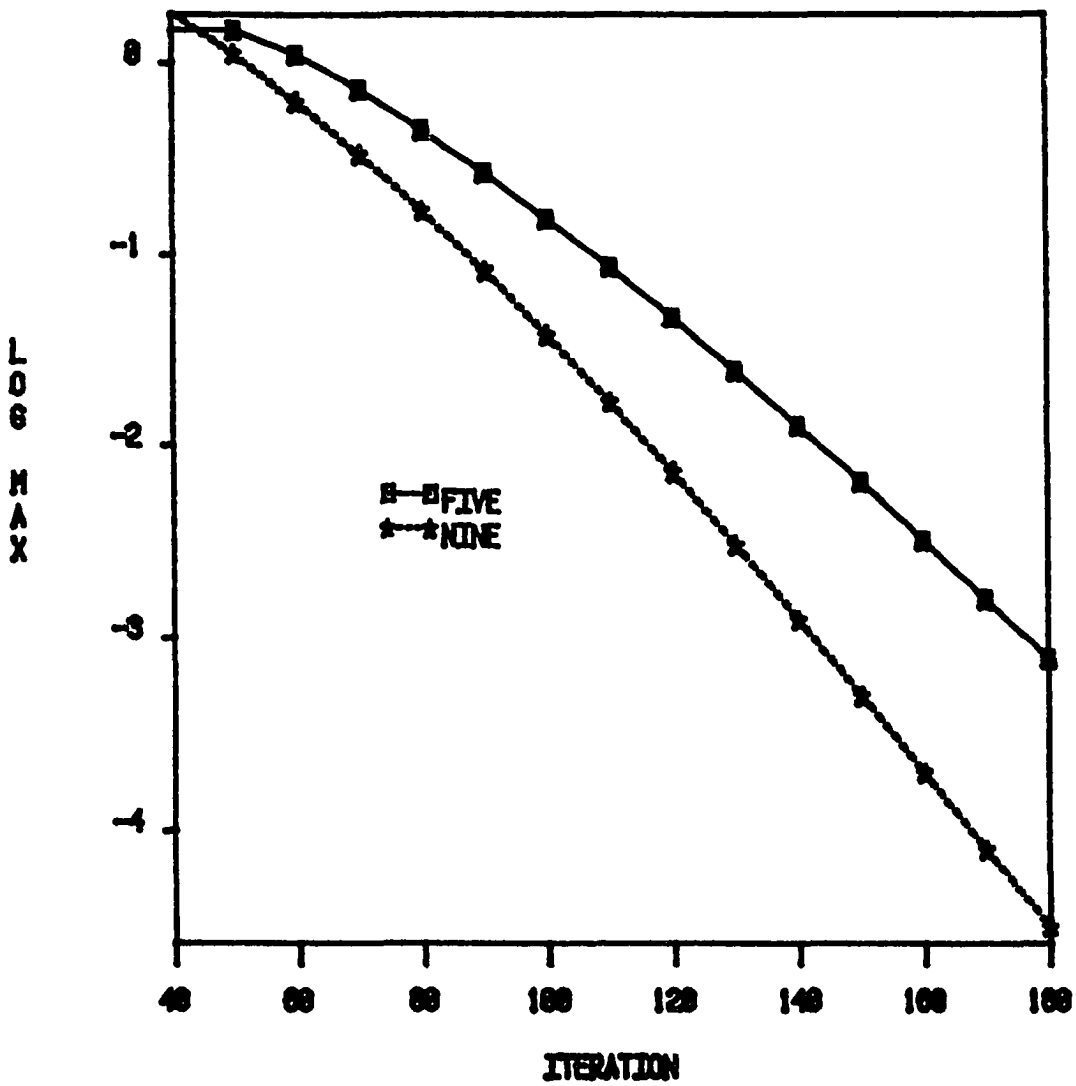

Figure 5.15. Residual norm for the nine- and five-point approximations (unsteady-state case with $K = K_o (1 + \xi T)$)

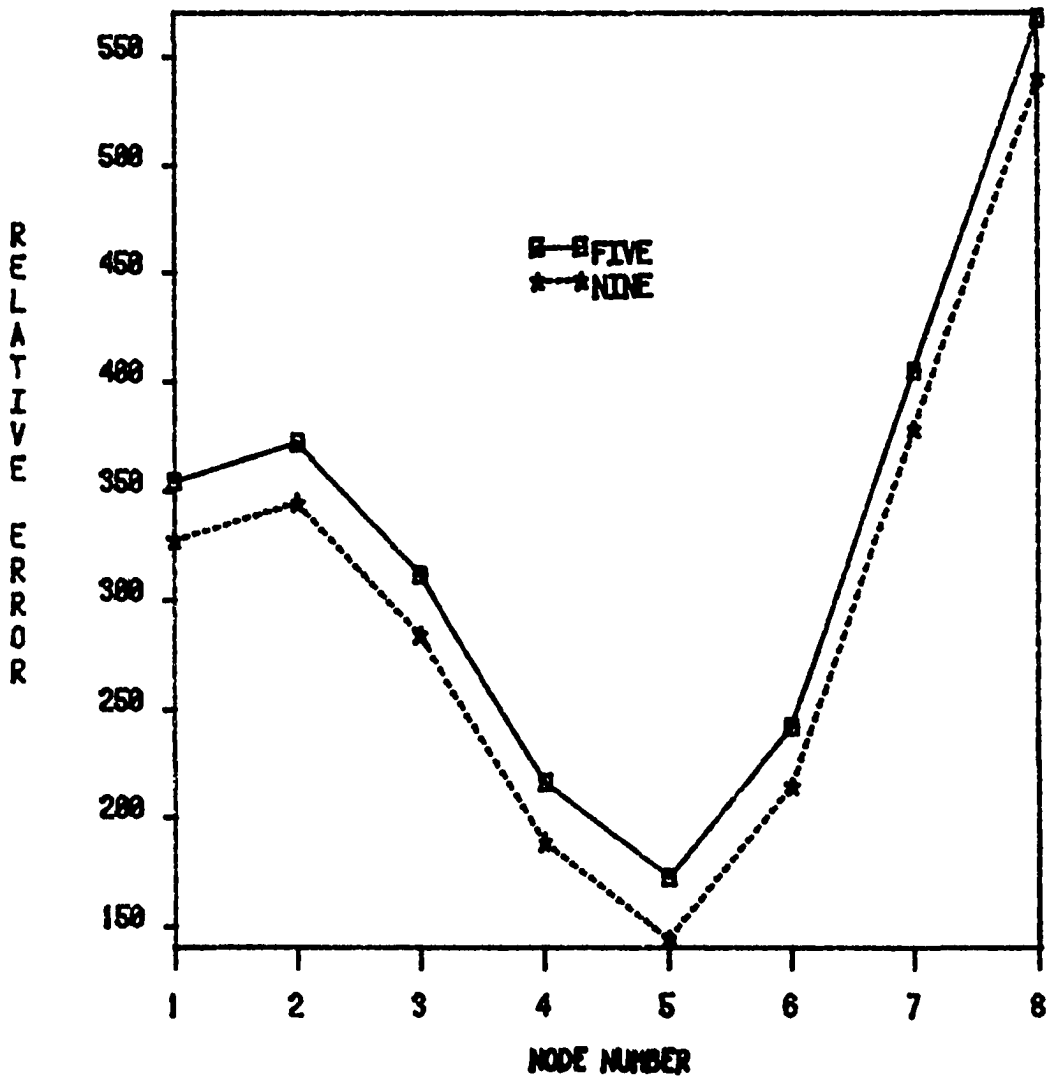

Figure 5.16. Relative error comparison along the y-axis in case of unsteady-state with $S = S_o XY$

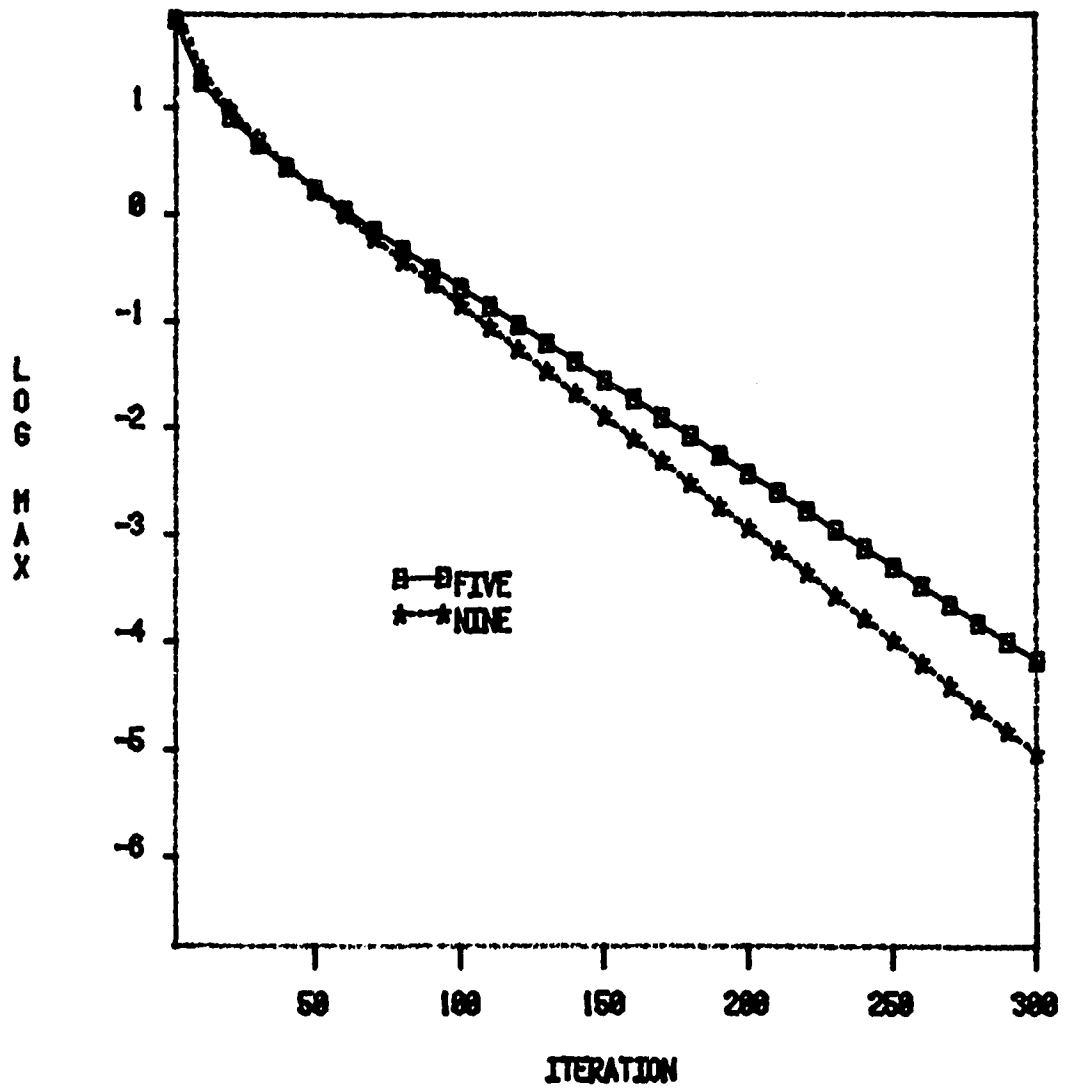

Figure 5.17. Residual norm for the nine- and five-point relations in the case of unsteady-state with $S = S_o XY$

6. SUMMARY, CONCLUSIONS AND SUGGESTIONS FOR FURTHER STUDY

6.1 Summary

As stated previously, the objective of this study was the comparison of two-dimensional finite difference relations for the heat conduction equation over a nuclear fuel element: the two methods are the nine-point relation developed in Chapter 2, and the usual five-point relation. The comparison was made to show the higher accuracy of the nine-point relation and also to determine which relation converged more rapidly. This was done through the comparison of the solution error and speed of convergence. In order to make the analysis, it was necessary to relate the accuracy of the numerical solution to the number of grid points used. This was done through the use of a logarithmic plot of L_2 error norm versus the number of grid points used. In some cases, the absolute or relative errors were plotted as a function of the grid spacing.

To generate the data necessary for such plots, numerical and reference analytical solutions of problems applied to several different regions were calculated. The regions were of constant shape and size, and had the same range of x and y values. The data varied with the number of grid points used for each calculation. Thus from these solutions, specific error values could be calculated.

Most of the error calculations were made without any attempt for the optimization of the SOR parameter α.

Equations were developed for the nine-point, five-point relations, and for the reference analytical methods. These equations were based on the following assumptions.

1. The power generated in the fuel was either a function of x and y or a constant.
2. No heat was generated in the clad.
3. The fuel-clad gas gap was negligible.
4. The axial conduction was negligible.
5. The thermal conductivity of the fuel was known either as a linear function of temperature (this resulted in a non-linear governing equation for the temperature), or a constant.
6. The heat capacity and the density of the fuel were constant.
7. The thermal conductivity, the heat capacity and the density of the clad were constant.
8. The coolant and the fuel boundary temperatures were constant.

6.2 Conclusions

In assessing the work presented in the previous chapters, two types of problems were examined in most cases. One was an application of the techniques to a general mechanical slab for which an analytical method can be solved for the purpose of a reference case, and to test the program. The other problem was a direct application of the techniques to a nuclear fuel element that was an approximation of a fuel rod as shown in Figure 3.10.

The application of the nine-point and five-point relations to the steady-state heat conduction equation was considered with constant thermal properties and constant heat generation in Section 3.3. The nine-point relation provided a more accurate result than the five-point relation. However, up to an accuracy of 3.35×10^{-4} in terms of relative error (see Figure 3.13), approximately 12 grid points only were needed for the nine-point, whereas the five-point used more than 79 grid points for the same problem. Also, the nine-point converged faster than the five-point relation. The convergence rate was approximately 14% higher for the nine-point relation as compared to the five-point relation.

The heat generated in the nuclear fuel element was taken as a second order polynomial function in x and y in Section 3.4. A careful use, as mentioned in the dissertation, of the nine-point relation with the parameter, p, being taken as all the terms given by Equation (3.20) turned out to be more accurate than the five-point relation. Figure 3.16 shows that approximately, up to an accuracy of 1.23×10^{-4} for the relative error, 84% fewer grid points were needed for the nine-point relation. In this case, Equation (3.20) was used for the parameter, p. About 58% fewer grid points were needed for the nine-point relation when the parameter, p, was given by Equation (3.21) . Also, in both cases the nine-point relation converged faster than the five-point relation. On the average, the convergence rate was about 65% higher for the nine-point relation with p given by Equation (3.20), and 18% higher with p given by Equation (3.21).

The thermal conductivity of the nuclear fuel element was taken as a linear function of the temperature in Section 3.5 and the numerical relations were developed for equal spacing. The parameter, p, was a sum of three different terms (see Equation (3.39)). Except for the first term of p (i.e. $p_1 = 0.333$), the other terms were dependent on the solution itself. It was concluded from the computational results that the nine-point relation in both cases (i.e. $p = p_1$ and $p = p_1 + p_2 + p_3$) turned out to be more accurate than the five-point relation. However, the nine-point relation with $p = p_1 + p_2 + p_3$ was more accurate than the nine-point relation with $p = p_1$, especially in the case where a small number of grids were used. In cases where a 2 by 2 grid was used, the nine-point relation with $p = p_1 + p_2 + p_3$ had a 91% higher accuracy, whereas the nine-point relation with $p = p_1$ had a 32% higher accuracy as compared to the five-point relation (Figure 3.23). From the convergence point of view, the nine-point relation with $p = p_1 + p_2 + p_3$ was found not to converge as fast as the nine-point relation with $p = p_1$ when a large number of grids were used. This disadvantage was overcome by using the SOR technique with a specific optimum α.

Finally, in the steady-state case, the thermal conductivity of the nuclear fuel element was taken as a linear function of temperature. The heat generation was taken as a second order polynomial function in x and y. The computational results for this case showed a higher accuracy for the nine-point relation with $p = p_1 + p_2 + p_3$ than the nine-point relation with $p = p_1$ or the five-point relation.

Throughout this study, some verifications of the numerical values of the parameter, p, were made by considering a backward problem in which the solution to the problem was assumed given. This was done to verify the accuracy of the developments.

An illustrative problem was investigated by using convective boundaries with a large heat transfer coefficient in the steady-state case. The nine-point finite difference relation with the parameter, p, given by Equation (3.21) was compared to the five-point relation as developed in Section 3.8.2. It was concluded that the nine-point relation provided a higher degree of accuracy and had a faster convergence rate than the five-point relation.

Chapter 4 illustrated the application of the numerical techniques in regions where there was no heat generated such as the clad region of the nuclear fuel element. A slab was chosen as an example which was subjected at one of its boundaries to either a uniform or an exponential temperature distribution. The slab was made of a uniform material either aluminum or zirconium. The nine-point relation here again provided a higher accuracy and a faster convergence rate than the five-point relation.

Finally, Chapter 5 reflected the time-dependent behavior of the numerical techniques developed for the study, and in some problems already considered in the steady-state case. The equations were developed using an explicit method which was convenient for such a problem.

Section 5.3 provided the results of computations in the case of constant heat generation and thermal properties. Here, the second term of the parameter, p, of the nine-point relation (Equation 5.9) was not zero as the corresponding steady-state case. It was concluded that the nine-point relation in both cases provided more accurate results than the five-point relation. However, there was no significant difference between the two cases of the nine-point relation, but in terms of convergence, it was higher for the nine-point relation when all terms for p (see Equation (5.9)) were used.

An optimization of the error was investigated in the unsteady-state case by changing the step size Δt. It was concluded that the errors decreased as the step size Δt approached its optimum value.

In the case of variable thermal conductivity or heat generation in the time dependent case, the computational results showed again a higher accuracy and a faster convergence rate for the nine-point relation.

6.3 Suggestion for Further Study

The nine-point finite difference formulation may be extended to the heat conduction equation in the three-dimensional rectangular network.

The present work may also be extended to fields dealing with configurations using irregularly shaped regions, such as in Figure 6.1. It could also be possible to develop the nine-point relation in the R-ϕ cylindrical geometry. This will be of particular interest for the calculation of the temperature distribution in a nuclear fuel rod.

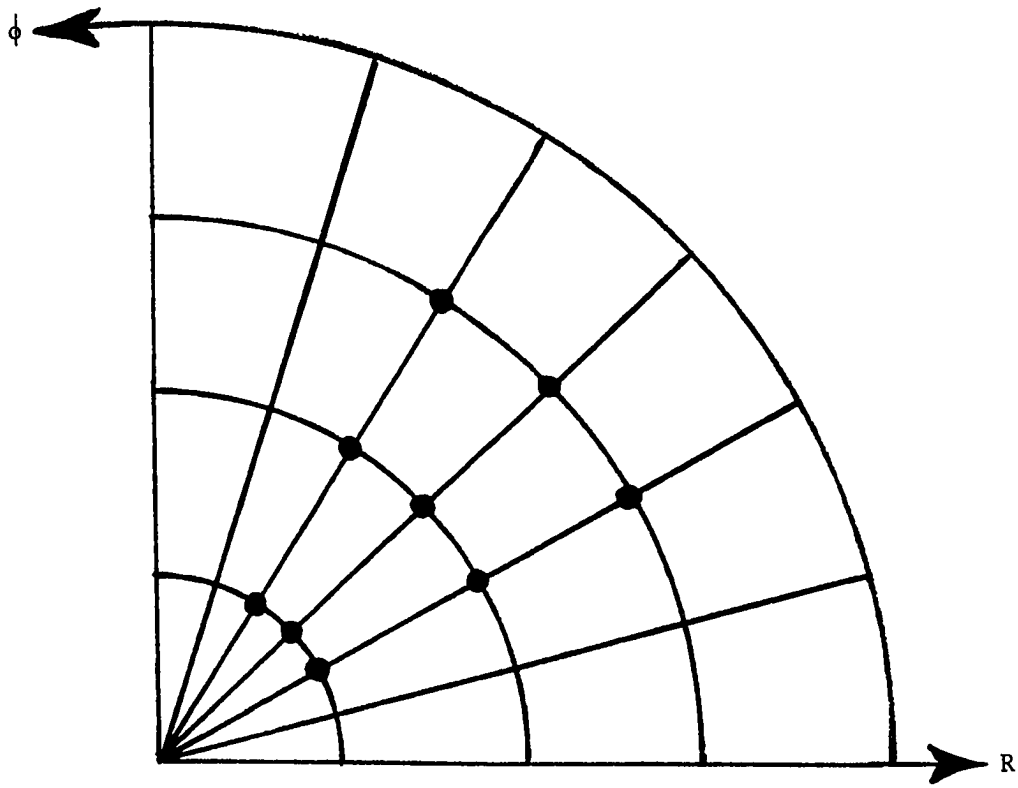

Figure 6.1. Irregular cylindrical region

7. REFERENCES

1. W. D. Turner and J. S. Crowell, Notes on heating: An IBM 360 heat conduction program, CTC-INF-980, Oak Ridge, TN, November 21, 1969.

2. Invert 1.0: A program for solving the nonlinear inverse heat conduction problem for one-dimensional solids, EGG.2068, Department of Energy, Idaho Falls, Idaho, February 1981.

3. John A. McClure, Too dee: A two-dimensional, time-dependent heat conduction program, IDO-17227, Phillips Petroleum Company, Idaho Falls, Idaho, April 1967.

4. W. D. Turner, D. C. Elrod and Siman-Tov, Heating 5: An ABM 360 heat conduction program, ORNL/CSD/TM-15, Oak Ridge, TN, March 1977.

5. Siman-Tov and W. D. Turner, Heatup: A computer program for the thermal analysis of LOCA accident in an HTGR, ORNL/CSD/TM-16, Oak Ridge, TN, November 1976.

6. W. D. Turner and M. Siman-Tov, Heating 3: An ABM 360 heat conduction program, ORNL-TM-3208, Oak Ridge, TN, February 1971.

7. R. B. Smith and J. Spainer, Hot-1: A two-dimensional steady-state heat conduction program for the Philco-2000, WAPD-TM-465, Westinghouse Electric Corp., Pittsburg, July 1964.

8. J. Spainer and W. D. Peterson, Hot-2: A two-dimensional transient heat conduction program for the CDC-6600, WAPD-TM-669, Bettis Atomic Power Lab, June 1967.

9. G. Lebon and Ph. Mathieu, A numerical calculation of nonlinear transient heat conduction in the fuel elements of a nuclear reactor, J. Heat Transfer 22, 1187-1198 (1979).

10. S. K. Fraley, T. J. Hoffman and P. N. Stevens, A Monte Carlo method of solving heat conduction problems, J. Heat Transfer 102, 121-125 (1980).

11. M. N. Özisik, Boundary Value Problems of Heat Conduction (International Textbook Company, Scranton, PA, 1968).

12. M. N. Özisik, Heat Conduction (John Wiley and Sons, Inc., New York, 1980).

13. V. S. Arpaci, Conduction Heat Transfer (Addison-Wesley Publishing Company, Massachusetts, 1966).

14. M. M. El-Wakil, Nuclear Heat Transport (International Textbook Inc., Scranton, PA, 1971).

15. A. F. Rohach, Nine-point difference approximation to Laplacian operator, Trans. Am. Nucl. Soc. 17, 232-233 (1973).

16. E. F. Eckholt, A computational study of a nine-point numerical approximation to the two-dimensional Poisson equation, M.S. Thesis, Iowa State University, 1976.

17. J. M. Clark and K. F. Hansen, Numerical Method of Reactor Analysis (Academic Press, New York, 1964).

18. T. E. Guidotti, K. L. Peddicord and L. H. Nielsen, Transient fuel pin temperature calculations using describing functions NP-2278, Research Project 1321-2, EPRI, California, February 1982.

19. L. S. Tong and J. Weisman, Thermal Analysis of Pressurized Water Reactors (American Nuclear Society, LaGrange Park, IL, 1979).

20. J. Cornette, Department of Mathematics, Iowa State University. Private communication, 1983.

21. A. J. Chapman, Heat Transfer, 3rd edition (Macmillan Publishing Company, Inc., New York, 1974).

22. P. A. Loretan, Laplace-variational method for transient multidimensional temperature distributions, Ph.D. Thesis, Iowa State University, 1965.

8. ACKNOWLEDGMENTS

The author wishes to express his deepest gratitude to his major professor, Dr. Alfred Rohach, whose guidance and helpful contributions made this work possible. In addition, the author expresses appreciation to the Government of Algeria for its financial support.

In conclusion, sincere gratitude is given to my wife for her help and encouragement throughout my graduate study.

9. APPENDIX A: DERIVATION OF FIVE-POINT FINITE DIFFERENCE REALTION

The temperature is expressed as a function of the two independent variables, x and y, in rectangular coordinates. In the steady-state case, the pertinent equation is the Poisson equation [12],

$$\frac{\partial^2 T}{\partial x^2} + \frac{\partial^2 T}{\partial y^2} + \frac{S}{K} = 0 \ . \qquad \text{(A.1)}$$

The field is divided into a fine grid of widths Δx and Δy, Figure 9.1.

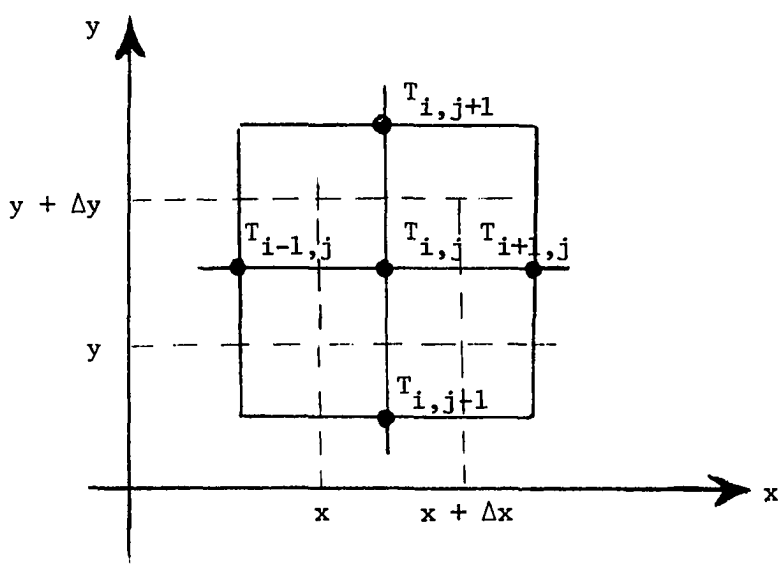

Figure 9.1. Nodes in a two-dimensional system

Equation (A.1) can be approximated by a five-point finite difference equation. Using the Taylor's series expansion

$$T(x \pm \Delta x) = T(x) \pm \Delta x\, T'(x) + \frac{(\Delta x)^2}{2!} T''(x)$$

$$\pm \frac{(\Delta x)^3}{3!} T'''(x) \pm \ldots . \qquad (A.2)$$

Using a finite difference grid as shown in Figure 9.1, and expanding each of the four axial points about the center point results in

$$T_{i+1,j} + T_{i-1,j} = 2\, T_{i,j} + (\Delta x)^2 \frac{\partial^2 T_{ij}}{\partial x^2} + O(h^4) \qquad (A.3)$$

and

$$T_{i,j+1} + T_{i,j-1} = 2\, T_{i,j} + (\Delta y)^2 \frac{\partial^2 T_{ij}}{\partial y^2} + O(h^4) \; . \qquad (A.4)$$

Equations (A.3) and (A.4) can now be solved for $\frac{\partial^2 T_{ij}}{\partial x^2}$ and $\frac{\partial^2 T_{ij}}{\partial y^2}$. The addition results in

$$\frac{\partial^2 T_{ij}}{\partial x^2} + \frac{\partial^2 T_{ij}}{\partial y^2} = \frac{1}{(\Delta x)^2} [T_{i+1,j} + T_{i-1,j} - 2\, T_{i,j}]$$

$$+ \frac{1}{(\Delta y)^2} [T_{i,j+1} + T_{i,j-1} - 2\, T_{i,j}] - O(h^2) \; . \qquad (A.5)$$

Using $\beta = \Delta x/\Delta y$ in Equation (A.5) and rearranging Equation (A.1) can be rewritten for the node (i,j) as

$$\frac{1}{(\Delta x)(\Delta y)} \left[\frac{1}{\beta} (T_{i+1,j} + T_{i-1,j}) + \beta (T_{i,j+1} + T_{i,j-1}) \right.$$

$$\left. - 2\left(\frac{1}{\beta} + \beta\right) T_{ij} \right] + \frac{S_{ij}}{K_{ij}} = 0 \; . \qquad (A.6)$$

Then, solving Equation (A.6) for T_{ij} results in

$$T_{ij} = \frac{1}{2(\frac{1}{\beta} + \beta)} \left[\frac{1}{\beta} (T_{i+1,j} + T_{i-1,j}) + \beta(T_{i,j+1} + T_{i,j-1} + (\Delta x)(\Delta y) \frac{S_{ij}}{K_{ij}} \right] + O(h^2) \quad . \tag{A.7}$$

This is the standard five-point finite difference approximation for unequal spacing for the heat conduction equation. If $\Delta x = \Delta y$ (equal spacing), Equation (A.7) reduced to

$$T_{ij} = \frac{1}{4} \left[T_{i+1,j} + T_{i-1,j} + T_{i,j+1} + T_{i,j-1} + (\Delta x)^2 \frac{S_{ij}}{K_{ij}} \right] + O(h^2) \quad . \tag{A.8}$$

10. APPENDIX B: THEORETICAL DEVELOPMENT OF THE SECOND-ORDER RITZ PROFILE FOR THE STEADY-STATE CASE

The steady-state problem in terms of Figure 10.1 is [13]:

$$\frac{\partial^2 T}{\partial x^2} + \frac{\partial^2 T}{\partial y^2} + \frac{S}{K} = 0 \tag{B.1}$$

$$\frac{\partial T(0,y)}{\partial x} = 0 \ , \quad T(A,y) = 0 \tag{B.2}$$

$$\frac{\partial T(x,0)}{\partial y} = 0 \ , \quad T(x,B) = 0 \ . \tag{B.3}$$

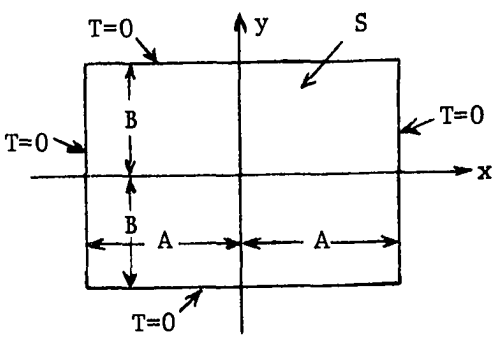

Figure 10.1. Slab with internal heat generation S and zero boundary temperatures

The thermal symmetry of the problem with respect to the coordinate axes of Figure 10.1 suggests the generalized Ritz profile

$$T(x,y) = (A^2 - x^2)(B^2 - y^2)(a_o + a_1 x^2 + b_1 y^2 + a_2 x^4 + b_2 y^4 + C_2 x^2 y^2 + \ldots) \ . \tag{B.4}$$

In Equation (B.4), either $(a_o + a_1x^2)$ or $(a_o + b_1y^2)$ may be used as the last term of the second-order approximation. Here,

$$T(x,y) = (A^2 - x^2)(B^2 - y^2)(a_o + a_1x^2) \tag{B.5}$$

is used arbitrarily. Equation (B.5), having two unknowns, a_o and a_1, to be determined, requires that two conditions be specified. The integral form of the governing differential equation, Equation (B.6), may be used as one of these conditions

$$\int_o^A \int_o^B \left(\frac{\partial^2 T}{\partial x^2} + \frac{\partial^2 T}{\partial y^2} + \frac{S}{K}\right) dxdy = 0 \tag{B.6}$$

Substitution of Equation (B.5) into Equation (B.6) results in

$$4 \int_o^A \int_o^B \{- 2(B^2 - y^2)\ [(a_o - a_1A^2) + 6\ a_1x^2]$$

$$- 2(a_oA^2 + a_1A^2x^2 - a_ox^2 - a_1x^4)$$

$$+ \left(\frac{S}{K}\right)\}\ dxdy = 0\ . \tag{B.7}$$

After simplification,

$$(B^2 + A^2)\ a_o + A^2(B_2 + A^2/5)\ a_1 = \frac{3S}{4K}\ . \tag{B.8}$$

The second condition related to the differential formulation of the problem is satisfied at the origin by Equation (B.5) and gives

$$(B^2 + A^2)\ a_o - A^2a_1 = S/2K\ . \tag{B.9}$$

Solving Equations (B.8) and (B.9) for a_o and a_1 yields

$$a_o = \left(\frac{S}{4K\ B^2}\right) \frac{5 + \left(\frac{2}{5}\right)(A/B)^2}{[1 + (A/B)^2][2 + \left(\frac{1}{5}\right)(A/B)^2]} \tag{B.10}$$

$$a_1 = \left(\frac{S}{4K\ B^2}\right) \frac{(1/A)^2}{2 + \left(\frac{1}{5}\right)(A/B)^2} \cdot \tag{B.11}$$

Hence, the second-order Ritz profile is found to be

$$T(x,y) = \left(\frac{SA^2}{K}\right) \cdot \frac{1}{4} \frac{[1 - (x/A)^2][1 - (y/B)^2}{[2 + \left(\frac{1}{5}\right)(A/B)^2]}$$

$$\left[\frac{S + \left(\frac{2}{5}\right)(A/B)^2}{1 + (A/B)^2} + \left(\frac{x}{A}\right)^2\right] . \tag{B.12}$$

Equation (B.12) is used in the program for the second-order Ritz profile for the steady-state case with constant thermal conductivity, K, and internal heat source, S.

11. APPENDIX C: SEPARATION OF VARIABLES ANALYTICAL METHOD IN THE STEADY-STATE CASE

The differential equation, Equation (B.1), being nonhomogeneous, is not separable. The solution of the problem, as given in Appendix B, is now assumed to be [13]

$$T(x,y) = \theta(x,y) + \phi(x) \ . \tag{C.1}$$

The differential equation to be satisfied by the two-dimensional problem, $\theta(x,y)$, can be made homogeneous. Thus, $\theta(x,y)$ is suitable for separation of variables. However, the complete formulation of $\phi(x)$, and $\theta(x,y)$ requires that the boundary conditions of these be specified. Here, $\phi(x)$ is assumed to satisfy the one-dimensional form of Equation (B.2). Hence,

$$\frac{d^2\phi}{dx^2} + \frac{S}{K} = 0 \ ; \quad \frac{d\phi(0)}{dx} = 0 \ ; \quad \phi(A) = 0 \ . \tag{C.2}$$

Then, combining Equations (B.1), (B.2), (B.3), (C.1), and (C.2), we find that $\theta(x,y)$ is satisfied by

$$\frac{\partial^2\theta}{\partial x^2} + \frac{\partial^2\theta}{\partial y^2} = 0 \tag{C.3}$$

$$\frac{\partial\theta(0,y)}{\partial x} = 0 \ , \quad \theta(A,y) = 0 \tag{C.4}$$

$$\frac{\partial\theta(x,0)}{\partial y} = 0 \ , \quad \theta(x,B) = -\phi(x) \ . \tag{C.5}$$

Thus, the solution of the nonseparable problem $T(x,y)$ is reduced to that of the separable problem $\theta(x,y)$. The result, including $\phi(x)$ is

$$T(x,y) = \left(\frac{S\,A^2}{K}\right) \left\{\frac{1}{2}\left[1 - \left(\frac{x}{A}\right)^2\right]\right.$$

$$\left. - 2 \sum_{k=0}^{\infty} \frac{(-1)^k}{(\beta_k A)^3} \left(\frac{\cos h\, \beta_k y}{\cos h\, \beta_k B}\right) \cos \beta_k x\right\}, \qquad (C.6)$$

where $\beta_k A = (2k + 1)\, \pi/2$, $k = 0,1,2....$ Equation (C.6) is used in the program for the exact analytical solution for the temperature distribution in the case of steady-state with constant K and S.

12. APPENDIX D: THE ANALYTIC SOLUTION OF THE NONLINEAR PROBLEM, THE KIRCHHOFF TRANSFORMATION

When the thermal conductivity varies with temperature, then a change of the dependent variable by means of the Kirchhoff transformation one can move the thermal conductivity K(T) outside the differential operator as now described [12],

Consider the heat conduction equation in the form

$$\nabla. \, [K(T) \, \nabla T] + S(r,t) = \rho(T) \, C_p(T) \, \frac{\partial T}{\partial t} \tag{D.1}$$

where C_p, ρ, and K are assumed to depend on temperature.

A new dependent variable U is defined according to Kirchhoff transformation as

$$U = \int_{T_o}^{T} \frac{K(T')}{K_o} \, dT' \tag{D.2}$$

where T_o is a reference temperature and K_o is the value of K(T) at T_o. Equation (D.1) is rearranged as

$$\nabla. \, [K(T) \, \frac{\partial T}{\partial U} \, \nabla U] + S(r,t) = \rho \, C_p \, \frac{\partial T}{\partial U} \, \frac{\partial U}{\partial t} \, . \tag{D.3}$$

From Equation (D.2), we have

$$\frac{\partial U}{\partial T} = \frac{K(T)}{K_o} \quad \text{or} \quad \frac{\partial T}{\partial U} = \frac{K_o}{K(T)} \, . \tag{D.4}$$

Introducing Equation (D.4) into Equation (D.3), one obtains

$$\nabla^2 \, U(r,t) + \frac{1}{K_o} \, S(r,t) = \frac{1}{\alpha_T} \, \frac{\partial U}{\partial t} \tag{D.5}$$

where $\alpha_T \equiv \alpha_T(T)$. Equation (D.5) is still nonlinear because α_T depends on temperature, but it is in a form that is more suitable for analysis than Equation (D.1). If $\alpha_T(T)$ varies little with temperature, then it can be assumed constant and Equation (D.5) becomes linear.

In the case of steady-state, the nonlinear differential equation of heat conduction is transformed to a linear equation by the Kirchhoff transformation, since the right-hand side of Equation (D.5) is zero for the steady-state case.

Let's now transform the boundary conditions by the Kirchhoff transformation. For the boundary condition of the first kind as given by Equation (1.3) in Chapter 1,

$$T = f(r,t) \ . \tag{D.6}$$

If considering K(T) as a linear function of T in the form

$$K(T) = K_o \ (1 + \xi T), \tag{D.7}$$

then the transformation (Equation D.2) becomes

$$U = \int_{T_o}^{T} (1 + \xi T')dT' = (T - T_o) + \frac{\xi}{2} (T^2 - T_o^2) \tag{D.8}$$

and the transformation of the boundary condition (Equation D.6) gives

$$U = (f - T_o) + \frac{\xi}{2} (f^2 - T_o^2) = f^*(r,t) \tag{D.9}$$

which is also a boundary condition of the first kind. In the same manner, one can proceed for the second and third kind boundary condition given by Equations (1.4) and (1.5).

If the reference temperature T_o is taken zero, and for our problem f = 0, then, the problem is transformed as

$$\frac{\partial^2 U}{\partial x^2} + \frac{\partial^2 U}{\partial y^2} + \frac{S(r,t)}{K_o} = \frac{1}{\alpha_T} \frac{\partial U}{\partial t} \qquad \text{(D.10)}$$

$$K_o \frac{\partial U}{\partial x} = 0 \qquad \text{at } x = 0$$

$$K_o \frac{\partial U}{\partial y} = 0 \qquad \text{at } y = 0$$

$$U = 0 \qquad \text{at } x = A \text{ or } y = B \ .$$

The transformation (Equation D.8) reduces to

$$U = T + \frac{1}{2} \xi T^2 \ . \qquad \text{(D.11)}$$

The inverse transformation becomes

$$T(\bar{r},t) = \frac{1}{\xi} \left[\sqrt{1 + 2\xi\, U(\bar{r},t)} \ -1\right] \ . \qquad \text{(D.12)}$$

This result is good for both steady-state and transient problems.

13. APPENDIX E: ANALYTICAL DEVELOPMENT OF THE STEADY AND UNSTEADY-STATES OF THE HEAT CONDUCTION EQUATION WITH HEAT GENERATION AS FUNCTION OF SPACE USING GREEN'S FUNCTION

The mathematical formulation of this problem is given as [12]

$$\frac{\partial^2 T}{\partial x^2} + \frac{\partial^2 T}{\partial y^2} + \frac{1}{K} S(x,y) = \frac{1}{\alpha} \frac{\partial T}{\partial t} \qquad \text{(E.1)}$$

where $\alpha = \frac{\rho C_p}{K}$ = thermal diffusivity,

$T = 0$ at all boundaries, for $t > 0$, and

$T = F$ (any constant as example for the temperature distribution at $t = 0$ in the slab).

To determine the appropriate Green's function, consider the homogeneous version of this problem as

$$\frac{\partial^2 \theta}{\partial x^2} + \frac{\partial^2 \theta}{\partial y^2} = \frac{1}{\alpha} \frac{\partial \theta}{\partial t} \quad 0 \leq x \leq A, \quad 0 \leq y \leq B \qquad \text{(E.2)}$$

$\theta = 0$ at $x = A$ and $y = B$, $t > 0$

$\theta = F$ at $t = 0$.

The solution of the problem (E.2) is obtained by separation of variables in the form

$$\theta(x,y,t) = X(x) \cdot Y(y) \cdot \Gamma(t) \quad . \qquad \text{(E.3)}$$

The complete solution of $\theta(x,y,t)$ in terms of these separated functions is written as

$$\theta(x,y,t) = \sum_{m=1}^{\infty} \sum_{n=1}^{\infty} C_{mn}\, e^{-\alpha(\gamma_m^2 + \eta_n^2)t}\, X(\gamma_m,x)\, Y(\eta_n,y) \qquad (E.4)$$

The application of the initial condition gives

$$F = \sum_{m=1}^{\infty} \sum_{n=1}^{\infty} C_{mn}\, X(\gamma_m,x)\, Y(\eta_n,y)\ . \qquad (E.5)$$

The unknown coefficient C_{mn} is determined by operating on both sides of the above equation (Equation E.5) and using the orthogonality of the eigenfunctions, $X(\gamma_m,x)$ and $Y(\eta_n,y)$. We obtain

$$C_{mn} = \frac{1}{0(\gamma_m) \cdot 0(\eta_n)} \int_{x'=0}^{A} \int_{y'=0}^{B} X(\gamma_m,x')\, Y(\eta_n,y') \cdot F \cdot dx'dy' \qquad (E.6)$$

where

$$0(\gamma_m) = \int_o^A X^2(\gamma_m,x)dx$$

$$0(\eta_n) = \int_o^B Y^2(\eta_n,y)dy$$

and

$$X(\gamma_m,x) = \sin \gamma_m x$$

$$Y(\eta_n,y) = \sin \eta_n y \qquad (E.7)$$

and

γ_m's are roots of $\sin \gamma_m A = 0$

η_n's are roots of $\sin \eta_n B = 0$,

that is,

$$\gamma_m = \frac{m\pi}{A} , \quad m = 1,2,3....$$

$$\eta_n = \frac{n\pi}{B} , \quad n = 1,2,3....$$

Substituting the above equations into Equation (E.6) and then into Equation (E.4), the solution becomes

$$\theta(x,y,t) = \frac{4}{A.B} \sum_{m=1}^{\infty} \sum_{n=1}^{\infty} e^{-\alpha(\gamma_m^2 + \eta_n^2)t} \cdot \sin \gamma_m x \sin \eta_n y$$

$$\cdot \int_{x'=0}^{A} \int_{y'=0}^{B} \sin \gamma_m x' \sin \eta_n y' \cdot F \cdot dx'dy' \quad (E.8)$$

or, for purpose of comparison, in the form

$$\theta(x,y,t) = \int_{x'=0}^{A} \int_{y'=0}^{B} [\frac{4}{AB} \sum_{m=1}^{\infty} \sum_{n=1}^{\infty} e^{-\alpha(\gamma_m^2 + \eta_n^2)t}$$

$$\cdot \sin \gamma_m x \sin \eta_n y \sin \gamma_m x' \sin \eta_n y' \cdot F \cdot dx'dy' . \quad (E.9)$$

Also, the solution of the problem (Equation E.1) in terms of Green's function is given as

$$\theta(x,y,t) = \int_{x'=0}^{A} \int_{y'=0}^{B} G(x,y,t|x',y',\tau)\Big|_{\tau=0}$$

$$\cdot F \cdot dx'dy' . \quad (E.10)$$

A comparison of Equations (E.10) and (E.9) gives

$$G(x,y,t|x',y',\tau)\Big|_{\tau=0} = \frac{4}{AB} \sum_{m=1}^{\infty} \sum_{n=1}^{\infty} e^{-\alpha(\gamma_m^2 + \eta_n^2)t}$$

$$\cdot \sin \gamma_m x \sin \eta_{ny}$$

$$\cdot \sin \gamma_m x' \sin \eta_n y' \quad . \tag{E.11}$$

The desired Green's function is obtained by replacing t by $(t-\tau)$ in Equation (E.11); as

$$G(x,y,t|x',y',\tau) = \frac{4}{AB} \sum_{m=1}^{\infty} \sum_{n=1}^{\infty} e^{-\alpha(\gamma_m^2 + \eta_n^2)(t - \tau)}$$

$$\cdot \sin \gamma_m x \sin \eta_n y \cdot \sin \gamma_m x' \sin \eta_n y' \quad . \tag{E.12}$$

Then, the solution of the nonhomogeneous problem (Equation E.1) is given in terms of the above Green's function after some manipulations as

$$T(x,y,t) = \int_{x'=0}^{A} \int_{y'=0}^{B} G(x,y,t|x',y',\tau)\Big|_{\tau=0} \cdot F \cdot dx'dy'$$

$$+ \frac{\alpha}{K} \int_{\tau=0}^{\tau} dr \int_{x'=0}^{A} \int_{y'=0}^{B} G(x,y,t|x',y',\tau)$$

$$\cdot S(x',y') \, dx'dy' \tag{E.13}$$

where the Green's function is as defined by Equation (E.12).

The solution of the problem becomes

$$T(x,y,t) = \frac{4}{AB} \sum_{m=1}^{\infty} \sum_{n=1}^{\infty} e^{-\alpha(\gamma_m^2 + \eta_n^2)t} \cdot \sin \gamma_m x \sin \eta_n y$$

$$\cdot \int_{x'=0}^{A} \int_{y'=0}^{B} F \sin \gamma_m x' \sin \eta_n y' \cdot dx'dy'$$

$$+ \frac{4}{AB} \sum_{m=1}^{\infty} \sum_{n=1}^{\infty} e^{-\alpha(\gamma_m^2 + \eta_n^2)t} \cdot \sin \gamma_m x \sin \eta_n y$$

$$\cdot \int_{t'=0}^{t} e^{\alpha(\gamma_m^2 + \eta_n^2)t'} dt' \cdot \int_{x'=0}^{A} \int_{y'=0}^{B} \frac{\alpha}{K}$$

$$\cdot \sin \gamma_m x' \sin \eta_n y' \; S(x',y')dx'dy' \; . \qquad \text{(E.14)}$$

In the case where, for example, the heat generation is taken in the form

$$S = S_o(X.Y), \qquad \text{(E.15)}$$

with an initial temperature distribution in the slab of F = 37.8°C (100°F), using these in Equation (E.14) and after performing the different integrations (simple integrations and integration by parts for the last double integral), one gets the following final expression for the temperature distribution in the slab as

$$T(x,y,t) = \frac{4}{AB} \sum_{m=1}^{\infty} \sum_{n=1}^{\infty} \sin \gamma_m x \sin \eta_n y$$

$$\cdot \left[100\left(\frac{1 - \cos \gamma_m A}{\gamma_m}\right)\left(\frac{1 - \cos \eta_n B}{\eta_n}\right)\right.$$

$$\cdot e^{-\alpha(\gamma_m^2 + \eta_n^2)t} + \left(\frac{\sin \gamma_m A}{\gamma_m^2} - \frac{A \cos \gamma_m A}{\gamma_m}\right)$$

$$\cdot \left(\frac{\sin \eta_n B}{\eta_n^2} - \frac{B \cos \eta_n B}{\eta_n}\right) \cdot \frac{S_o}{K(\gamma_m^2 + \eta_n^2)}$$

$$\left. \cdot \left(1 - e^{-\alpha(\gamma_m^2 + \eta_n^2)t}\right)\right] \qquad \text{(E.16)}$$

which is the equation used in the program for this specific problem, and as the time is taken sufficiently large ($t \to \infty$), one gets the steady-state temperature distribution in the slab.